INVESTIGATIONS INTO ELECTRONIC STOPPING REGIME SPUTTERING OF URANIUM TETRAFLUORIDE

Thesis by

Charles Kenneth Meins, Jr.

In Partial Fulfillment of the Requirements

for the Degree of

Doctor of Philosophy

California Institute of Technology

Pasadena, California

1982

(Submitted Jan. 14, 1982)

ACKNOWLEDGEMENTS

I would like to thank my advisor, Tom Tombrello, for the support and encouragement shown to me during the course of this work. Thanks also go to the students and postdocs who aided with suggestions, revelations, and physical labor, notably J. Griffith, M. Dumke, Y. Qiu, B. Cooper, M. Mendenhall, J. Osborne, T. Skelton, L. Seiberling, R. Kremer, and C. Watson.

The love and support of my wife, Gwen, made all of this possible. The God of Spinoza and Einstein made all of this necessary.

ABSTRACT

Yields were measured for ^{235}U sputtered from UF_4 by ^{16}O, ^{19}F, and ^{35}Cl over the energy range ~.12 to 1.5 *MeV/* amu using a charge equilibrated beam in the stripped beam arrangement for all the incident ions and in the transmission arrangement for ^{19}F and ^{35}Cl. In addition, yields were measured for ^{19}F incident in a wide range of discrete charge states. The angular dependence of all the measured yields were consistent with $\cos\vartheta$. The stripped beam and transmission data were well fit by the form $\left[\frac{Az_{eq}^2\ln(B\varepsilon)}{\varepsilon}\right]^4$ where ε was the ion energy in *MeV/* amu and $z_{eq}(\varepsilon)$ was taken from Zeigler(80). The fitted values of B for the various sets of data were consistent with a constant B_0, equal to 36.3±2.7, independent of incident ion. The fitted values of A show no consistent variation with incident ion although a difference can be noted between the stripped beam and transmission values, the transmission values being higher.

The incident charge data were well fit by the assumptions that the sputtering yield depended locally on a power of the incident ion charge and that the sputtering from the surface is exponentially correlated to conditions in the bulk. The equilibrated sputtering yields derived from these data are in agreement with the stripped beam yields.

In addition, to aid in the understanding of these data, the data of Hakansson(80,81a,81b) were examined and contrasted with the UF_4 results. The thermal models of Seiberling(80) and Watson(81) were discussed and compared to the data.

TABLE OF CONTENTS

I. Introduction

The experiments described in this thesis are the continuation of investigations by Griffith(79) and Seiberling(80, 81) on the sputtering of UF_4 caused by ions with energies near the peak of the electronic stopping power ($\sim$.1-2*MeV*/amu). The techniques used to measure sputtering were described in detail by Griffith. For this reason, only a general description is presented here. However, as the experimental equipment was constructed particularly for the experiments described in this thesis, it will be discussed thoroughly.

The focus of this work was to determine the detailed dependence of the sputtering yield on the energy and charge of the incident ion.

Previous experiments used beams of a single charge state and the yield showed a dependence on this charge. To eliminate this effect and see the true energy dependence of the sputtering mechanism, two related sets of experiments were performed. Both purported to look at the sputtering caused by a beam in charge equilibrium, i.e., a beam in which the relative populations of charge states are unaffected by the passage of the beam through matter. In one, the transmission experiments, the sputtering target, UF_4, was placed on the back of a thin carbon foil. As the beam traversed ~3000Å of matter before reaching the free surface of the UF_4 it had ample opportunity to reach equilibrium. In the second, the stripped beam experiments, a carbon foil was placed 1.2*cm* in front of the target. It was assumed that the beam came to equilibrium in the foil and that it remained in equilibrium in emergence from the foil and traversal of the vacuum to the target. These experiments are shown schematically in fig.1.

The sputtering yield was also investigated over a wider range of incident charge state than previously examined. To achieve this range a carbon foil was used to strip the beam after its emergence from the accelerator. This arrangement is shown in fig.2. Examination of these data allowed a separate determination of the sputtering yield at equilibrium charge.

It was desired to measure $\frac{dE}{dx}$ in UF_4 for comparison of its energy dependence with that of the sputtering yield. This was done using Rutherford scattering. This technique was also used to look for the effects of charge equilibration in $\frac{dE}{dx}$ in both UF_4 and UO_2 and to set a limit on the number of fluorine atoms sputtered per uranium atom in UF_4.

Sputtering, whether it be initiated by events near the surface of a material or deep in the bulk, is essentially a surface phenomenon and depends strongly on the condition of the surface. In the experiments performed, care was taken to ensure the cleanliness of the surface of the UF_4. The UF_4 was evaporated onto backings in a clean, good vacuum ($\leq 1\times10^{-6} torr$) to ensure cleanliness of the bulk material. During the experiments, and for some time before as well, the targets were held at elevated temperatures (140-160°C) and low pressures ($\leq 5\times10^{-9} torr$) to drive contaminants off the surface.

To achieve the temperatures and pressures needed for these experiments and to allow integration of the incident ion beam current, care was taken in the selection and preparation of the materials used in the construction of the experimental equipment. The major portion of the equipment consisted of 304 stainless steel (no other steels were used in the UHV chamber). Stainless steel has a very low vapor pressure at the

temperatures used and is readily cleaned by various acid baths. The 304 grade, though more difficult to machine than other grades of stainless, was chosen as it is the material used in commercially available UHV flanges and blankoffs. Using the same grade throughout helped to assure the vacuum-worthiness of the welded joints.

One large part was made from 2024 aluminum. The presence of an aluminum alloy caused concern as its vapor pressure, due mostly to trace zinc, varies from sample to sample. However this piece rode on a steel rod and it was felt that the use of two such dissimilar metals was needed to avoid vacuum welding problems. Such was the case and the chamber pressure was unaffected. In addition, there were several small pieces made from aluminum out of expediency. They were added one at a time and, as no adverse effects were noted on the attainable vacuum, they were allowed to remain.

Aluminum foil (Alfa-Ventron Co.) was used to catch the sputtered uranium atoms. It was high purity aluminum and was known to cause no vacuum problems (Griffith(79)).

Copper was used both because of its heat conductivity and the ability of UF_4 to adhere to it in thin layers. For the integrity of the vacuum, only OFHC (oxygen free, high conductivity) copper was used.

Electrical insulation caused the most difficulty. All organic insulators and even teflon had unacceptable vapor pressures. Only glass and Macor were usable. Macor is a machinable glass-mica compound marketed by Corning. It is composed of white opal glass doped with fluorine. Under heat treatment mica crystals appear in the matrix and grow until they are ~20μm in length and occupy ~55% of the volume. The random orientation of these crystals give the material its machinability; during

machining fractures can propagate only the length of one mica crystal before they touch a crystal of different orientation and are stopped.

All parts that were placed in the UHV chamber, with the exception of the aluminum catcher foils, were UHV cleaned.

II. Sputtering Experiments

A. Equipment

All of the experiments described herein were performed using the EN Tandem Van de Graaff accelerator in the Kellogg Radiation Laboratory. The sputtering experiments were performed in the UHV chamber on the N10° beamline while the experiments using Rutherford scattering were performed in the center leg scattering chamber.

The UHV chamber was designed by J.E. Griffith expressly for sputtering experiments. The chamber and N10° beamline are shown in fig.3. The chamber was a 304 stainless steel cylinder, 6" in diameter, 13" in length, with standard 8" CFF flanges on both ends. There were three 1½" ports mounted radially, all in the same plane, 5" from one end of the cylinder. All three had standard 2¾" CFF flanges. They were spaced at intervals of 90° around the chamber. As the chamber was mounted on the N10° leg, two of the ports were collinear with the beamline and the third was at the top of the chamber. The ports at the top and back of the chamber were sealed with quartz window blankoffs. The front port was connected to the beamline.

The vacuum system for this chamber was mounted on the 8" flange farthest from the 1½" ports. It consisted of an Ultek 80 ℓ/sec D-I ion pump and an Ultek sorption pump. The ion pump was mounted directly to the chamber. A grounded wire grid was placed over the mouth of the pump to impede electrons escaping from the pump from reaching the target. In between the ion and sorption pumps were a Granville-Philips 1" gold seal right-angle valve, a double-faced flange equipped with a Nupro

Co. needle valve, a U.S. Gauge absolute pressure gauge, and a Teledyne Hastings-Raydist DV-6M thermocouple vacuum gauge, and a Viton seal valve. The needle valve was connected to a bottle of dry nitrogen gas equipped with a regulator via ¼" copper tubing. A coldtrap was formed in the tubing by wrapping six turns in it (diameter ~6") and placing it in a liquid nitrogen dewar. Between the needle valve and the coldtrap was a tee with a 3 psig relief valve and a throttle valve on the free leg.

A liquid nitrogen inline coldtrap isolated the chamber from the beamline. Between the coldtrap and the chamber were a Granville- Phillips straight-through valve and a cross which held a 3*mm* tantalum collimator. The collimator was mounted on a single pin electrical feedthru so that it could both be biased and any current impinging upon it could be measured. A large permanent magnet, with its field perpendicular to the beamline, sat on top of the cross to deflect any electrons escaping from the collimator.

The experimental apparatus was mounted on the remaining 8" flange. The major portion of the apparatus was an 8" CFF blankoff. On this blankoff were three 1½" ports with 2¾" CFF flanges and one ¾" port with a rotatable CFF mini flange. All of these were made of 304 stainless steel.

As arranged for these experiments, only the 1½" ports were used. The ¾" port was installed in case the need arose for more electrical feedthrus than could be provided with a single 1½" port; the need never materialized. One port was used for electrical feedthrus, an eight pin feedthru being installed in it. The pins were composed of Kovar and hollow; they were welded shut on the chamber-side ends. The other ports held linear motion feedthrus, one with 2" of travel and the other with 6".

In addition to the ports, several holes were drilled in the chamber-side of the blankoff, all ~½" deep and tapped with 8-32 threads.

At the heart of the apparatus were the UF_4 target and the aluminum catcher foils. The foils were held on the inside surface of a stainless steel cylinder (3"O.D., 2.875"I.D., 4.625" in length) by two steel runners on opposite sides of the cylinder. Each runner was held in place by two 2-56 screws, one at each end. Two 4"×½" slots, running the length of cylinder, were cut on opposite sides of the cylinder. One of the slots gave the ion beam entrance while the other allowed viewing of the target. The cylinder was held by an assembly consisting of steel clamps at the top and bottom of the cylinder attached to Macor blocks which were in turn attached to an aluminum block. The Macor served to electrically isolate the cylinder. The aluminum block rode on a ¼" steel rod which, along with two other steel rods of the same length, was screwed into an 8-32 tapped hole in the blankoff. All three rods were connected at their other ends by an aluminum plate for rigidity. The aluminum block was connected to the 6" linear motion feedthru. In this manner the position of the catcher foil cylinder could be varied.

A second of the rods held a ~½" section of alumina tubing. This piece served as an insulated support for the copper wire connecting the cylinder to a feedthru pin.

The cylinder was held such that its axis passed through the center of the target.

The assembly holding the target was of more complexity than that which held the catcher foils. At the heart of the assembly was an OFHC copper block, 1¼" wide by 2" high by .188" thick. Two openings were cut through the face of the block, a .438" hole centered .313" from the top of

the block and a .375" hole ¾" lower. Both were on the centerline of the block. The .438" hole held a quartz disc for viewing the beamspot while the sputtering target was placed over the .375" hole. Since the target was evaporated onto a .010" tantalum foil holder (for transmission experiments) or a .010" copper backing (for forward direction experiments), a .010" recess was machined into the face of the block. In this way, the target was held flush with the surface of the copper block.

Collimating plates were attached to the block above and below the target with two 2-56 screws on each. These were semicircular plates made from .031" steel or .020" aluminum (used only for the stripped beam experiments). In all of the experiments, a pair of collimators was attached to the UF_4 side of the block. For transmission experiments an additional pair was attached to the opposite side. The target side collimators, as their name implies, collimated the sputtered atoms into bands on the catcher foils. In addition they helped to trap any secondary electrons and thus improve charge integration. Charge integration was the sole purpose of the second pair of plates in transmission experiments. Fig.4 shows the apparatus as set up for transmission experiments. The second pair of collimators has been omitted for clarity.

In the stripped beam experiments the stripper foil was attached to the upper aluminum collimator plate so that the foil was centered between the collimators. On each collimator a ½" wide C-shaped cut was made; the interior of the C was bent away from the beamline to form flaps on the outside of the collimators. The flap on the upper collimator had a hole drilled through it and the foil holder was attached to it with a 2-56 screw. The foil holder was a piece of .020" aluminum with a .375" hole for the foil. The foil sat 1.2*cm* in front of the target.

In contrast to the catcher cylinder, the target assembly was attached directly to the 2" linear motion feedthru. A .375" steel rod was attached to the feedthru and was collinear to it. At the top of the rod was a steel block, .375" thick. Attached to the back of this was a Macor block, 1.3" by 1¼" by ¼". The copper block was attached to the front of the Macor by four 2-56 screws. Since the Macor was mounted .188" off of the center of the feedthru, the target side of the .188" copper block was on the feedthru axis.

The Macor block served several purposes. It insulated the target electrically and thermally from the blankoff and provided a convenient location for the target's resistive heater. The heater element was ~10" of .015" tungsten wire coiled into a recess in the surface of the Macor facing the copper block. The recess was formed by two circular depressions, ½" in diameter and .031" deep, which overlapped each other by ~.001". The tungsten wire entered the recess from the back of the Macor through a .030" hole in one circle, crossed through the overlap to the other circle, and exited out a second .030" hole to the back of the Macor. Two sapphire discs, ½" in diameter and .019" thick, covered the wire in the recess and electrically isolated the heater from the target. The combination of wire and discs protruded .002" from the surface of the Macor to ensure mechanical contact. By using sapphire, the heater remained in good thermal contact with the target.

The heater resistance was .54Ω when cold and .65Ω when a current of 3.7*A* flowed through it (while the electrical feedthrus were rated at 4.*A* the heater could be seen glowing a dull red through the Macor at this current and it was feared that structural damage would result at higher currents). The temperature that the target could achieve varied

depending on which collimators were in use. With both pairs of steel collimators, as used in transmission experiments, the target reached only 150°C with a current of 3.7*A*. With a single pair of aluminum collimators, the temperature reached 210°C with 3.2*A*.

A chromel-constantan thermocouple was mounted in the copper block to monitor its temperature. To guarantee that the temperature measured was at least a lower bound to the target temperature, the thermocouple was positioned with the UF_4 target between it and the heater. A .128" hole was drilled through the width of the copper block between the holes for the quartz and the target. The thermocouple was fed through this hole with a lead extending from each end. The leads were insulated with alumina tubing (.126"O.D., .064"I.D.) except for the thermocouple junction which was forced into contact with the copper block.

The thermocouple leads were not attached directly to the electrical feedthrus. Instead, they were attached to bolts fastened through the Macor. Leads from the feedthrus were attached to the other ends of the bolts, a chromel lead on the chromel side and a constantan lead on the constantan side. This arrangement put the thermocouple's reference junction on the electrical feedthru which was held to room temperature by the thermal mass of the steel blankoff. The reason for this added complexity, which was repeated with the leads to the heater, was to allow the target assembly, with its many small pieces and fine wires, to be assembled independently of the heavy steel blankoff.

There were five electrical connections to the target assembly, two each to the heater and thermocouple and one for charge integration. Three of the wires were copper while the thermocouple leads were chromel and constantan, as stated above. All five were threaded through

a Macor guide block attached to the steel blankoff. Between the guide and the target, the leads were insulated with ~1" sections of glass tubing. Connected in this fashion, the target assembly could be moved up and down without fear of the leads shorting against each other, the blankoff, or the cylinder. In addition, the placement of the guide against the blankoff directly under the edge of the cylinder, assured that the leads could not interfere with the movement of the cylinder.

The leads were attached to the electrical feedthru by wrapping them around the Kovar pins. They were secured by copper alligator clips. The pins on which the cylinder and target were attached were connected together on the outside of the blankoff. During experiments they were further connected to a 300^{V} battery via a large resistor (~1MΩ) which put a 300^{V} bias on both cylinder and target. The collected current was sent to a Brookhaven Nuclear Instruments Corp. Model 1000 current meter and integrator by RG-58 cable. The output of the integrator was sent to a Tennelec TC 550 scaler from which the charge incident on the target was read.

As read on the current meter, the leakage current on the target, i.e., the target current in the absence of beam, was typically $-.18nA$. This current was due to electrons escaping from the ion pump and passing through the grounded grid to be accelerated onto the target. When the pump was off, the leakage current dropped to $<50.pA$.

Some of the experiments performed required higher charge states than the normal operation of the accelerator could provide. In a tandem Van de Graaff, the beam is injected into the machine either neutral or with a single negative charge per atom. As the beam passes through the terminal, it encounters matter in the form of thin foils or, in the case of

the Kellogg EN machine, N_2 gas. Collisions with this matter strip away electrons from the beam, leaving the atoms with an overall positive charge. These positive ions are then accelerated away from the positively charged terminal so that the ions have a greater energy on exit than on entrance. The distribution of charge states in the exit beam is that corresponding to the beam energy at the terminal and is thus lower than that corresponding to the exit energy. For the ^{19}F beams produced by the tandem (~2-35MeV), the average exit charge is 2 to 4 lower than appropriate for the exit energy.

To get higher charge states, a carbon foil was placed at the object of the 90° spectrometer magnet as shown in fig.2. The placement was chosen as the 90° magnet could then be used to select the desired charge state from the beam. Also, the focusing properties of the magnet helped to overcome the angle straggling caused by passage through the foil. The foil holder was a piece of aluminum on a steel rod which was mounted on a lucite viewport. The aluminum was bent into a dogleg so that rotating the rod brought the foil in and out of the beamline. When out of the beam, the holder did not interfere with the movement of the object tantalum/quartz beam diagnostics.

As originally mounted, the carbon foil was 20.$\mu g/cm^2$ thick and was supported on a .001" thick, 90% transmission nickel screen over a ¾" hole. The nickel was intended to aid in dispersion of heat from the foil. Instead, it served to destroy the foil by melting when exposed to beams of >1μA of ^{19}F with energies between ~5 and 15MeV. The holder was remade, the ¾" hole being replaced by a ¼" by ¾" slot. The nickel was discarded and a 46.$\mu g/cm^2$ carbon foil was mounted. This arrangement proved to be more resilient; it withstood ~3μA of $^{35}Cl^{+4}$ at 15.MeV.

B. Vacuum Procedure

The procedure for pumping out the chamber was the following. After the chamber was sealed up, the sorption pump was cooled and the right angle valve and the Viton seal valve were opened. When carbon foils were used in the chamber, the Viton valve was opened slowly and, monitoring with the U.S. Gauge absolute pressure gauge, the pressure in the chamber was allowed to drop at no more than $.1 psi/sec$. The pumping speed of the sorption pump dropped severely at pressures under $100\mu m$, possibly due to a crack opening up when the pump was cooled (at room temperature the pump was helium leak-tight). Because of this, the inline coldtrap was filled and the straight through valve opened when the chamber pressure was below $100\mu m$. The Viton valve was closed at the same time. Opening the straight through valve allowed the N10° diffusion pump to evacuate the chamber. The coldtrap impeded the flow of diffusion oil into the chamber. After the chamber pressure dropped below $5\mu m$, both gold seal valves were closed and the ion pump turned on. After the ion pump was started, both the coldtrap and the sorption pump were allowed to warm up. The sorption pump was vented after it reached room temperature.

As soon as the chamber pressure fell to below $1\times10^{-5} torr$, the chamber walls were heated by a heat tape wrapped around the chamber. The heat tape was powered by a Variac. With 120^{V} across the heat tape, the chamber walls were at ~100°C. The 1½" port on the blankoff on which the target was mounted only reached ~25°C. The tape was turned off and the chamber allowed to cool to room temperature before the experiments were performed.

Heating the chamber increased the rate of outgassing of the material adsorbed on the inside of the chamber (e.g., H_2O, CO_2) and permitted this material to be pumped out of the chamber more quickly. Use of the Variac allowed control of this outgassing so that the chamber pressure never rose above $1\times10^{-5} torr$.

After the chamber itself had been outgassed, i.e., after the heat tape had been brought to full power and the chamber pressure had resumed its descent, the target heater was turned on and the outgassing procedure repeated. The outgassing of the cylinder and target were performed separately as the rates of outgassing were unpredictable and thus consecutive outgassing periods gave greater control over the chamber pressure.

After both chamber and target were outgassed, the chamber pressure would drop by a factor of 30-100 when the chamber was allowed to cool to room temperature. If the target was cooled as well, the pressure dropped below readability ($\leq 5\times10^{-10} torr$).

During the experiments the target temperature was held at 150°C.

The chamber was filled with dry nitrogen gas to bring it up to atmospheric pressure. The throttle valve on the copper tubing and the valve on the nitrogen bottle were opened. Once the flow rate was adjusted ($\sim 1 psi$ difference on the regulator with the throttle valve opened and closed), the coiled section of tubing was immersed in liquid nitrogen to freeze out any impurities in the gas. The throttle valve was closed after the nitrogen stopped boiling. If the section between the right-angle and the Viton valves was not at vacuum ($\leq 5mm$), the sorption pump was cooled and the section pumped out. With the line at an acceptable pressure, the ion pump was turned off and the right-angle valve opened. If no carbon foils

were inside, the needle valve was opened wide. If there were, the pressure was monitored with the absolute pressure gauge and the needle valve was opened slowly, the pressure allowed to rise at no more than $.1 psi / sec$.

Once the chamber was at atmospheric pressure, the needle valve and the nitrogen bottle regulator were closed, the throttle valve opened, and the copper coils removed from their liquid nitrogen bath. The impurities frozen in the coils would then boil off and exit violently through the throttle valve.

C. Target Preparation

The sputtering targets used in these experiments consisted of ~2000 Å ($\sim 140 \mu g / cm^2$) of UF_4 on either a copper or carbon backing. The former was used for all forward sputtering experiments and the latter for the transmission runs. The uranium was enriched to 93.08% ^{235}U.

The copper backings were made of .010" copper sheet. After being cut to size and screw holes drilled, the blanks were polished to optical smoothness. First 600 grit sandpaper and then 5, 2, and $1 \mu m$ polishing compound, suspended in methanol, were used to achieve this finish. At every change of polishing agent the blanks were given an ultrasonic bath in methanol. After the polishing, the blanks were given the standard UHV copper cleaning.

The carbon backings were foils made by the Arizona Carbon Foil Co. The thickness of the foils, as claimed by the manufacturer, ranged from 18.3 to 21.7 $\mu g / cm^2$ (~800 to 1000Å). The foils were mounted over a .438" hole in a .010" thick tungsten backing. Before mounting the foils, the

tungsten was cleaned by the same procedure as used for copper.

Once the backings were readied, the procedure went independently of the backing material. Application of the UF_4 layer was done by evaporation in a Veeco VE-775 vacuum system. The UF_4 was loaded into a .005" 'closed' tungsten boat, $\sim \frac{1}{2} mg$ at a time. This amount would suffice for ~4 evaporations. The backings were mounted ~8" away from the boat and an aluminum foil tent was arranged around the two to minimize the amount of uranium evaporated onto the belljar itself. The boat was baked, typically at 40.*A* overnight, to drive the water and other contaminants off the slightly hydroscopic UF_4. With the liquid nitrogen coldtrap filled, the belljar pressure fell to below $3 \times 10^{-7} torr$.

The rate of evaporation of the UF_4 was a compromise between time and pressure. It was thought desirable to complete the evaporation in the shortest time and under the lowest pressure possible so that the layer of UF_4 laid down would contain the fewest number of trapped residual gas molecules (typically N_2 and diffusion pump oil). Unfortunately, the rate of evaporation could only be raised by raising the boat temperature. This in turn raised the outgassing rate of the boat and increased the belljar pressure. The best compromise that could be struck was to hold the pressure under $1 \times 10^{-6} torr$ in which case the evaporation could be completed in less than 90 sec.

In one of the $\frac{dE}{dx}$ experiments, a UO_2 target was used. This was formed by first evaporating a layer of depleted uranium onto a copper backing and then heating it in air to form the oxide. The evaporation was performed in the same manner as the UF_4, except that the boat used was a a .005" open tungsten boat instead of a closed one. The uranium layer evaporated, $13. \mu g / cm^2$, while adequate, was thinner than planned as the

boat melted during the evaporation. Melting occurred at ~140.*A* of boat current; Mendenhall(80) has demonstrated that these boats will withstand currents in excess of 240.*A*. This melting serves to bolster molten uranium's reputation as a universal solvent of metals. Future evaporations of uranium should be done in an alumina lined boat.

After the uranium layer was laid down, it was oxidized by placing it in a test tube which was immersed in boiling water. After ~5 minutes, the color which was originally a dark yellow changed very slightly to a yellow-brown which remained unchanged on further heating.

III. Analysis

A. Sputtering Yield

Uranium atoms sputtered from the target were caught on the aluminum foils on the inside of the catcher cylinder. The collimators on the target assembly limited the atoms to a band ~.4" wide along the foils. The cylinder and foils were moved ½" between runs. After exposure, the foils were removed from the cylinder and cut into pieces less than ~2" by ~1½". These dimensions were nominally those of the muscovite mica sheets used as a sort of photographic positive to expose the locations of the sputtered uranium atoms. The mica sheets, ~.010" thick, were cleaved to provide clean surfaces between which the exposed foils were placed. These sandwiches, along with a control composed of a cloven mica and two pieces of uranium doped glass, were clamped in a lucite holder. The entire assembly was placed in the center vertical column of the UCLA research reactor and the reactor run at $100kW$ for 30 minutes. This bathed the assembly in $\sim 3.1\times10^{15}$ neutrons/cm^2 and fissioned $\sim 1.4\times10^{-4}$% of the uranium atoms. After this, the micas were removed and etched in 48% HF for 15 minutes. This etching converted the paths along which the fission fragments traveled into voids, or tracks, which were visible under a microscope.

The tracks were counted with a Leitz Wetzlar microscope at either 625X or 1250X magnification. A reticule of known area allowed the counted numbers to be converted into areal densities. Approximately 200,000 tracks were counted by the author in the course of the work.

The uranium doped glass was included to provide a more accurate, or at least more consistent, measure of neutron dose than the UCLA reactor operators could provide. The glass was obtained from the National Bureau of Standards and carried the appellation NBS-612. It contained 8.95×10^{-6} fraction by weight of ^{235}U. By measuring the number of tracks occurring under such a glass, the total neutron flux, or, more simply, the conversion from densities of tracks to uranium atoms, could be determined. This was complicated by the fact that the fission fragments emerged from a solid and that the lengths of the tracks produced in the mica ranged from $\sim 10\mu m$ down to 0. Tracks with zero length are, of course, hard to count. However, since all of the tracks were counted by the same observer, it is felt that the sputtering yields reported in this work are at least internally consistent. In addition, the measured neutron doses were in close agreement with those observed by Griffith(79).

A further complication is the lack of accurate measurements in the average range of fission fragments. This range is proportional to the number of uranium atoms per area whose fission fragments can escape the doped glass and cause tracks. In keeping with earlier work in Kellogg(Gregg(77), Griffith(79), Seiberling(80)), the range was assumed to be $2.24\times10^{-3} g/cm^2$.

The sputtering yield S was calculated by the following procedure. The track density was fit to the form

$$n(x) = n_0 \cos\left[\frac{x}{R}\right] \tag{3.1}$$

by least squares. Several runs were χ^2-fit for comparison. The differences in n_0 were typically <1%, the worst case being 1.5%. The least squares fit was used as, since all calculations were performed on an HP-67

calculator, it was a great deal faster than the χ^2 fit.

The background, due to trace fissionable elements in the mica and foils, was subtracted off after the fit was performed. This was possible, and desirable, as the background was measured independently by counting the tracks between the bands of foil exposed to the sputtered uranium atoms. That these tracks were due to trace fissionable elements in the foils and mica and not to sputtered atoms bouncing one or more times before sticking is evidenced by the observation that the number of number tracks showed no x dependence.

The subtraction was done in the following manner. What was actually fit was

$$n(\vartheta) = n_0 \cos\vartheta + \Delta n \tag{3.2}$$

where

$$\vartheta = \frac{x}{R} \tag{3.3}$$

For constant Δn, a least squares procedure yields

$$n_0 = \frac{\sum_i (n_i - \Delta n)\cos\vartheta_i}{\sum_i \cos\vartheta_i^{\,2}} \tag{3.4a}$$

$$= \frac{\sum_i n_i \cos\vartheta_i}{\sum_i \cos\vartheta_i^{\,2}} - \Delta n \left[\frac{\sum_i \cos\vartheta_i}{\sum_i \cos\vartheta_i^{\,2}} \right] \tag{3.4b}$$

To find the total number of tracks, N_{tot}, eqn.3.1 with the n_0 from eqn.3.4 was integrated over the hemisphere exposed to the sputtered atoms,

$$N_{tot} = \int_A n(x)\, dA \tag{3.5}$$

Converting from x to ϑ yields

$$N_{tot} = \int_{2\pi} n(\vartheta)\, R^2 d\Omega \tag{3.6}$$

$$= 2\pi R^2 \int_0^{2\pi} n_0 \cos\vartheta \sin\vartheta \, d\vartheta$$

$$= \pi R^2 n_0$$

The sputtering yield, S, was N_{tot} divided by the number of ions, N_i, to strike the target. For a beam of charge state q and total charge Q, N_i was

$$N_i = \frac{Q}{qe} \tag{3.7}$$

where e is the electron charge. Therefore S was

$$S = \frac{qe\, N_{tot}}{Q} \quad . \tag{3.8}$$

B. Error Analysis

Uncertainties appear in the sputtering yield from three sources: geometry of the experimental apparatus, integration of the beam current, and statistical uncertainties in the counting of the sputtered atoms. They will be discussed in that order.

The analysis of the sputtering data is done under assumptions that the source of sputtered atoms is pointlike and at the center of the

cylinder on which catcher foil is located. Also, that the band of the cylinder examined is narrow enough to be considered spherical. Of these, the 'sphericalness' of the cylinder and the location of the foil against the cylinder are the better assumptions. The exposed portion of the foil was ~.4" wide and was centered on the beamspot. Thus the variation in distance from target to foil was at most 1% of the cylinder's 3.63cm radius. Whenever possible, data were taken from the center of the bands. As for the foil, in no case did it sit more than ~1mm off of the inner surface of the cylinder and such wrinkles were no more than ~3mm out of the ≤52mm foil length. Their effect on the sputtering yield was estimated to be less than 1%, i.e.,

$$Error \sim \left[\frac{3mm}{52mm}\right]\left[1-\left[\frac{36-3mm}{36mm}\right]^2\right] \qquad (3.9)$$

$$\sim .3\% \ .$$

Estimating the effects of the finite beamspot and the nonconcentricity of the target and foil was more involved. (Since translation of the target transverse to the beam direction produced an effect equivalent to a beamspot of finite extent, only the translation will be examined in detail.) Lacking a rigorous analytical technique, the effects of target translation were examined numerically. A point source was assumed to be at (x_0,y_0) where the beam direction was along the y-axis. The collecting surface was at $x^2+y^2=a^2$. The source emitted atoms with the distribution

$$n(\varphi) = \frac{a^2\cos\varphi}{r^2(\varphi)} \qquad (3.10)$$

The geometry is shown in fig.5. The areal distribution of atoms on the collector in terms of the angle ϑ was

$$n(\vartheta) = \frac{a^2\cos\varphi}{r^2(\varphi)}\cos(\vartheta-\varphi) \qquad (3.11)$$

$$= \frac{a^2\cos\vartheta\cos(\vartheta-\varphi)}{a^2+x_0^2+y_0^2+2ax_0\sin\varphi+2ay_0\cos\varphi},$$

$$\varphi = \vartheta-\arcsin\left[\frac{(x_0^2+y_0^2)^{1/2}}{a}\cos\left[\vartheta-\arctan\left[\frac{y_0}{x_0}\right]\right]\right]$$

Given a point (x_0,y_0) this function was calculated at 18 evenly spaced points from ϑ = -85° to +85° (the data gathered were taken typically at constant intervals). These values were fit to the form $n_0\cos\vartheta$ by a least squares procedure. The departure of n_0 from 1 was taken to be the error introduced by the translation to (x_0,y_0) from the origin. The errors at a selected set of points are shown in table 1. The results show that the sputtering yield is very insensitive to translations in the transverse direction and thus also to the finite extent of the beamspot. At the maximum displacement possible, 3.*mm*, the error is only 1.0%. For translations in the beam direction the case is much worse. The target and cylinder could conceivably have moved 2.*mm* before touching each other. This would have resulted in a ~9% error in the yield.

A check on translations in the beam direction could be made for the stripped beam experiments. In these runs a portion of the catcher foil was shadowed from the beamspot by the stripper foil holder. The distance along the foil required to go from exposed to shadow, along with the target geometry, provided a measure of the beamspot size, typically 1.2*mm* FWHM. Once the beamspot size was known, the shadowing on the foil caused by the collimators near ϑ=0° was used to determine the target

offset in the beam direction. For the stripped beam runs, this displacement was $\leq 1.mm$, corresponding to a 5% uncertainty. This was the uncertainty used for all the runs.

Estimation of the uncertainty in beam integration was difficult as there were no direct checks, such as Rutherford scattering, that could be used to measure the efficiency of charge collection. Instead, great faith was placed in the design of the experimental equipment. The target, collimation plates, and catcher cylinder formed a Faraday cup. In addition, a bias of $+300^{V}$ was applied to the apparatus to impede the escape of secondary electrons.

An experiment bearing on this question was performed by Qiu(81). This was a sputtering experiment performed in the same N10° UHV chamber as the experiments described here. The apparatus, which held up to four target and catcher foil combinations at once, did not form a Faraday cup and the integrity of charge integration was maintained only by the bias on it. The sputtering yields measured reproduced to within ~10% for the targets run at the same time. Several runs were performed with different target biases to determine the minimum bias necessary to assure run-to-run reproducibility. It was found that biases of $+300^{V}$ and above brought the run-to-run reproducibility down to the ~10% intra-run reproducibility.

It is assumed that the charge integration uncertainty was 10%.

In fitting the data, distance along the mica, x, was converted to angular displacement, ϑ. It was assumed that the mica was an exact copy of the catcher foil it had been exposed to. If the foil had been in perfect contact with the inner surface of the catcher cylinder, ϑ would be given by

$$\vartheta = \frac{x}{R}$$

where R was the inner radius of the cylinder. The contact was not perfect, as noted before. However the difference in length so caused was typically less than $1\mu m$ so it was ignored.

A more significant uncertainty was the determination of the point x_0 corresponding to ϑ=47°. This was particularly true for the transmission runs where almost the full 180° was viewed. The length of exposed aluminum foil was $105.0mm$. The foil was cut into two so as to be placed in the mica sandwiches. The cuts were accurate to $\sim.5mm$ so that the resulting pieces were $52.5\pm.5mm$ long. The micas were $51.4mm$ long. Thus the foils overlapped the micas by .5-1.5mm and made the determination of x_0 uncertain by the same amount. To see the effect of this on the fit to the data, two runs were fit with different offsets and the values of n_0 examined versus the offset. The values of n_0 varied approximately linearly with the offset at the rate of 4% per mm of offset. An offset of $1mm$ produced a noticeable skewing to the fit to the data. For this reason it was assumed that only offsets of less than $1mm$ escaped notice. The total error in both halves of the foil was taken to be 6%.

This error applies only to transmission runs. For all other experiments the foils could be conveniently cut into pieces smaller than the micas. For these, the location of the edges, and thus x_0, was limited by the random location of tracks. In all cases x_0 could be determined to within $.1mm$. The error associated with this was ignored.

There was also an uncertainty in n_0 due to the statistics of the distribution of tracks.

For all the runs performed, the density of tracks due to sputtered atoms was large enough compared to those caused by contamination of the mica and foils that the cross term from the uncertainty in background was not a significant fraction of the uncertainty in n_0. Ignoring the effects of background, the uncertainty in n_0 was

$$\sigma(n_0) = \left[\frac{n_0}{\sum_i \cos\vartheta_i}\right]^{1/2} \tag{3.12}$$

The value of $\sigma(n_0)$ was typically 3% of n_0 whereas the uncertainty in Δn, when weighted as in the subtraction term of eqn.3.4b, was a third of this.

Adding all of the above uncertainties in quadrature yields an uncertainty of ~13% for the transmission experiments and ~12% for the stripped beam and charge state experiments. The error bars shown on the points in the figures are those appropriate for each point.

IV. Discussion

A. Theory

At energies near the peak of $\frac{dE}{dx}$, an ion can transfer considerable energy to the matter through which it passes. For example, ^{19}F deposits $\sim 300eV$ per Å of UF_4. Thus it appears that there is no scarcity of available energy to cause sputtering. The key here is available. The energy given directly to nuclei is very small, less than $.2eV/Å$ in the example above. The rest goes to electrons causing both electronic excitation and ejection of electrons from atoms. For atoms to be sputtered from a material, this electronic energy must be shared with the nuclei and it must be shared quickly enough that the energy remains localized. Otherwise, the energy will be distributed over too many atoms for any one atom to have a sufficient amount to enable it to leave the bulk. The observation that sputtering does occur in such insulators as UF_4 (Griffith(79)), water ice (Cooper(81)), and large organic molecules (Macfarlane and Torgerson(76)) shows that such a transfer does take place.

Several mechanisms have been advanced to explain how this transfer occurs. Macfarlane(76) suggested that the ejected electrons move freely in the bulk material, oscillating about and through the line of ionized atoms. Repeated collisions between the electrons and the atoms would transfer energy from the electrons to the atoms. Seiberling(80) has shown that this mechanism cannot work in UF_4. The time required for the electrons to transfer a sufficient amount of energy to the uranium atoms is an order of magnitude greater than the time for the thermal energy to diffuse into the bulk.

Krueger(77) has tried to explain the sputtering of large, polar bound organic molecules by a variation of the Franck-Condon effect. The energy and charge behavior of such sputtering is similar to that seen in UF_4. He proposed that the large, time varying electric field (~5V/Å) created by the ionization caused by a fast ion is sufficient in itself to lift the molecules into an unbound state. Unfortunately, this model has not been developed to the point of predicting the dependence of the sputtering yield on the energy or charge of the incident ion. It is also unclear how to extrapolate from one target material to another.

Haff(76) has attempted to make use of the ion explosion proposed by Fleischer, Price, and Walker(75) to explain the formation of tracks in dielectrics. The ion explosion works as follows. An ion passes through a material, ionizing adjacent atoms along its path. The rate of such ionizations per length is denoted by $\frac{dJ}{dx}$ and was first calculated by Bethe(30). In the Born approximation it takes the form

$$\frac{dJ}{dx} = \frac{Az_{eq}^2 \ln(B\varepsilon)}{\varepsilon} \tag{4.1}$$

where A and B are constants dependent on the incident ion and the target material, ε is the ion energy per mass, and z_{eq} is the equilibrated charge of the ion. Zeigler(80) gives for this charge the empirical form

$$\frac{z_{eq}}{z_0} = \left(1-e^{-6.32\varepsilon^{1/2}-1.2\varepsilon-14.43\varepsilon^2}\right)\left(1-e^{-A(1.034-.1777e^{-.08114z_0})}\right) \tag{4.2}$$

$$A = B+.0378\sin(\tfrac{1}{2}\pi B)$$

$$B = 5.6\,\varepsilon^{1/2} z_0^{-2/3}$$

where ε is the ion energy per mass in *MeV*/amu and z_0 is the nuclear

charge. Another commonly used form for z_{eq} is that of Heckman et al.(63),

$$z_{eq} = z_0\left[1-e^{-\varepsilon^{1/2}/z_0^{55}}\right] \tag{4.3}$$

This form differs from eqn.4.2 in that for small ε it gives a greater charge, the difference being greater as the charge of the ion increases. For ions up to ^{35}Cl the difference between eqns.4.2 and 4.3 is small.

If the electrical conductivity is low enough the ejected electrons will take a long time to return to the ionized atoms. This delay will allow the ions to electrostatically repel each other, converting their electrostatic energy into kinetic energy. After a few collisions with neighboring atoms, the energy is further converted into thermal energy. Eventually this heat dissipates by diffusion to the rest of the target material. In this picture, the atoms dislocated along the path of the incident ion form a region highly susceptible to chemical etching. The void remaining after such an etch would be labeled a track.

Haff noted that at the surface of a material undergoing such an upheaval, atoms would be ejected. Such ejection of atoms is, by definition, sputtering. The number of particles ejected was assumed to be proportional to to the energy deposited by the incident ion. This energy was the electrostatic energy caused by the ionization from the ion and was proportional to the square of the charge per length so created. Since the charge per length was given by $\frac{dJ}{dx}$, the sputtering yield was proportional to

$$S \sim \left[\frac{dJ}{dx}\right]^2 \tag{4.4}$$

This was the first model to predict the existence of such sputtering

There are a number of thermal models of which two will be discussed at length here, those of Seiberling(80) and Watson(81). In these models energy deposited by the ion is converted to thermal energy in a region around the ion path. This region is called the hot core. Atoms then evaporate from the surface of this hot core. These models can be divided into two portions, the deposition of energy into the core and the subsequent thermal history of the core. The latter is the same in both of the models to be described and will be presented first.

After a few collision times ($\sim 5\times10^{-13}$sec for 1eV ^{235}U in UF_4), the atoms in the core are assumed to be in local thermal equilibrium. The velocity distribution is thus a Maxwell-Boltzmann

$$F(v)dv = n\left(\frac{M}{2\pi kT}\right)^{\frac{3}{2}} e^{-Mv^2/2kT}\, 4\pi v^2\, dv \tag{4.5}$$

where n is the number density of atoms with mass M and velocity $\vec{v}$. If we assume the presence of a step potential U at the surface, the flux of atoms emitted into a solid angle $d\Omega$ at an angle ϑ from the surface normal is

$$\varphi(u,\vartheta)\, du\, d\Omega = n\left(\frac{M}{2\pi kT}\right)^{\frac{3}{2}} e^{-(U+\frac{1}{2}Mu^2)/kT}\cos\vartheta\, u^3\, du\, d\Omega \tag{4.6}$$

where $\vec{u}$ is the velocity of the atom after emerging from the surface.

To arrive at the total number of sputtered atoms, the flux must be integrated over the area and the lifetime of the hot core and the velocity and solid angle of the sputtered atoms.

Integrating over velocity and solid angle first yields

$$s = \int\int \varphi \, du \, d\Omega \tag{4.7}$$

$$= n\left(\frac{kT}{2\pi M}\right)^{\frac{1}{2}} e^{-U/kT} \, .$$

This quantity is the rate of sputtering per unit area. A notable feature of the sputtering rate is the prediction that atoms of type i will be sputtered as

$$s_i \sim M_i^{-\frac{1}{2}} e^{-U_i/kT} . \tag{4.8}$$

The temperature T will be common to the different atomic species as they are in thermal equilibrium.

In the case of UF_4 the ratio of rates, and thus to a first approximation the ratio of the total numbers of sputtered atoms, of ^{19}F and ^{235}U is

$$\frac{s_F}{s_U} \approx \frac{N_F}{N_U} = \left(\frac{235}{19}\right)^{\frac{1}{2}} e^{(U_U - U_F)/kT} \tag{4.9}$$

$$= (3.52) e^{(U_U - U_F)/kT}$$

Thus, considering the composition of UF_4, it would be expected that 14.1 ^{19}F per ^{235}U will be sputtered if their surface binding energies are equal. This result is exact only if the temperature remains constant during the evaporation of the atoms. It also assumes that UF_4 breaks up during sputtering. This assumption is probably not good as UF_4 is known to evaporate without dissociation (Griffith(79)).

Returning to eqn.4.7, in order to make the physics more apparent, an exact integration will be foregone and a zeroth order integration will be

performed over time and area. For this the core can be pictured as having a constant radius r_0 and a constant temperature T_0. If the lifetime of the core is τ_0, the sputtering yield is given by

$$S = \int 2\pi r dr \int dt \; s(T(r,t)) \tag{4.10}$$

$$\approx \pi r_0^2 \; \tau_0 \, n \left(\frac{kT}{2\pi M}\right)^{\frac{1}{2}} e^{-U/kT} \tag{4.11}$$

At this point the dependence of r_0, T_0 and τ_0 on incident ion and the target material must be examined. Seiberling(80) views the situation as a thermalized ion explosion and thus dependent on the rate of ionization, $\frac{dJ}{dx}$, caused in the target by the incident ion. The temperature is related to the deposited energy E_d by

$$\frac{3}{2}kT = E_d + \frac{3}{2}kT_0 \tag{4.12}$$

T_i is the initial temperature of the material. E_d is the electrostatic energy created by the ionization of the incident ion.

In this model the ionization given by $\frac{dJ}{dx}$ is contained inside the radius r_0. If the distribution of charge inside this radius is independent of $\frac{dJ}{dx}$, the electrostatic energy E_e is proportional to

$$E_e \sim \frac{\left(\frac{dJ}{dx}\right)^2}{r_0^2} . \tag{4.13}$$

Equating E_e with E_d, T_0 is given by

$$T_0 = T_i + a\frac{\left(\frac{dJ}{dx}\right)^2}{r_0^2} \tag{4.14}$$

where a is a constant.

The velocity distribution of ^{235}U sputtered from UF_4 has been measured at $\vartheta = 0°$ for two incident beams, $4.74 MeV\ ^{19}F$ and $13. MeV\ ^{35}Cl$ (Seiberling(81)). These are shown in figs.6 and 7. Using eqn.4.6 it is possible to assign temperatures to these distributions. For the ^{19}F, the temperature was 3620°K and for the ^{35}Cl it was 5240°K. The temperature rise, T_0-T_i, caused by the ^{35}Cl was only 50% higher than that caused by ^{19}F even though $\frac{dJ}{dx}$ from eqn.4.13 was 195% higher. For comparison, $\frac{dE}{dx}$ from Zeigler(80) was 204% higher. Thus, to a first approximation,

$$r_0 \sim \frac{dJ}{dx} \tag{4.15}$$

From the thermal diffusivity κ the lifetime can be estimated to be

$$\tau_0 = \frac{r_0^2}{4\kappa} \tag{4.16}$$

Combining these with eqn.4.11 yields

$$S = n\left(\frac{\pi r_0^4}{4\kappa}\right)\left(\frac{kT}{2\pi M}\right)^{1/2} e^{-U/kT}. \tag{4.17}$$

$$\sim \left(\frac{dJ}{dx}\right)^4. \tag{4.18}$$

Watson(81) has considered a different mechanism for the conversion of deposited ion energy into atomic thermal energy. He assumed the atoms to be described by the Thomas-Fermi model, i.e., as clouds of free electron gas around nuclei. The passing ion deposits energy into these clouds which thermalize quickly. The hot clouds attempt to expand and so exert pressure on the neighboring colder clouds which causes them to

move. As a cloud moves, so does the nucleus within it. In this manner, electronic energy is rapidly and efficiently converted into atomic energy.

Watson considers the energy deposited by the ion to be radially distributed as r^{-2}. This distribution is cut off at the lower end by assuming a constant value for radii less than the lattice spacing, l. The upper limit is set by the maximum radial travel of electrons Rutherford scattered by the ion, i.e., the range of the delta rays. The scale of the deposited energy density, $\rho(r)$, is set by the requirement that

$$\frac{dE}{dx} = \int_0^{r_{max}} 2\pi r dr\ \rho(r) \tag{4.19}$$

$$= \int_0^{l} 2\pi r dr\ \rho_0 + \int_l^{r_\delta} 2\pi r dr \frac{l^2 \rho_0}{r^2}$$

$$\rho_0 = \frac{1}{\pi l^2} \frac{dE}{dx} (1+2\ln(r_\delta / l))^{-1} \tag{4.20}$$

For ρ greater than ρ_{cr},

$$\rho_{cr} = \frac{U}{V} \tag{4.21}$$

where U is the surface binding energy and V is the atomic volume, the band structure will disappear and the atoms can be treated as in the Thomas-Fermi model. The energy density greater than ρ_{cr} will be shared with atoms out to r_{co} such that

$$\pi r_{co}^2\ \rho_{cr} = \int_0^{r_{co}} 2\pi r dr \rho(r) \tag{4.22}$$

$$r_{co} = \left\{ \frac{V}{U} l^2 (1+2\ln(r_{co}/l)) \rho_0 \right\}^{1/2} \tag{4.23}$$

$$= \left\{ \frac{1}{\pi} \frac{V}{U} \frac{dE}{dx} \frac{1+2\ln(r_{co}/l)}{1+2\ln(r_\delta/l)} \right\}^{1/2}$$

ρ will equilibrate on a time scale τ_e

$$\tau_e = \frac{\tau_0}{N_e}\left(\frac{G}{kT_e}\right)^2 e^{G/kT_e} \tag{4.24}$$

where

$$\tau_0 = \frac{\hbar^3}{2me^4}$$

$$N_e = n_e V$$

n_e is the electron density at the surface of a Thomas-Fermi atom and V is its volume. G is the band gap energy. T_e can be set by

$$\Delta E_e \approx \frac{\pi^2}{4} N_e \frac{(kT_e)^2}{\varepsilon_F} \tag{4.25}$$

where ε_F is the Fermi energy. ΔE_e is the increase in electronic energy of the atom due to raising its temperature from 0 to T_e. It is set equal to U.

The energy is assumed to diffuse out of the core in a random walk fashion. The lifetime of the core is thus

$$\tau_s = \frac{3}{4}\left(\frac{r_{co}}{l}\right)^2 \tau_e \tag{4.26}$$

where l is assumed to be the step length.

The hot electronic cloud exerts a pressure P given by

$$P = \frac{2}{3}\frac{\Delta E_e}{V} \tag{4.27}$$

The force exerted on a neighboring atom is then

$$F = PA \tag{4.28}$$

$$\approx \frac{2}{3}\frac{\Delta E_e}{l}$$

since V is approximately l^3. The energy transferred to atomic motion is

$$\Delta E_a \approx \frac{1}{2M}(F\tau)^2 \tag{4.29}$$

The time τ is that in which the two atoms lose contact and is approximately the time required to travel $\frac{1}{2}l$. Therefore

$$\frac{l}{2} = \frac{1}{2}\left[\frac{F}{M}\right]\tau^2 \tag{4.30}$$

Inserting this into eqn.4.29,

$$\Delta E_a = \frac{Fl}{2} \tag{4.31}$$

$$= \frac{1}{3}\Delta E_e$$

Correcting for the cooling of the expanding atom yields

$$\Delta E_a = (0.24)\Delta E_e \tag{4.32}$$

The atomic temperature is

$$T_a = \frac{2}{3}\frac{\Delta E_a}{k} \tag{4.33}$$

$$\approx (0.16)T_e$$

One further point is the treatment of the surface binding energy appearing in the exponential in eqn.4.12. Watson replaces this by an effective energy U_{eff}. The atoms inside the radius r_{co} are all assumed to have an electronic energy U; U_{eff} is thus zero initially. ΔE_a of this is then

transferred to atomic energy and is therefore taken to be the final U_{eff}. As ΔE_a is simply $\frac{3}{2}kT$, the exponential in eqn.4.12 reduces to the constant 0.22.

Putting all of these pieces in eqn.4.12 gives for the sputtering yield

$$S = (0.22)\,\pi r_{co}^2\,\tau_s\,n_a\left(\frac{kT_a}{2\pi M}\right)^{1/2} \tag{4.34}$$

$$\sim r_{co}^4 \sim \left[\frac{dE}{dx}(r_{co})\right]^2$$

S depends on the portion of $\frac{dE}{dx}$ deposited within a radius r_{co}, i.e., it is the restricted $\frac{dE}{dx}$, $\frac{dE_{re}(r_{co})}{dx}$.

All of the theoretical predictions hold only for ions in charge equilibrium.

B. Results

The requirements of beam focusing and energy selection allow the beam from a Van de Graaff to be in one charge state only and all of the data on the sputtering of UF_4 previous to this work were collected using beams incident on the UF_4 in single charge states. These data are shown in fig.8, the numbers beside the data points being the charge states of the beams used. The data indicate a dependence on the charge state showing that the sputtering mechanism is at work at depths less than those required to establish charge equilibration. Therefore it was necessary to eliminate the process of equilibration in order to see only the sputtering mechanism.

To effect equilibration, two types of experiments were performed, transmission and stripped beam sputtering. Figs.9, 10, and 11 show the sputtering yields versus ion energy for ^{16}O, ^{19}F, and ^{35}Cl, respectively. The ^{16}O data consist only of stripped beam points while for the ^{19}F and ^{35}Cl there are both stripped and transmission data. These data are given in table 2 as well. The curves show the least squares fits to $\left[\frac{dJ}{dx}\right]^4$ with the values of A and B shown. Fig.10 and 11 show the yields as calculated by Watson(81). Fits to $\left[\frac{dE}{dx}\right]^2$ and $\left[\frac{dE}{dx}\right]^4$, as measured in **V.B.**, are shown in fig.12 for stripped beam ^{19}F along with $\left[\frac{dJ}{dx}\right]^2$ and $\left[\frac{dJ}{dx}\right]^4$. The best fit is given by $\left[\frac{dJ}{dx}\right]^4$.

For comparison, the data of Hakansson et al.(80) for Cs^+ sputtered from CsI by ^{16}O,^{32}S, ^{63}Cu, and ^{127}I are shown in fig.13. Fig.14 shows the Hakansson et al. data for CsI, glycylglycine, and ergosterol sputtered by ^{63}Cu. The latter two targets are organic molecules of weight 132 and 396 amu, respectively. The sputter products observed were $(M+H)^+$ where M was the target molecule. Along with the data are χ^2 fits to $\left[\frac{dJ}{dx}\right]^4$ The data were fit with eqn.4.3 for z_{eq} instead of eqn.4.2 as with the UF_4 data. For ^{16}O, the difference was small while for ^{127}I the data could not be reasonably fit with eqn.4.2.

Despite the differences between CsI, glycylglycine, ergosterol, and UF_4, the energy dependence is quite similar. The values of A and B derived from all of the $\left[\frac{dJ}{dx}\right]^4$ fits are given in table 3.

The magnitude of the transmission data is consistently greater than that of the stripped beam experiments, being ~40% higher for ^{19}F and ~100% for the ^{35}Cl. These results are to be contrasted with the findings of Hakansson(81a) for CsI. For an incident beam of 42.*MeV* ^{16}O, the stripped beam and transmission yields were indistinguishable, as can be seen in fig.15.

By taking the equilibration process into account it was possible to extract the equilibrated sputtering yield from the single charge state data. To look at individual charge states, it is first necessary to calculate the evolution of the charge state distribution. This evolution can be described by the set of rate equations

$$\frac{1}{n}A'_k(x) = -(\sigma_c(k)+\sigma_l(k))A_k+\sigma_l(k-1)A_{k-1}+\sigma_c(k+1)A_{k+1} \qquad (4.35)$$

where A_k is the fraction of the beam in the k^{th} charge state, σ_c and σ_l are the cross sections for electron capture and loss respectively, and n is the atomic density of the target. This ignores the effect of multielectron transfers. According to Betz(72), these transfers are small for the ions used in these experiments.

In equilibrium $A'_k(x)=0$ and, using the $k=z_0$ equation,

$$\frac{1}{n}A'_{z_0} = -\sigma_c(z_0)A_{z_0}+\sigma_l(z_0-1)A_{z_0-1} \qquad (4.36)$$

one derives a ratio for σ_c and σ_l of neighboring states

$$\frac{\sigma_c(k+1)}{\sigma_l(k)} = \left[\frac{A_k}{A_{k+1}}\right]_{eq} \qquad (4.37)$$

A common practice (Betz) for parametrizing these data is to assume the exponential forms

$$\sigma_c(k) = \alpha e^{ak} \tag{4.38}$$

$$\sigma_l(k) = \beta e^{-bk}$$

Eqn.4.36 now reads

$$\left[\frac{A_k}{A_{k+1}}\right]_{eq} = \left[\frac{\alpha e^{a}}{\beta}\right] e^{(a+b)k} \tag{4.39}$$

As fig.16 shows, this form provides a good fit to the charge fraction data of Wittkower and Betz(73) for ^{19}F at 28.*MeV*.

Unfortunately, this gives only the sum of the length scales a and b. For simplicity they will be assumed to be equal. For a and b not equal, the effect will be to skew the length scales of the $A_k(x)$. This skewing only serves to confuse the overall length scale and does not alter the dependence of the sputtering yield on the incident charge state.

The magnitude of σ_c and σ_l was estimated by comparing the data of Angert et al.(68) for lithium, nitrogen, and iodine in N_2 with the general theoretical consensus that the cross sections vary as

$$\sigma_c \sim \sigma_l \sim Z_T^{2/3} E^{-2} \tag{4.40}$$

where Z_T is the nuclear charge of the target. It is known (Betz(72)) that the cross sections for polyatomic systems are less than the sum of the individual cross sections and further that extrapolation from the region referenced to atoms as heavy as uranium tends to overestimate. Because of this, the length scale was considered uncertain to a factor of ~2.

Thus armed with tentative values for the cross sections, the rate equations can be solved. First, the equations are cast in matrix form

$$A'_k(x) = R_{kl} A_l(x) \tag{4.41}$$

The solutions are of the form

$$A_k(x) = \xi_k e^{\alpha x} \tag{4.42}$$

where the ξ_k's and the α's are the eigenvectors and eigenvalues of R. The full solution is

$$A_k = \sum_j a_j \; \xi_{kj} \; e^{\alpha_j x} \quad , \tag{4.43a}$$

$$a_j = \sum_l (\xi)^{-1}_{jl} A_l(0) \tag{4.43b}$$

The sum over j and l should properly extend, for example, from -1 to 9 in the case of ^{19}F. Experimentally it is seen that few of these charge states have measurable populations at any given ion energy. Limiting the summations to these states simplifies calculations considerably.

Fig.17 shows the charge fractions versus x for ^{19}F at 28. MeV for z_i = 5.

In terms of the charge state fractions, $A_k(x)$, the average charge is replaced by

$$z(x) \rightarrow \sum_k k A_k(x) \tag{4.44}$$

and the n^{th} power of the average charge by

$$z^n(x) \rightarrow \sum_k k^n A_k(x) \tag{4.45}$$

Second, assume that the removal of atoms from a surface is exponentially correlated to the conditions in the bulk material, i.e., by

$$g(x,x') = \frac{1}{\lambda_s} e^{-|x-x'|/\lambda_s} \tag{4.46}$$

This has been shown to be exact for the case of collisional sputtering (Sigmund(81)). Since the sputtering yield S varies as z^n with n=8, as indicated by the $\left[\frac{dJ}{dx}\right]^4$ fits, the sputtering yield is given by

$$S = A\int_0^\infty dx\ g(x,0)\ z^n(x) \tag{4.47}$$

$$= A\int_0^\infty dx\ g(x,0)\sum_k k^n A_k(x)$$

$$= A\int_0^\infty dx\ \frac{1}{\lambda_s} e^{-x/\lambda_s} \sum_k k^n \sum_j \sum_l A_l(0)(\xi)^{-1}_{lj}\ \xi_{jk}\ e^{\alpha_j x}$$

$$= A \sum_{jkl} A_l(0)(\xi)^{-1}_{lj}\xi_{jk}\ k^n\ (1-\alpha_j\lambda_s)^{-1} \tag{4.48}$$

where A is the ubiquitous constant.

A simpler way of taking equilibration into account was by a suggestion of Griffith(81). Assume that the distribution of charge states can be well characterized by the average charge and that this charge varies exponentially from the initial to the equilibrium value as

$$z(x) = z_{eq} - (z_{eq} - z_i)e^{-x/\lambda_c} \tag{4.49}$$

Substituting this into eqn.4.47, the sputtering yield is given by

$$S = A\ z_{eq}^n \frac{\lambda_c}{\lambda_s} \int_0^\infty dy\ e^{-\frac{\lambda_c}{\lambda_s}y}\left[1+\left(\frac{z_i}{z_{eq}}-1\right)e^{-y}\right]^n \tag{4.50a}$$

$$= A\, z_{eq}^{n}\, s\left(\frac{\lambda_c}{\lambda_s}, n, \frac{z_i}{z_{eq}}\right) ,$$

$$s = {}_2F_1\left[-n, \frac{\lambda_c}{\lambda_s}; \frac{\lambda_c}{\lambda_s}+1; \frac{z_{eq}-z_i}{z_{eq}}\right] \tag{4.50b}$$

where A is a constant.

If n is an integer, s simplifies to the n^{th} degree polynomial

$$s = \sum_{k=0}^{n} \frac{n!}{k!(n-k)!}\left[1+\frac{\lambda_c}{\lambda_s}k\right]^{-1}\left[\frac{z_i}{z_{eq}}-1\right]^{k} \tag{4.51}$$

Incident charge data for ^{19}F at 28.5MeV are plotted in fig.18 along with arbitrarily normalized S from eqn.4.48 with λ=700Å and n=8. The corresponding fit to eqn.4.51 is shown for comparison. It is apparent that taking the individual charge states into account has little effect.

The two approaches differ in the values they predict for the sputtering yield of a beam in charge equilibrium. This quantity is denoted by S_{eq}. In the average charge model, S_{eq} is simply the value of the fitted curve at z_{eq} and is given by Az_{eq}^{n} from eqn.4.50a since $s=1$ at $z=z_{eq}$. In the charge fraction picture, S_{eq} is $A\sum_k k^n$ by eqn.4.48. The A in eqns.4.48 and 4.50a are the same. Thus, S_{eq} is the $z=z_{eq}$ value times the quantity η given by

$$\eta = \frac{\sum_k k^n A_k}{\left(\sum_k k A_k\right)^n} \tag{4.52}$$

The denominator is z_{eq}^{n}. η varies from ∞ to 1 as the energy varies from 0 to ∞ and is ~1.5 in the region of interest. It was calculated using the data of Wittkower and Betz(73).

Eqn.4.51 was used to fit the incident charge data. Taking z_{eq} from Zeigler's empirical expression, eqn.4.2, the fits on figs.19, 20, and 21 for E = .25, .5, and 1.*MeV/* amu were obtained. These data are given in table 4 as well. The derived values for $\frac{\lambda_c}{\lambda_s}$ are shown in fig.22. Table 5 gives these values of $\frac{\lambda_c}{\lambda_s}$ along with those from Hakansson(81b), which are discussed below.

Using the fitted value of .46 for $\frac{\lambda_c}{\lambda_s}$ at 1.*MeV/* amu, the exponent n was varied to fit the data. This gave n=9.6±1.0. Taking n=8, the data were fit to z_{eq}. This gave z_{eq}=5.9±1.3 as opposed to the value of 6.74 given by eqn.4.14. A similar procedure at 1.5*MeV/* amu yielded n=8.24±.83 and z_{eq}=7.35±.33. Eqn.4.2 gave z_{eq}=7.29 at this energy.

Once the $\frac{\lambda_c}{\lambda_s}$ were determined, S_{eq} could be calculated at each energy. The S_{eq} are shown in fig.23 along with the stripped beam and transmission data.

To appreciate the difference between S_{eq} and the stripped beam and transmission data, other data should be examined. Hakansson(81b) has performed this experiment with 20.*MeV* ^{16}O as the beam and glycylglycine, ergosterol, and CsI as the targets. Glycylglycine and ergosterol are organic molecules of weight 132 and 396 amu respectively while CsI is an ionic compound. The observed products were $(M+H)^+$ for the organics and Cs^+ for CsI. These data, along with χ^2 fits to eqn.4.51, are shown in figs.24, 25, and 26. In addition, the experiment was done with a gold stripper foil in front of the glycylglycine. The data with and without the stripper foil are shown in fig.24. In contrast to the UF_4 results, the stripped beam yields fall below the S_{eq} from the incident charge state data.

The difference in conditions between the experiments described here and those of Hakansson et al. are unclear. The distance between the stripper foil and the target is not stated, although the requirements of their experiment force the placement of the stripper much farther from the target than was possible for the experiments described here. Because of this, it is possible that atomic states excited in passage through the foil were still present when the beam struck the UF_4. Another possibility is that the shower of energetic electrons generated by the ion in passage through the foil in some manner enhanced the sputtering yield in the UF_4. Such enhancement has been seen by Ahn et al.(75). Both of these effects would have been present in the transmission experiments as well. In the Hakansson et al. experiments, both excited atomic states and the electron shower would have had a chance to dissipate before the beam reached the target.

V. Rutherford Scattering Experiments

A. Equipment

All Rutherford scattering experiments were performed in the center leg scattering chamber. The targets were clamped to the brass bracket on the linear motion feedthru. A quartz crystal was also mounted on the bracket to aid in beam focusing. Surrounding the targets was a cylinder, ~4" in diameter, made of copper screen. This cylinder served as a secondary electron suppression grid and aided charge integration. It stood on a lucite block and was biased to -300^{V}. The targets, on the insulated feedthru, were biased to $+300^{V}$. Two slots were cut into the cylinder to allow an entrance for the beam and an exit for the scattered atoms. The slot on the beam side of the target extended from ~90° to 200°, and the second from ~20° to 70° in terms of the scattering angle. Both were ½" wide and centered in the plane of the beam. The second slot allowed foil targets to be examined at small scattering angles with concomitant large cross sections. For such targets, a graphite block attached to the back of the brass bracket served as a beam dump.

The collected charged was sent to a Brookhaven Nuclear Instruments Corp. Model 1000 current meter and integrator via RG-58 cable. The output of the integrator was in turn sent to a Tennelec TC 550 scaler from which the total charge incident on the target was read. As read on the current meter, the leakage current on the target was $<50pA$.

The detector used was an Ortec BA-23-50-100 surface barrier detector. It was mounted on one of the two detector mount arms in the scattering chamber. These arms are concentric with the target bracket

and can be rotated through a full 360°. The detector mount was placed so that its collimating aperture was 8.5cm from the target.

The second detector arm was used to support a 18.8$\mu g / cm^2$ carbon foil on an aluminum holder. A lucite block insulated the aluminum from the arm; the aluminum was connected to the brass target bracket by a short piece of copper wire. The carbon foil was 1" from the target and could be swung in and out of the beam in front of the target. A baffle on the aluminum holder prevented atoms from scattering from the carbon and entering the detector.

Fig.27 shows the equipment described above.

The output of the Ortec detector was sent to a Nuclear Data ND 4420 MCA via a Systems Research Corp. preamp and a Canberra 2010 amplifier with RG-58 cable. An Ortec 210 power supply was used to put 50^V of bias on the detector (with .23μA of leakage current). This bias produced an active depth of 100.μm in the detector, significantly longer than the 75.μm range of 23.9MeV ^{19}F which was the most penetrating beam to enter the detector. To guard against drifting of the gains of the amplifier and preamp, the output of a BNC DB-2 pulse generator was fed into the test input of the preamp during the experiments. The output level was adjusted so that the test pulses appeared above the spectra on the MCA. The width of the resulting peak served as an indicator of the gain stability of the detector system. The use of the pulse generator was suggested by B.H. Cooper.

The target used for measuring the relative numbers of sputtered ^{235}U and ^{19}F atoms was a carbon foil which had been used as the stripper foil in the ^{16}O stripped beam experiments. After the ^{16}O runs were completed the catcher foils were moved out of the way and an additional 3×10^{12} ^{19}F at

9.5*MeV* were put onto the target. Since the stripped sputtering yield at this energy was 14.2, the carbon foil, sitting at 1.2*cm*, was struck by 1.0×10^{13} $^{235}U/cm^2$. This was in addition to the $7.\times10^{12}$ $^{235}U/cm^2$ incident during the ^{16}O runs. Thus, if all the incident ^{235}U atoms stuck, the carbon foil held a layer of 1.7×10^{13} $^{235}U/cm^2$. This was ~.01 monolayer of ^{235}U and ~.2 monolayer of ^{19}F (if $U_U=U_F$). While a thicker layer would have been desired, the unknown probabilities for uranium and fluorine sticking on each other would have made analysis difficult.

B. Analysis and Results

The target was analyzed with 1.5*MeV* alphas at a scattering angle of 55°. Fig.28 shows the measured spectrum. Clearly visible are the carbon and uranium peaks. In addition, there are peaks due to oxygen, magnesium, chlorine, and copper. The oxygen was probably in the form of CO, CO_2, and H_2O absorbed on the foil surfaces. The amount of oxygen seen is consistent with ~1 monolayer on each side. It should be noted that the oxygen layer was probably laid down after the UF_4 sputtering occurred as the UHV conditions prevailing during sputtering were sufficient to clean the carbon foil. The chlorine derives from the $BaCl_2$ used in fabrication of the carbon foil (any barium was buried under the uranium peak). The origin of the magnesium and copper is unclear.

The carbon and uranium peaks were fit with gaussians on their high energy side. The low energy sides were ignored as energy straggling through the foil gave them a different half width than their high energy partners. Using the fitted locations of the peaks and the energies at which 1.5*MeV* alphas scattered from carbon and uranium lie, the energy

scale was established. Table 6 gives the energies and channel numbers of the important nuclides.

The contaminants oxygen and magnesium were fit with the shape of the carbon as they were equally likely to be on both sides of the foil. The fluorine peak, or rather the absence of it, was treated as having the shape of the uranium peak.

At the location of fluorine, there is only a flat background. As fig.29 shows, the spectrum in this region can be satisfactorily described by the tails of oxygen and magnesium peaks and a flat background of 68.0 counts/channel. Any fluorine peak present was surely less than 3σ of this or ~25 counts/channel. The uranium peak on the other hand had a height of 620 counts/channel. For this combination of energy and angle, the ratio of cross sections for alphas on fluorine and uranium was

$$\frac{\sigma(F)}{\sigma(U)} = 105. \tag{5.1}$$

Combining all of these, the ratio of the numbers of sputtered fluorine and uranium atoms was

$$\frac{N(F)}{N(U)} \leq 4. \tag{5.2}$$

at the 3σ level. Using the temperature measured with $4.74 MeV$ ^{19}F, 3620°K (Seiberling(80)), this limit implies

$$U_F - U_U > .4\text{eV} \tag{5.3}$$

assuming that the fluorine and uranium atoms are ejected seperately. Considering the relative electronegativities of fluorine and uranium, this limit is physically plausible. It should be noted that this result is

susceptible to charge build up on the target surface. If the secondary emission rate of UF_4 is greater than one, a positive voltage will appear on the surface of the electrically insulating UF_4. Since the uranium and the fluorine initially appear as U^{4+} and F^-, such a voltage would inhibit the emission of fluorine while enhancing that of uranium if no chemical changes take place. It is known that the chemistry of the uranium does change as Seiberling(80) observed the sputtered uranium to be neutral or singly charged only.

The UF_4 target used for $\frac{dE}{dx}$ measurements was ~1600 Å of UF_4 on a copper backing. It had been used as the target for a stripped beam run with ^{19}F. It was kept in the UHV chamber under vacuum until it could be mounted in the scattering chamber. This was done to minimize the target's exposure to air as it was known to be hydroscopic. In transferring it from chamber to chamber, it spent less than ~½ hr. at atmosphere. To aid in energy calibration, a bare piece of copper was mounted along with it.

The detector was set at a scattering angle of 160°. A .0935" aperture ($.0443 cm^2$) was placed in front of the detector. A typical spectrum, in this case $E(^{19}F)=19. MeV$, is shown in fig.30.

Analyzing the data required that an energy scale had to determined for every setting of amplifier gain. As the gain was changed with each beam energy to allow the spectra to occupy a comfortable portion of the MCA display, the energy calibration was performed at every beam energy used (if an energy was repeated, so was the calibration). The uranium in the UF_4 and bare copper gave two points through which a straight line was fit. No attempt was made to force the line through the origin as the scattered atoms lost energy in the gold layer on the front of the detector and

thus produced an offset. The magnitude of this offset was small compared to the points of interest and followed the shape of $\frac{dE}{dx}$.

Since the Rutherford cross section varies as E^{-2}, the observed spectra tended to vary as E^{-2} as well. This rapid variation in the number of counts per channel hindered the location of the edges on the spectra. To get around this difficulty, the spectra were multipled through by the square of the channel number (which was almost proportional to the energy). This flattened the spectra very well. The location of the edges were determined by drawing a straight line through as many points as possible and reading off the channel number where the line went through half of the peak minus background value. This method appeared to give the edge location to within ~1-2 channels. The resolution of the uranium edges was typically better than that of the copper edges.

Using these two targets, two measures of $\frac{dE}{dx}$ were possible. The first was the width of the portions of the spectra due to scatterings from uranium, i.e., the difference in energy between the upper and lower edges of those portions. The second measure was the shift in position of the copper edge between the bare copper target and the copper with UF_4. Unfortunately in neither of these cases can values of $\frac{dE}{dx}$ be extracted unambiguously. This results from the kinematics of the scattering.

Consider for example a ^{19}F incident on a layer of UF_4 Δx thick with energy E_0. If the ^{19}F scatters from a ^{235}U at the surface at an angle ϑ, its energy drops to

$$E' = K_U E_0 \ , \tag{5.4a}$$

$$K_U = \frac{2m_U m_F(1-\cos\vartheta)}{(m_U+m_F)^2} \ . \tag{5.4b}$$

If the ^{19}F scatters from a ^{235}U at the back of the UF_4, it first loses energy due to $\frac{dE}{dx}$ in the UF_4, then loses a fraction 1-K_U of its energy in scattering, and again loses energy to $\frac{dE}{dx}$ as it passes out of the UF_4. In the second passage, the length of UF_4 seen by the ^{19}F is $\Delta x / \cos\vartheta$. If the $\frac{dE}{dx}$ losses are small enough so that $\frac{dE}{dx}$ can be assumed constant during each passage, the emergent ^{19}F has the energy

$$E'' = K_U(E_0 - \Delta E(E_0)) - \frac{1}{\cos\vartheta}\Delta E(K_U(E_0 - \Delta E(E_0))) \tag{5.5}$$

where

$$\Delta E(E_i) = \Delta x \frac{dE}{dx}(E_i) \ . \tag{5.6}$$

$\frac{dE}{dx}$ is considered to be positive.

The difference between E' and E'' is

$$D_U = K_U \Delta E(E_0) + \frac{1}{\cos\vartheta}\Delta E(K_U(E_0 - \Delta E(E_0))) \ . \tag{5.7}$$

The same situation holds for a ^{19}F scattering from a copper atom at the copper surface. For a bare copper target the ^{19}F energy after scattering is

$$E_1 = K_{Cu} E_0 \ . \tag{5.8}$$

When there is a layer Δx of UF_4 on the copper, the scattered energy, again assuming that the $\frac{dE}{dx}$ is constant during each passage, is

$$E_2 = K_{Cu}(E_0 - \Delta E(E_0)) - \frac{1}{\cos\vartheta}\Delta E(K_{Cu}(E_0 - \Delta E(E_0))) \ . \tag{5.9}$$

Thus the energy difference for copper scattering is

$$D_{Cu} = K_{Cu}\Delta E(E_0)+\frac{1}{\cos\vartheta}\Delta E(K_{Cu}(E_0-\Delta E(E_0))) \quad . \tag{5.10}$$

As can be seen, both measures of $\frac{dE}{dx}$, D_{ij} and D_{Cu}, involve $\frac{dE}{dx}$ at two different energies.

Without an 'endpoint' to start from, the D_i cannot be solved for the $\frac{dE}{dx}$. What was done instead was to calculate $\frac{dE}{dx}$ for ^{19}F in UF_4 from published tables using Bragg's rule. The $\frac{dE}{dx}$ so derived were used to calculate the D_i. These were then compared to the observed D_i. Two tables of $\frac{dE}{dx}$ were used. One was Northcliffe and Schilling(70), a widely used reference. The other was Zeigler(80) which is the most recent and thus hopefully the more accurate compilation of $\frac{dE}{dx}$.

The calculated and measured D_{ij} are shown in fig.31. The larger uncertainties of the D_{Cu} rendered them unusable for fitting purposes. The calculated D_{ij} were normalized to the measured D_{ij} at $.25 MeV/$ amu. As can be seen, Northcliffe and Schilling give the better fit to the observed values although it is consistently 15% high. The $\frac{dE}{dx}$ from Zeigler is seen to peak higher in energy than the D_{ij} indicate while Northcliffe and Schilling peaks at a lower energy. In addition, the peak of Northcliffe and Schilling is too sharp while that of Zeigler is too flat.

Based on these comparisons, it is felt that fig.32 shows the true $\frac{dE}{dx}$. The $\frac{dE}{dx}$ from Zeigler and Northcliffe and Schilling are shown for comparison.

Also performed with UF_4 were two runs with incident charge states much higher that those ordinarily produced by the tandem, namely +5 at E = 4.75*MeV* and +7 at 19.*MeV*. These were compared with runs performed with +2 and +4 respectively. The equilibrated charges, as computed by Zeigler's empirical formula, eqn.4.14, were +4.61 and +6.74. The aim of this experiment was to see if the charge equilibration length could be seen in $\frac{dE}{dx}$.

As a collection of ions enters a material, the average charge will go from that of the incident charge distribution to one characteristic of the ion species and energy (ignoring target effects). Let this change be modeled by eqn.4.34. Since dE/dx varies as z^2, in a thin layer of matter the energy loss will be given by

$$\Delta E = \frac{dE}{dx}\frac{1}{z_{eq}^2}\int_0^l dx\,(z_{eq}-(z_{eq}-z_i)e^{-\frac{x}{\lambda}})^2 \qquad (5.11)$$

$$= l\frac{dE}{dx}\left[1-2\frac{\lambda}{l}\left[\frac{z_{eq}-z_i}{z_{eq}}\right](1-e^{-\frac{l}{\lambda}})+\frac{\lambda}{2l}\left[\frac{z_{eq}-z_i}{z_{eq}}\right]^2(1-e^{-\frac{2l}{\lambda}})\right]$$

$$\equiv \Delta E(z_i)\ .$$

Therefore, by measuring ΔE with different incident charge states a value of λ/l could be obtained.

The measurements of ΔE made at 4.75*MeV* with z_i = 2 and 5 and at 19.*MeV* with z_i = 4 and 7 showed no z_i dependence. From Rutherford scattering, the UF_4 thickness was measured to be 106.$\mu g/cm^2$ giving l the value of 1580Å. Using this, the limits on λ are

$$\lambda(4.75 MeV) \leq 39.\text{Å} \tag{5.12a}$$

$$\lambda(19. MeV) \leq 170.\text{Å} \tag{5.12b}$$

at the 3σ level.

A problem complicating the $\frac{dE}{dx}$ measurements with UF_4 is that the UF_4 sputters away during the measurements. For this reason it was necessary to limit the amount of beam used and thus also the statistical quality of the observations. For most measurements this was not significant. Only for the $\Delta E(z_i)$ experiments did this prove to be a limitation. For these experiments it was decided to use a UO_2 target as UO_2 is known to have a small sputtering yield in the energy region of interest (Seiberling(81)). It is shown in fig.33. The erosion of such a target could be ignored. It appeared that UO_2 was close enough to UF_4 in atomic and electronic density that a comparison between the two was appropriate.

The UO_2 target was bombarded with ^{19}F with energies of 9.5, 19., and 28.5*MeV*. Half of the beams at each energy were in the tandem-selected charge states. The rest were passed through the carbon foil mounted on the detector arm before striking the target. It was assumed that this passage put the beam into charge equilibrium.

The data were analyzed with the same method used for UF_4. Due to the higher number of counts in the spectra, the resolution was better than with UF_4, ranging from .2 channels at 9.5*MeV* to .4 at 28.5*MeV*. The quantity actually measured was D_{Cu} (the thinness of the UO_2 layer ensured that D_U only measured the detector resolution). To extract ΔE, $\frac{dE}{dx}$ was assumed to have the shape of Zeigler's data while the normalization was set by comparing the calculated D_{Cu} to the measured values.

Again no z_i dependence was found for ΔE. Assuming a thickness of 110.Å for the UO_2 layer, as implied by Rutherford scattering, the only limit that could be given on λ was at $9.5 MeV$ where

$$\lambda(9.5 MeV) \leq 75.\text{Å} \tag{5.13}$$

at the 3σ level. At the other energies, λ was consistent with infinity.

VI. Conclusions

In summary, yields were measured for ^{235}U sputtered from UF_4 by ^{16}O, ^{19}F, and ^{35}Cl over the energy range ~.12 to 1.5 *MeV/* amu. The yields were measured for a charge equilibrated beam in the stripped beam arrangement for all the incident ions and in the transmission arrangement for ^{19}F and ^{35}Cl. In addition, yields were measured for ^{19}F incident in a wide range of discrete charge states.

The angular dependence of all the measured yields were consistent with a cosine distribution. The χ^2/N derived from fitting to a cosine were typically one with N=16 to 40, the worst case being $\chi^2/N=1.5$ with N=16. All of the stripped beam and transmission data can be well fit by the form

$$S \sim \left[\frac{dJ}{dx}\right]^4 \qquad (6.1)$$

$$= \left[\frac{Az_{eq}^2(\varepsilon)\ln(B\varepsilon)}{\varepsilon}\right]^4$$

where ε is the ion energy in *MeV/* amu and z_{eq} is taken from either Heckman et al.(63) or Zeigler(80). The data are inconsistent with $\left[\frac{dJ}{dx}\right]^2$, $\left[\frac{dE}{dx}\right]^2$, and $\left[\frac{dE}{dx}\right]^4$. $\frac{dE}{dx}$ was measured for ^{19}F in UF_4 by Rutherford scattering for the purpose of comparison with the data.

The fitted values of B in eqn.6.1 for the various sets of data are consistent with a constant B_0, equal to 36.3±2.7, independent of incident ion. All experimental values of B are within 1.4σ of B_0. The fitted values of A show no consistent variation with incident ion although a difference can be noted between the stripped beam and transmission values, the transmission values being higher than those of the stripped beam.

The incident charge data were well fit by the assumptions that the sputtering yield depended locally on a power of the incident ion charge and that the sputtering from the surface is exponentially correlated to conditions in the bulk. For the two energies at which a suitably wide range of incident charge data were available, 1 and 1½ *MeV*/amu, fits to the data yielded the power on the charge to be 9.6±1.0 and 8.24±.83 respectively. These powers are not inconsistent with $\left(\frac{dJ}{dx}\right)^4$.

The equilibrated sputtering yields derived from these data are in reasonable agreement with the stripped beam yields although, on average, slightly lower.

In addition, to aid in the understanding of these data, the data of Hakansson et al.(80,81a,81b) were examined. The stripped beam data of Hakansson et al.(80) of Cs^+ sputtered from CsI by various ions can also be well fit by the form $\left(\frac{dJ}{dx}\right)^4$ although z_{eq} must be taken from Heckman et al.(63) instead of Zeigler(80) to fit the heavier ions. In these data, as with the UF_4 measurements, the fitted values of B are consistent with each other and, indeed, with those from the UF_4 data. Contrary to the UF_4 fits, the A showed a strong dependence on the ion, dropping a factor of 2.88 in going from ^{16}O to ^{127}I. In view of the different form used for z_{eq}, it is unclear if any importance should be attached to this variation.

A measurement was made of the sputtering yields for 42.*MeV* ^{16}O in stripped beam and transmission modes (Hakansson et al.(81a)). Contrary to the UF_4 results, the yields agreed. However, the ion energy was much greater than any used in UF_4 measurements so that the results may not be in conflict.

The incident charge data of Hakansson et al.(81b) for glycylglycine, ergosterol, and CsI sputtered by 20.*MeV* ^{16}O can also be well fit by the above assumptions. It should be noted that fits to these data require different ratios of the charge to sputtering equilibration lengths, demonstrating that the two lengths are not governed by the same mechanism; e.g., neither is proportional to the target electron density.

The magnitude of the transmission data for UF_4 is consistently greater than that of the stripped beam experiments, being ~40% higher for ^{19}F and ~100% for the ^{35}Cl. Assuming that the sputtering yield is proportional to z^8, as indicated by the $\left[\frac{dJ}{dx}\right]^4$ fit, these differences could be explained by letting z_{eq} be 4.3% higher in the transmission experiments than in the stripped beam for ^{19}F and 9.1% higher for ^{35}Cl. This effect could be caused by ions picking up electrons as they exit a solid, thus lowering the z_{eq} seen by the UF_4 in the stripped beam experiments. It should be noted that this is the converse of the expectation of Betz and Grodzins(70) and Bohr and Lindhard(54) who expect the emergent ions to be highly excited and thus lose electrons via the Auger mechanism as they exit.

Two other explanations for the variation in overall magnitude of the UF_4 yields are the existence of atomic states excited in the beam by passage through matter and the energetic electron shower generated by a fast ion in passage through matter. Both of these would change the electronic environment in the sputtered material and could thus effect the apparently electronic sputtering mechanism. Any excited state would be in equilibrium population while in passage through matter. Upon exiting, a fraction of such states would decay before the beam reencountered matter, as in the stripped beam experiments. An electron shower would

also be in equilibrium while the beam was in matter. On exiting it would disperse and on reentry would require time to reequilibrate. Thus the difference between stripped beam and transmission experiments. In incident charge experiments both of these effects would have been absent from the beam when it encountered the target. Due to the experimental arrangement, they also appear to have been absent in the Hakansson et al. experiments.

The extent of the role that excited atomic states could play in affecting sputtering is unclear. That they could have an effect is seen from the work on Rydberg atoms where atomic radii of many tens of angstroms have been seen (Zimmerman et al.(79)). Inside of such radii the charge as seen by a bombarded atom would be larger than the net ion charge. The lifetime of such states would also be very short, of order v_{ion} over the interatomic spacing. Such rapid depletion could be overcome by large populating cross sections.

The effect of energetic electrons is better understood although the state of knowledge is still incomplete. Ahn et al.(75) has shown that simultaneous bombardment of SiO_2 by low energy ions and electrons achieves a larger sputtering yield than ions alone. Knotek and Feibelman(79) have demonstrated a mechanism in a similar system, TiO_2, whereby electrons, or photons, of a sufficient energy sputter oxygen. The mechanism works as follows. Electrons of energy greater than $34.eV$ eject an electron from the $3p$ state of a Ti^{4+} on or very close to the surface. An electron from the $3p$ valence band of O^{2-} falls to fill it and the $31.eV$ liberated serves to Auger eject one or two electrons from the O^{2-}. The oxygen thus becomes neutral or positively charged and is driven off of the surface. Such a mechanism could conceivably be at work in SiO_2,

and UF_4 as well, to enhance the sputtering yield in the simultaneous presence of ions and electrons.

The velocity and angular distributions of the data strongly suggest that the sputtering mechanism is thermal in nature. Of the two thermal models discussed in IV.A., that of Seiberling(80) is the closest in agreement with the sputtering data, both for UF_4 and CsI and for the organics ergosterol and glycylglycine. Of these, only the first two are materials in which Seiberling's model should be appropriate. The model contains no provisions for the survival of large organic molecules. The model also considers the core temperature to be independent of incident beam whereas a 50% increase is seen from ^{19}F to ^{35}Cl. A final disagreement is to be found in the prediction that the yield is inversely proportional to the thermal diffusivity, κ. Griffith(81) has shown that the yield is the same for amorphous and crystalline SiO_2 despite the order of magnitude difference in κ for the two states of the compound.

Watson(81) has done calculations of the sputtering yield that are in general agreement with the ^{19}F data, reproducing the trend of the data with energy of the incident ion and giving the approximate magnitude. The yields calculated for ^{35}Cl are low by a factor of ~4. $\frac{dE}{dx}$ is taken as an input although assumptions as to the spatial extent of the deposited energy, i.e., $\frac{dE_{re}}{dx}$, are required. The atomic temperatures calculated, 2600°K for .25 *MeV/*amu ^{19}F and 4200°K for .37 *MeV/*amu ^{35}Cl are both lower than the experimental values, 3620°K and 5240°K respectively, but do reflect the trend of the data.

It should be noted that the model of Seiberling possesses two free parameters while that of Watson contains none.

To critique the theoretical work done on electronic regime sputtering, $\frac{dE}{dx}$ must be examined. $\frac{dE}{dx}$ can be broken into three parts; the energy given to electrons ejected from atoms, the energy given to atomic excitation, and the energy given directly to nuclei. It can also be divided into restricted energy loss, i.e., energy deposited inside or outside of a given radius. For the energy regime in question, the nuclear energy is some three orders of magnitude below the rest and will be ignored. In the models concerned with ejected electrons, the quantity of interest is the number of electrons (the primary ionization rate) rather than their energy. This quantity would thus be expressed as the energy transfer to electrons divided by the average energy so transferred.

A difficulty with all the realistic models proposed to date is that the portions of $\frac{dE}{dx}$ assumed to couple to atomic motion are inaccessible to direct experimental examination. For example, measurements of the primary ionization rate, $\frac{dJ}{dx}$, are clouded by secondary ionization. That is, a fraction of the electrons observed emanating from matter under ion bombardment are due to electrons originally ejected by the ion (primaries) ejecting other electrons (secondaries). The only way to separate the two varieties is to lower the target density sufficiently to make the secondary emission negligibly small. However, in doing so the electronic environment of the outermost, loosest bound electrons is considerably altered. Since these are the ones most likely to be ejected by a passing ion, they are the ones most affected by such a change in electronic configuration. This casts any attempt to measure the primary ionization rate in doubt.

A similar difficulty holds for the portion of $\frac{dE}{dx}$ representing atomic excitation, $\frac{dE_{ex}}{dx}$. The presence of secondary electrons demonstrate that atomic excitation, at least by the Auger process, takes place some distance from the ion path. This secondary excitation is probably too far from the ion path to assist in sputtering but will nevertheless appear in any measurement of $\frac{dE_{ex}}{dx}$. Whether a sufficiently selective measure of local excitation can be made is unclear. The same difficulty plagues the restricted energy loss, $\frac{dE_{re}}{dx}(r_0)$. As with $\frac{dJ}{dx}$, lowering the density of the system would remove the secondary complication but it would also rob the system of any collective modes of excitation. Thus it appears that both the atomic excitation and restricted portions of $\frac{dE}{dx}$ are also inaccessible.

As a further point it should be noted that one cannot discriminate between $\frac{dJ}{dx}$ and $\frac{dE_{ex}}{dx}$ by the invocation of a sum rule as $\frac{dE_{ex}}{dx}$ is a measure of energy and $\frac{dJ}{dx}$ is a measure of number. Therefore models using one cannot be directly compared to models using the other.

With these points in mind, it can be seen that comparison of the data with theoretical predictions is clouded by the uncertainty as to where any discrepancies arise. That is, whether the disagreement lies in the model itself or rather that the portion of $\frac{dE}{dx}$ input is inappropriate. Indeed, Duck et al.(80) have taken this point to its extreme by devising an empirical function, $f(v)$, from their organic sputtering data

$$f(v) = e^{-2.32v/v_B z_0} \qquad (6.2)$$

where v_B is the Bohr velocity such that

$$S \sim f(v) \frac{dE}{dx} \tag{6.3}$$

Until a method of determining the appropriate fraction of $\frac{dE}{dx}$ is devised, progress in theoretical understanding will be difficult.

As a guide for further theoretical work, it must be noted that all of the mechanisms discussed, namely electrostatic repulsion, both by direct ejection and by deposited heat, electronic pressure of excited atoms, and Auger-induced desorption, are physically capable of producing sputtering to varying degrees in different materials. A complete understanding of the phenomenon requires that all of these, and possibly others as well, be considered and allotted their due importance.

REFERENCES

Ahn J., Perleberg, C.R., Wilcox, D.L., Coburn, J.W., and Winters, H.F., 1975, J. App. Phys., **46,** No. 10, 4581.

Angert, N.B., Franzke, B., Moller, A. and Schmelzer, Ch., 1968, Phys. Lett., **44,** 28.

Bethe, H., 1930, Ann. Physik, **4,** 443.

Betz, H.-D., 1972, Rev. Mod. Phys., **44,** No.3, 465.

Betz, H.-D. and Grodzins, L., 1970, Phys. Rev. Lett., **25,** 211.

Bohr, N. and Lindhard, J., 1954, Kgl. Danske Videnskab. Selskab, Mat.-Fys. Medd. **28,** No. 7

Cooper, B.H., 1981, Ph.D. Thesis, California Institute of Technology

Duck, P., Treu, W., Frohlich, H., Galster, W. and Voit, H., 1980, Surface Science, **95,** 603.

Fleischer, R.L., Price, P.B. and Walker, R.M., 1975, **Nuclear Tracks in Solids** (University of California Press, Berkeley), pp. 11, 30-31.

Gregg, R., 1977, Ph.D. Thesis, California Institute of Technology

Griffith, J.E., 1979, Ph.D. Thesis, California Institute of Technology

Griffith, J.E., 1981, private communication

Griffith, J.E., Weller, R.A., Seiberling, L.E. and Tombrello, T.A.,

1980, Rad. Eff., **51**, 223.

Haff, P.K., 1976, Appl. Phys. Lett., **29**, 443.

Hakansson, P. and Sundqvist, B., 1980, TLU 77/80, Tandem Laboratory Report (Uppsala, Sweden).

Hakansson, P., Kamensky, I. and Sundqvist, B., 1981a, TLU 78/80, Tandem Laboratory Report (Uppsala, Sweden).

Hakansson, P., Jayasinghe, E., Johansson, A., Kamensky, I. and Sundqvist, B., 1981, Phys. Rev. Lett., **47**, 1227.

Heckman, H.H., Hubbard, E.L. and Simon, W.G., 1963, Phys. Rev., **129**, 1240.

Knotek, M.L. and Feibelman, P.J., 1979, Surf. Sci., **90**, 78.

Krueger, F.R., 1977, Z. Naturforsch., **32a**, 1084.

Macfarlane, R.D. and Torgerson, D.F., 1976, Phys. Rev. Lett., **36**, 486.

Mendenhall, M.H., 1980, private communication

Northcliffe, L.C. and Schilling, R.F., 1970, Nuclear Data Tables, **A7**, 270.

Qiu, Y., 1981, private communication

Seiberling, L.E., 1980, Ph.D. Thesis, California Institute of Technology

Seiberling, L.E., Meins, C.K., Cooper, B.H., Griffith, J.E., Mendenhall, M.H. and Tombrello, T.A., 1981, submitted to Nucl. Instr. and Meth.

Sigmund, P., 1981, private communication

Watson, C.C., 1981, private communication

Wittkower, A.B. and Betz, H.D., 1973, Atomic Data, **5**

Zeigler, J.F., 1980, **Handbook of Stopping Cross Sections for Energetic**

Ions in All Elements (Pergamon Press, New York).

Zimmerman, M.L., Littman, M.G., Kash, M.M. and Kleppner, D. 1979, Phys. Rev., **A20**, 2251.

Table 1

Errors in fit due to a target not at the center of the catcher cylinder. The sputtering data were fit to the form

$$n(\vartheta) = n_0 \cos\vartheta$$

which assumes that the target is at the cylinder center. For a target at (x,y), the distribution becomes

$$n(\vartheta) = \frac{\cos\vartheta\cos(\vartheta-\varphi)}{1+\left[\frac{x}{a}\right]^2+\left[\frac{y}{a}\right]^2+2\left[\frac{x}{a}\right]\sin\varphi+2\left[\frac{y}{a}\right]\cos\varphi}$$

$$\varphi = \vartheta - arcsin\left[\frac{(x^2+y^2)^{1/2}}{a}\cos\left[\vartheta - arctan\left[\frac{y}{x}\right]\right]\right]$$

where a is the cylinder radius. Forcing values from 18 equally spaced points from this form to fit $n_0\cos\vartheta$ with $n_0=1$ produces n_0'. The values in the table, Δn, are $|1-n_0'|$. These were taken to be the errors introduced by having a target at (x,y).

Table 1

Target Offset Error

$x(mm)$	$y(mm)$	$\Delta n(\%)$
0.	0.	0.
0.	1.	4.5
0.	2.	8.7
0.	3.	12.7
1.	1.	4.5
2.	2.	8.7
3.	0.	0.9
3.	3.	12.6

Table 2a

Yields of ^{235}U sputtered from UF_4 by ^{16}O in the stripped beam arrangement. As the uncertainty due to charge integration, assumed to be 10%, is the largest contribution to the uncertainty, σ is given with and without it to make clear the effects of the other uncertainties.

2b

Stripped beam and transmission yields for ^{19}F on UF_4.

2c

Stripped beam and transmission yields for ^{35}Cl on UF_4.

Table 2a

^{16}O Yields - Stripped Beam

$\varepsilon(MeV/\text{amu})$	S	$\sigma(tot-ch.)$	$\sigma(tot)$
0.125	2.74	0.15	0.28
0.25	5.84	0.32	0.60
0.5	6.10	0.34	0.63
0.75	3.83	0.21	0.39
1.5	2.14	0.12	0.22

Table 2b

^{19}F Yields - Stripped Beam

$\varepsilon(MeV/\text{amu})$	S	$\sigma(tot-ch.)$	$\sigma(tot)$
0.125	4.02	0.24	0.47
	5.40	0.31	0.62
0.25	13.87	0.78	1.60
	14.72	0.82	1.69
0.5	13.32	0.76	1.53
	17.16	0.96	1.97
0.75	9.75	0.56	1.12
	12.10	0.65	1.38
1.	8.72	0.50	1.00
	10.16	0.56	1.16
1.5	5.43	0.30	0.62
	6.08	0.34	0.69

^{19}F Yields - Transmission

$\varepsilon(MeV/\text{amu})$	S	$\sigma(tot-ch.)$	$\sigma(tot)$
0.125	7.70	0.67	1.02
	8.21	0.71	1.09
0.25	15.31	1.35	2.04
	18.89	1.66	2.51
0.5	21.30	1.77	2.77

	22.89	2.04	3.07
	26.56	2.20	3.45
0.75	15.96	1.37	2.11
1.	11.82	1.08	1.60
	12.59	1.08	1.66
1.5	6.56	0.56	0.86

Table 2c

^{35}Cl Yields - Stripped Beam

$\varepsilon(MeV/\text{amu})$	S	$\sigma(tot-ch.)$	$\sigma(tot)$
0.14	46.7	2.6	5.3
0.27	141.9	7.9	16.2
0.39	202.0	11.1	23.0
0.53	210.5	11.8	24.2
0.78	197.2	11.0	22.7
0.89	175.4	9.8	20.0
	192.0	10.8	22.1

^{35}Cl Yields - Transmission

$\varepsilon(MeV/\text{amu})$	S	$\sigma(tot-ch.)$	$\sigma(tot)$
0.125	65.3	5.3	8.4
	71.6	5.8	9.2
0.25	235.1	19.0	30.3
0.375	358.9	29.1	46.3
0.5	386.1	31.3	49.8
0.625	452.8	36.7	58.4

Table 3a

Values of A and B obtained from fitting the sputtering data to the form

$$S = \left[\frac{dJ}{dx}\right]^4$$

$$= \left[\frac{Az_{eq}^2(\varepsilon)\ln(B\varepsilon)}{\varepsilon}\right]^4$$

where $z_{eq}(\varepsilon)$ was taken from Zeigler(80). In accordance with the $\left[\frac{dJ}{dx}\right]^4$ fits, n was taken to be 8.

The "experiment" column refers to the type of experiment, stripped beam (s.b.) or transmission (tr.).

3b

Values of A and B derived from fitting the data of Hakansson(81b) for CsI to the form above. All of these data were taken in the stripped beam arrangement.

Table 3a

Parameters from $\left(\frac{dJ}{dx}\right)^4$ fits to UF_4

Beam	Exp.	A	$\sigma(A)$	B	$\sigma(B)$
^{16}O	s.b.	0.0097	0.0003	36.5	2.9
^{19}F	s.b.	0.0111	0.0003	31.7	2.1
	tr.	0.0113	0.0002	37.7	1.7
^{35}Cl	s.b.	0.0099	0.0001	38.38	0.55
	tr.	0.0119	0.0003	37.3	1.6

Table 3b

Parameters from $\left(\frac{dJ}{dx}\right)^4$ fits to CsI

Beam	A	$\sigma(A)$	B	$\sigma(B)$
^{16}O	0.00627	0.00008	42.7	1.2
^{32}S	0.00507	0.00016	38.5	2.4
^{63}Cu	0.00366	0.00001	35.5	0.8
^{127}I	0.00218	0.00003	39.6	0.9

Table 4

Incident charge sputtering yields for ^{19}F on UF_4. As in table 2, σ is given with and without the 10% charge integration uncertainty.

Table 4

^{19}F Incident Charge Yields

$\varepsilon(MeV/\text{amu})$	q	S	$\sigma(tot-ch.)$	$\sigma(tot)$
0.25	2	7.40	0.41	0.84
	5	11.29	0.62	1.29
	6	11.91	0.67	1.36
0.5	3	5.34	0.29	0.60
	6	7.80	0.41	0.88
1.	4	1.96	0.11	0.23
		2.19	0.12	0.25
	6	3.15	0.17	0.36
	7	4.22	0.24	0.49
	8	7.32	0.40	0.83
1.5	5	1.05	0.059	0.12
	7	2.35	0.13	0.27
	8	3.16	0.18	0.36
	9	8.83	0.48	1.01

Table 5

Values of $\frac{\lambda_c}{\lambda_s}$ from fits to incident charge data. The data were fit to the form

$$S(q) = S_0 \sum_{k=0}^{n} \frac{n!}{k!(n-k)!} \left[1 + \frac{\lambda_c}{\lambda_s} k\right]^{-1} \left[\frac{q}{z_{eq}} - 1\right]^k$$

where z_{eq} was taken from Zeigler(80) for the UF_4 data and from Heckman et al.(63) for the glycylglycine, ergosterol, and CsI data of Hakansson et al.(81b). λ_c is the charge equilibration length while λ_s is the equilibration length associated with sputtering. In accordance with the $\left[\frac{dJ}{dx}\right]^4$ fits, n was taken to be 8.

Table 5

Fitted ratios of equilibration lengths, $\frac{\lambda_c}{\lambda_s}$

Beam	ε(*MeV*/ amu)	Target	$\frac{\lambda_c}{\lambda_s}$	σ
^{19}F	.25	UF_4	0.087	0.029
	.5		0.17	0.08
	1.		0.46	0.03
	1.5		0.98	0.15
^{16}O	1.25	CsI	0.47	0.07
		ergosterol	0.58	0.05
		glycylglycine	0.39	0.06

Table 6

Nuclides of interest for a carbon stripper foil bombarded by uranium and fluorine atoms. The channel numbers are those of the 1.5 *MeV* alphas scattered at 55° from the various nuclides as shown in fig.28. The positions of elements with more than one stable isotope were averaged over those isotopes.

Table 6

Positions of Nuclides on Carbon Stripper Foil

Nuclide	Channel Number
^{12}C	546.5
^{16}O	590.1
^{19}F	610.8
^{24}Mg	635.3
Cl	666.0
Cu	695.2
^{235}U	723.0

Figure 1

Schematic of experiments designed to measured the sputtering yield of ions in charge equilibrium. The top figure is the stripped beam arrangement showing the placement of the carbon stripper foil. The target is on a thick copper backing. At the bottom is the transmission arrangement where the sputtering target is on the back of a carbon foil.

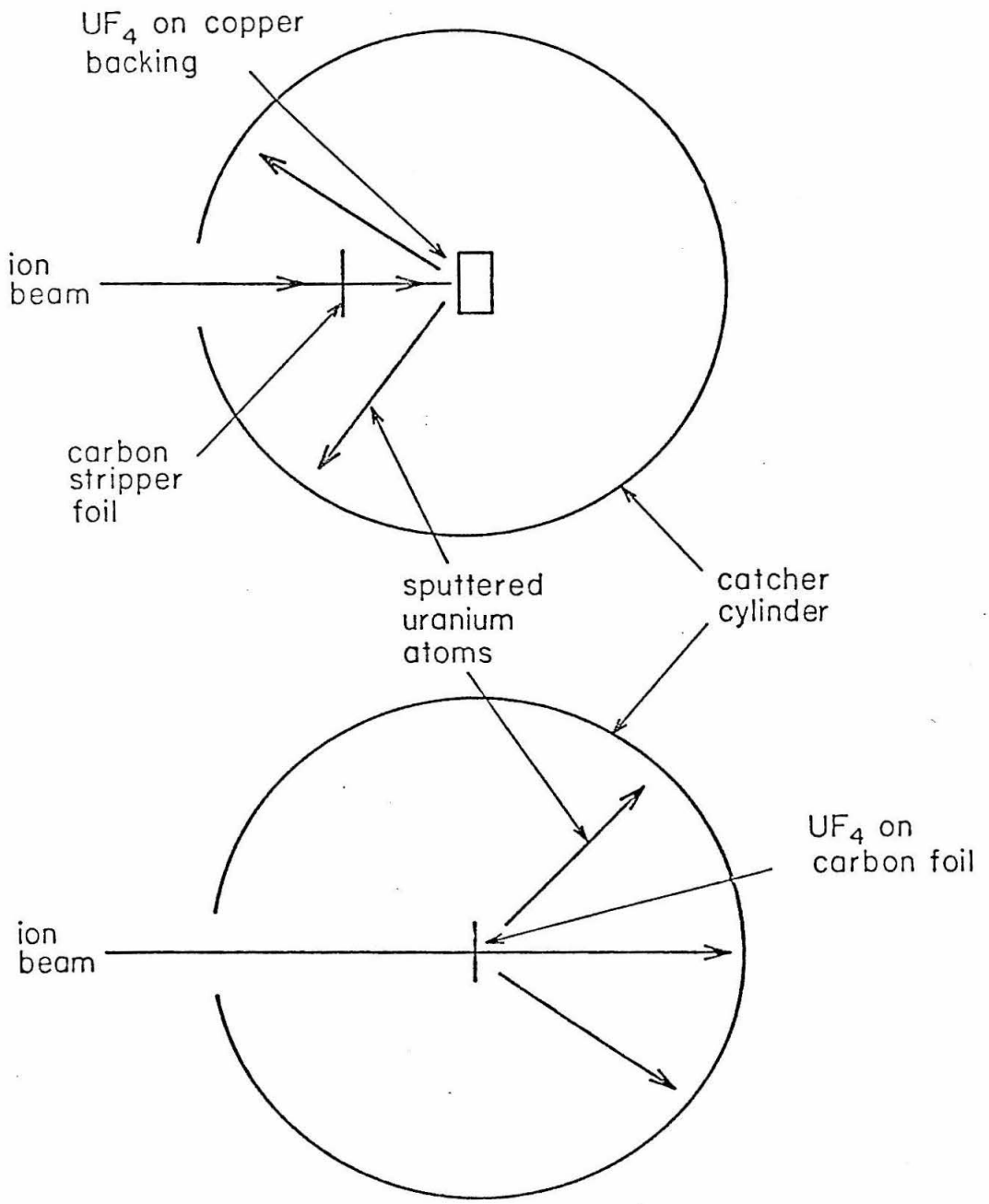
UF_4 on copper backing
ion beam
carbon stripper foil
sputtered uranium atoms
catcher cylinder
UF_4 on carbon foil
ion beam

Figure 2

Layout of the Tandem Van de Graaff accelerator. Negative ions were sent into the accelerator and stripped of electrons by N_2 gas as they passed through the terminal. Upon exiting, the ions were sent through the 90° spectrometer magnet which selected the ions with the desired energy and charge state. From here the ions were directed into the N10° beamline, focused by a quadrupole magnet, and sent into the UHV chamber.

A carbon foil was mounted on a dogleg in the beamline between the exit of the Tandem and the 90° magnet. This foil could be moved in and out of the beam and served to extend the range of charge states produced by the Tandem.

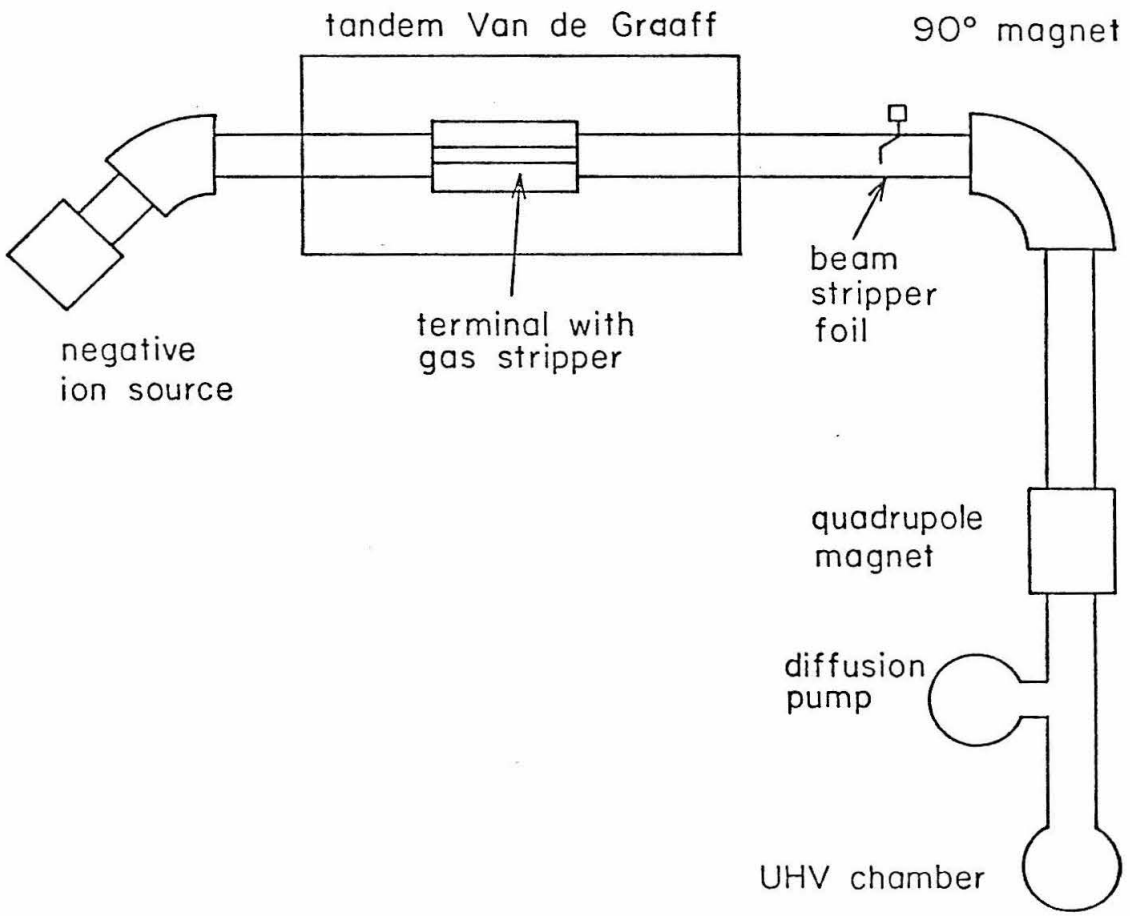
tandem Van de Graaff
90° magnet
beam
stripper
foil
terminal with
gas stripper
negative
ion source
quadrupole
magnet
diffusion
pump
UHV chamber

Figure 3

Outline of the N10° beamline and UHV chamber with its ancillary equipment. The beamline was pumped by a diffusion pump. A liquid nitrogen cooled trap isolated the beamline from the UHV chamber which was pumped by an ion pump.

A collimator was mounted in a cross in front of the cylinder. It was insulated and could be biased to suppress electron emission. Between the collimator and the chamber was a permanent magnet for deflection of electrons escaping from the collimator.

The ion pump was backed by a sorption pump. The chamber was brought to atmospheric pressure with N_2 which was passed through a liquid nitrogen cooled cold trap to remove impurities.

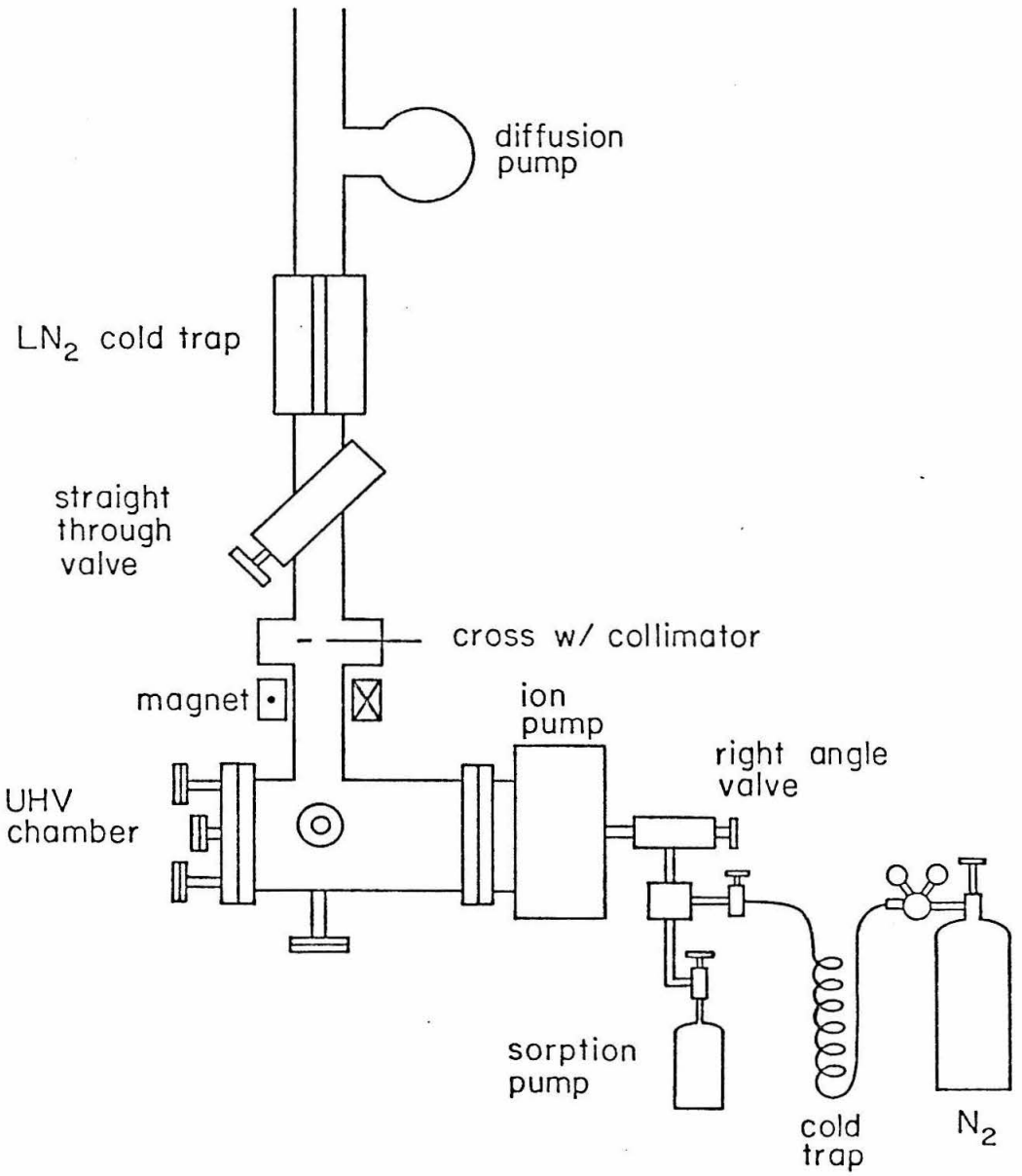
diffusion pump
LN_2 cold trap
straight through valve
cross w/ collimator
magnet
ion pump
right angle valve
UHV chamber
sorption pump
cold trap
N_2

Figure 4

Target mount and catcher cylinder in transmission arrangement. The front set of collimators has been removed for clarity. The target was mounted on a copper block which was in turn mounted on a Macor block. A chromel-constantan thermocouple was mounted in a hole drilled through the copper block between the target and the quartz beam viewing disc. The target heater was sandwiched between the copper and the Macor.

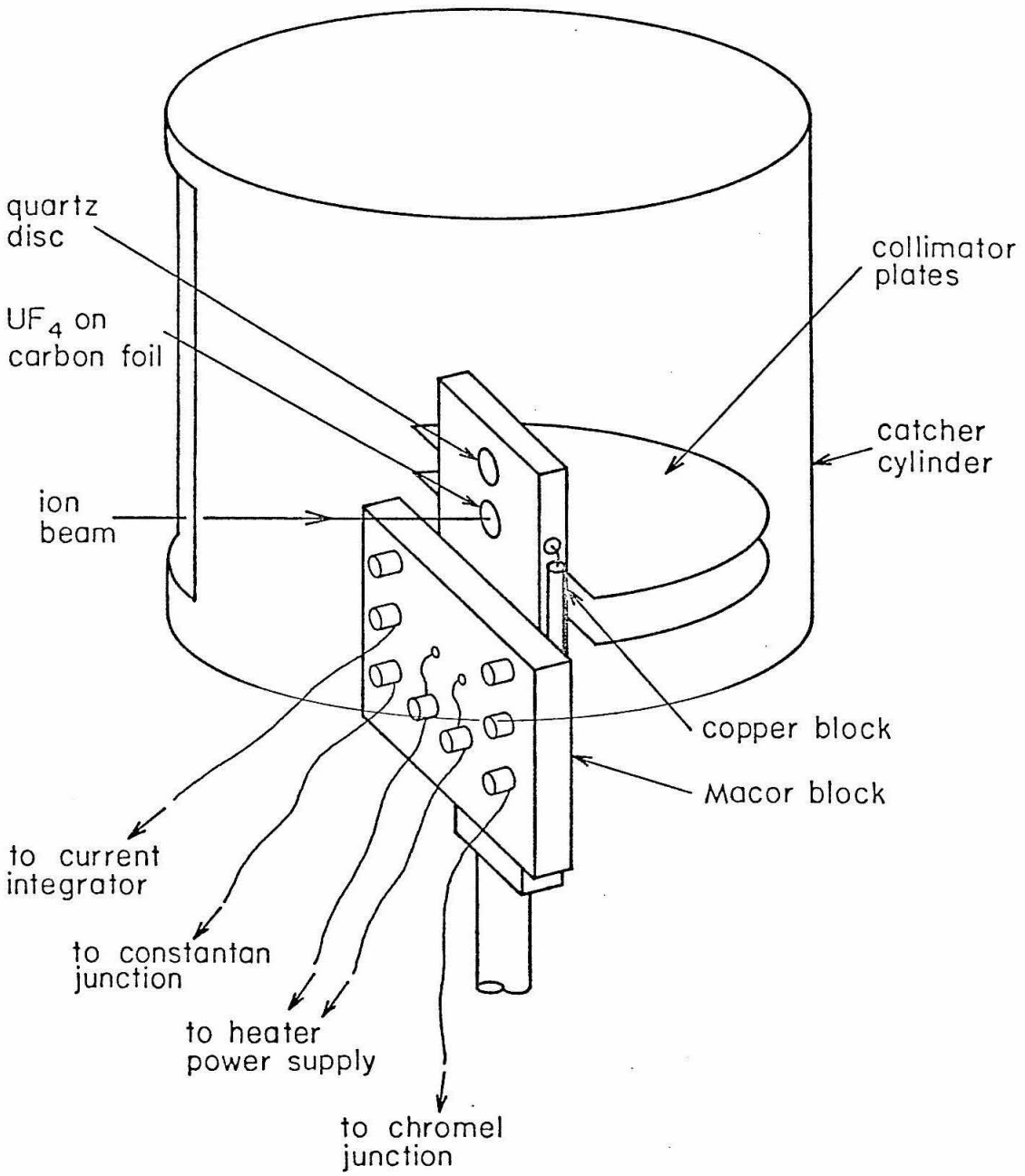
quartz
disc
UF_4 on
carbon foil
ion
beam
collimator
plates
catcher
cylinder
copper block
Macor block
to current
integrator
to constantan
junction
to heater
power supply
to chromel
junction

Figure 5

Geometry used for determining the effects of a target not at the center of the catcher cylinder.

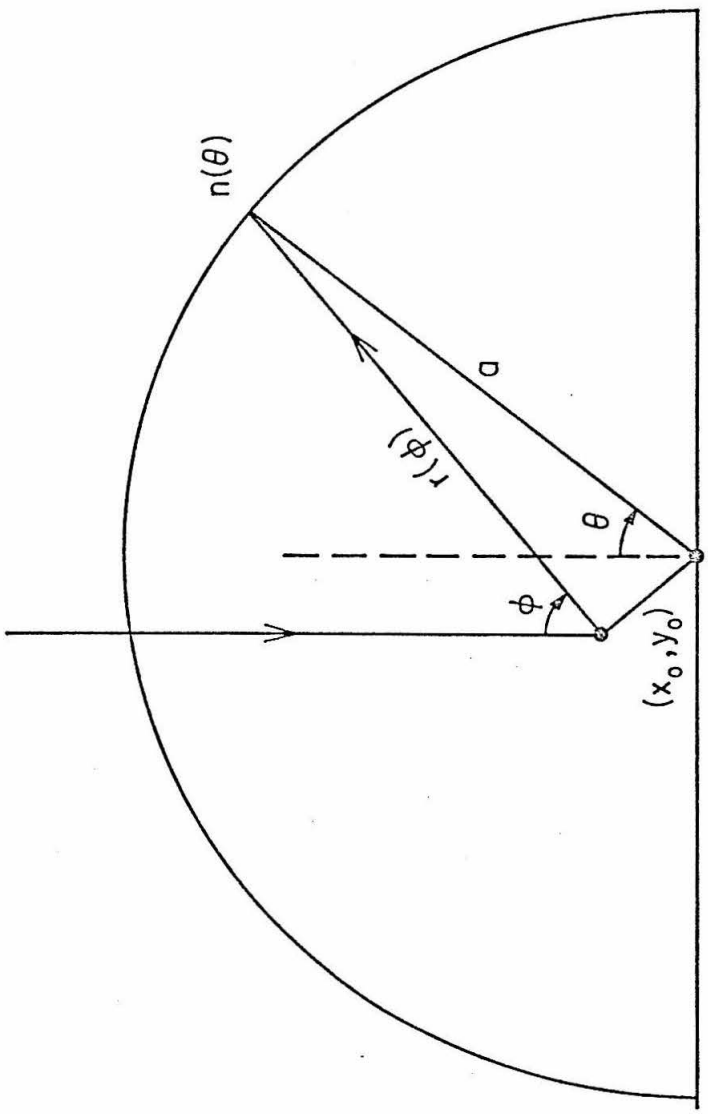
n(θ)
D
r(φ)
θ
φ
(x₀, y₀)

Figure 6

Velocity distribution of ^{235}U sputtered from UF_4 by 4.74 *MeV* ^{19}F (neutral component only).

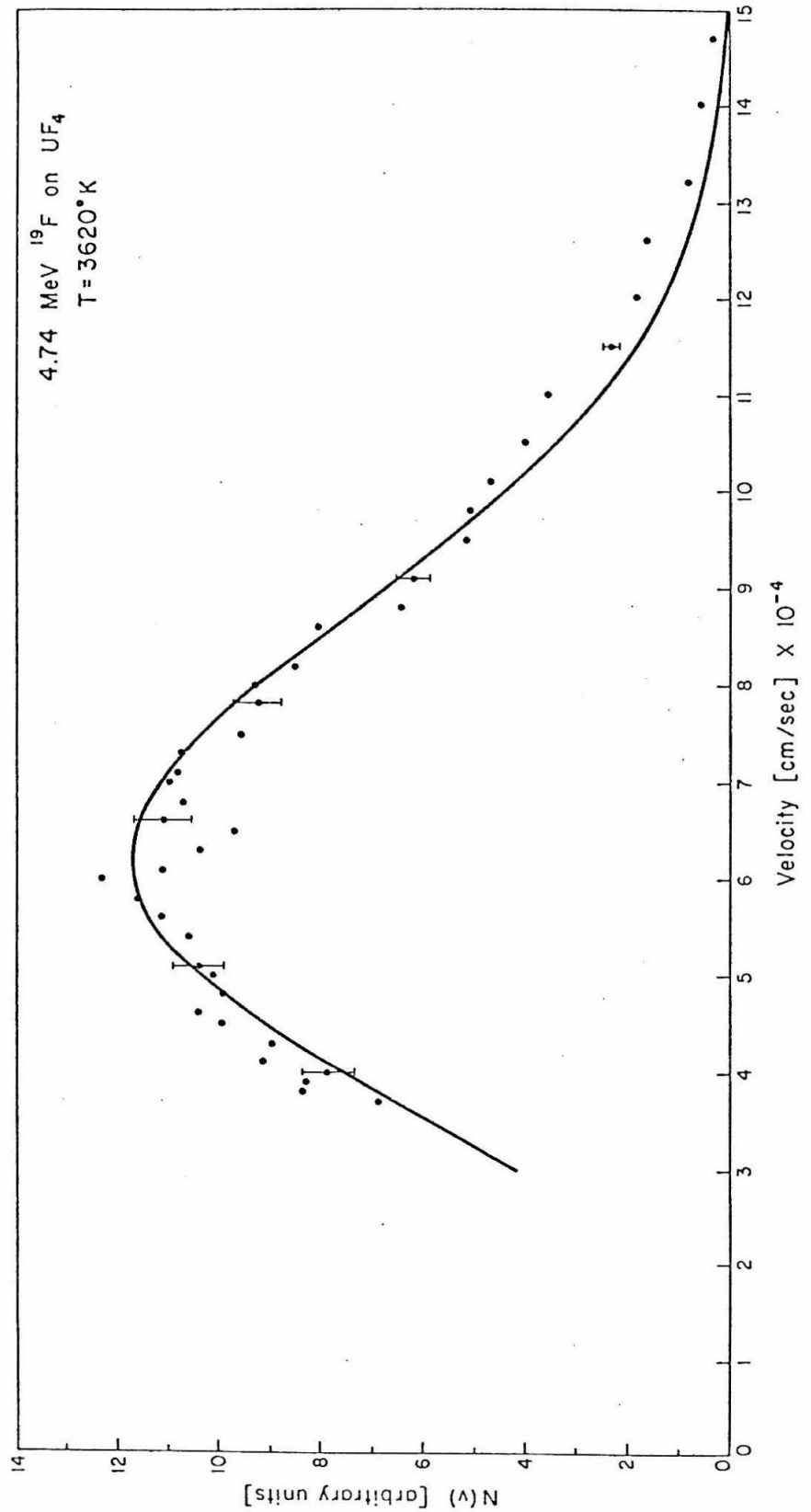
4.74 MeV ^{19}F on UF_4
T = 3620°K
N(v) [arbitrary units]
Velocity [cm/sec] X 10^{-4}
0
2
4
6
8
10
12
14
1
3
5
7
9
11
13
15

Figure 7

Velocity distribution of ^{235}U sputtered from UF_4 by 13. *MeV* ^{35}Cl (neutral component only).

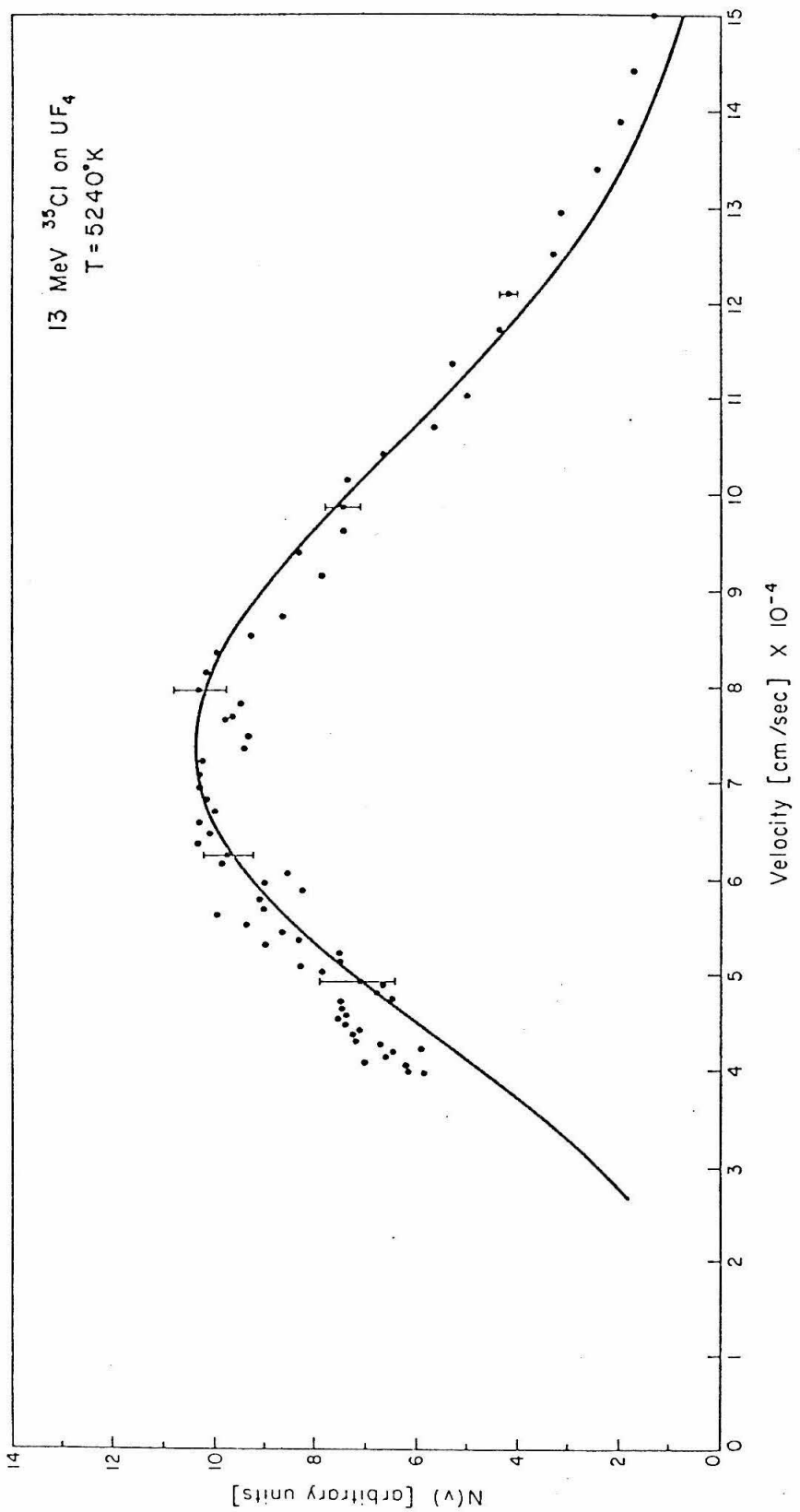
13 MeV ^{35}Cl on UF_4
T = 5240°K
N(v) [arbitrary units]
Velocity [cm/sec] X 10^{-4}
0
2
4
6
8
10
12
14
0
1
2
3
4
5
6
7
8
9
10
11
12
13
14
15

Figure 8

Yield of ^{235}U sputtered from UF_4 by ^{19}F (Griffith(79)). The numbers beside the points were the charge states of the ^{19}F incident on the UF_4.

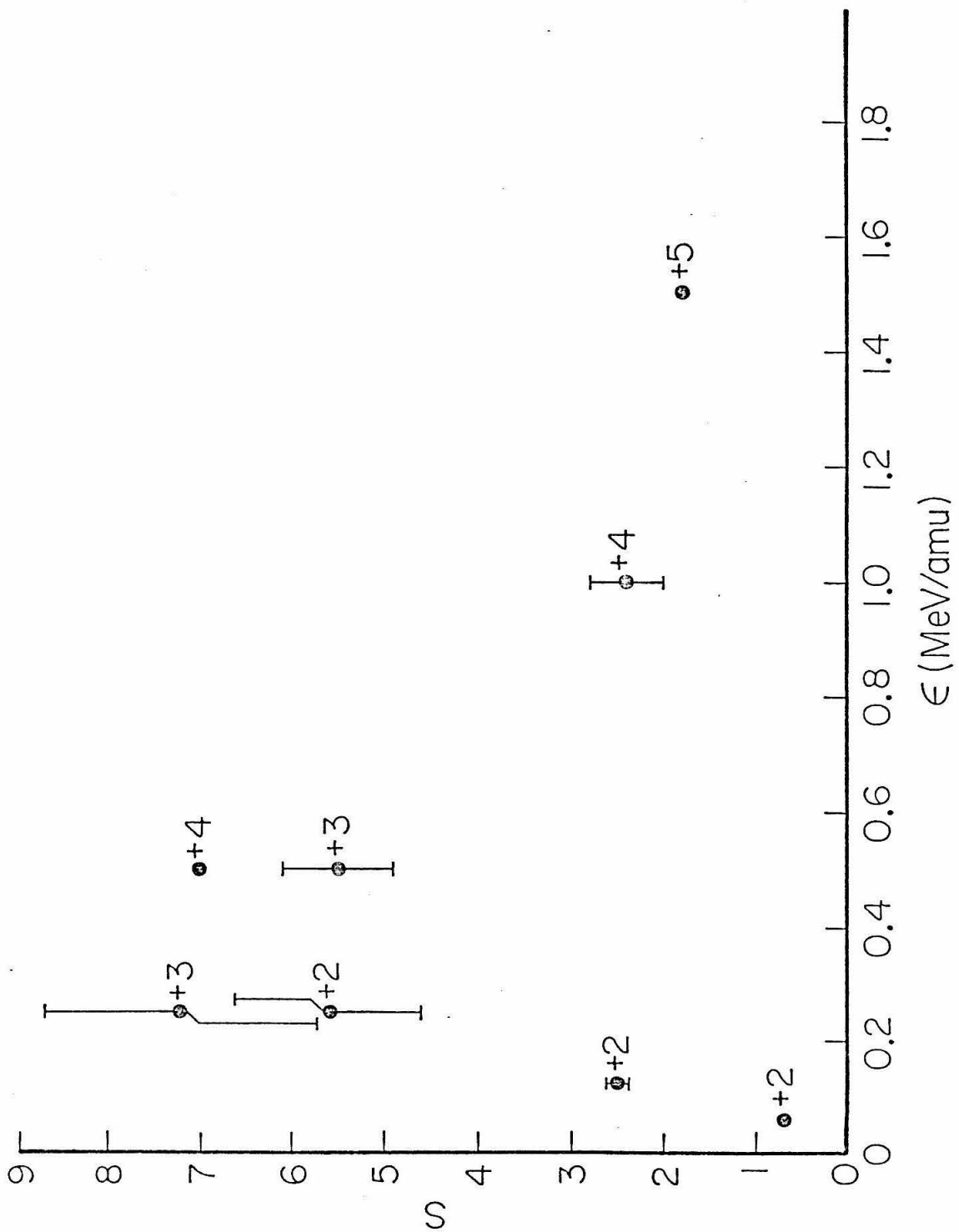
S
∈ (MeV/amu)
0
1
2
3
4
5
6
7
8
9
0
0.2
0.4
0.6
0.8
1.0
1.2
1.4
1.6
1.8
+2
+2
+4
+5
+3
+2
+3
+4

Figure 9

Yield of ^{235}U sputtered from UF_4 by ^{16}O in the stripped beam arrangement. The solid curve is a fit to

$$\left(\frac{dJ}{dx}\right)^4 = \left(\frac{Az_{eq}^2 \ln(B\varepsilon)}{\varepsilon}\right)^4$$

where ε is the energy per mass in $MeV/$amu of the ion. z_{eq} is taken from Zeigler(80). The fitted parameters, A^4 and B, are shown.

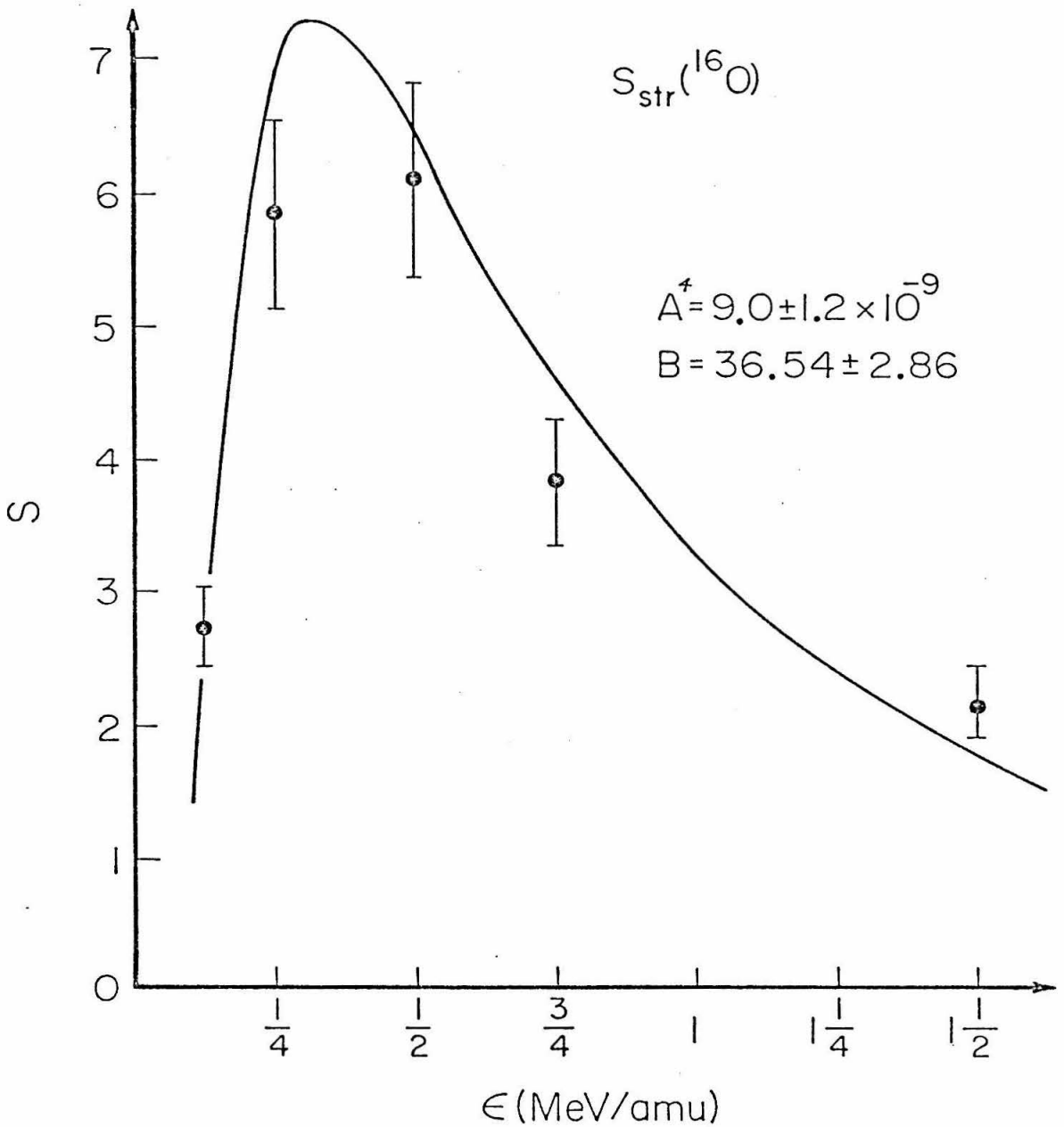
$S_{str}(^{16}O)$
$A^4 = 9.0 \pm 1.2 \times 10^{-9}$
$B = 36.54 \pm 2.86$
S
0
1
2
3
4
5
6
7
$\frac{1}{4}$
$\frac{1}{2}$
$\frac{3}{4}$
1
$1\frac{1}{4}$
$1\frac{1}{2}$
ϵ (MeV/amu)

Figure 10

Yield of ^{235}U sputtered from UF_4 by ^{16}F in the stripped beam and transmission arrangements. The solid curves are fits to $\left(\frac{dJ}{dx}\right)^4$ with the values of A^4 and B shown. Also shown are the yields calculated by Watson(81).

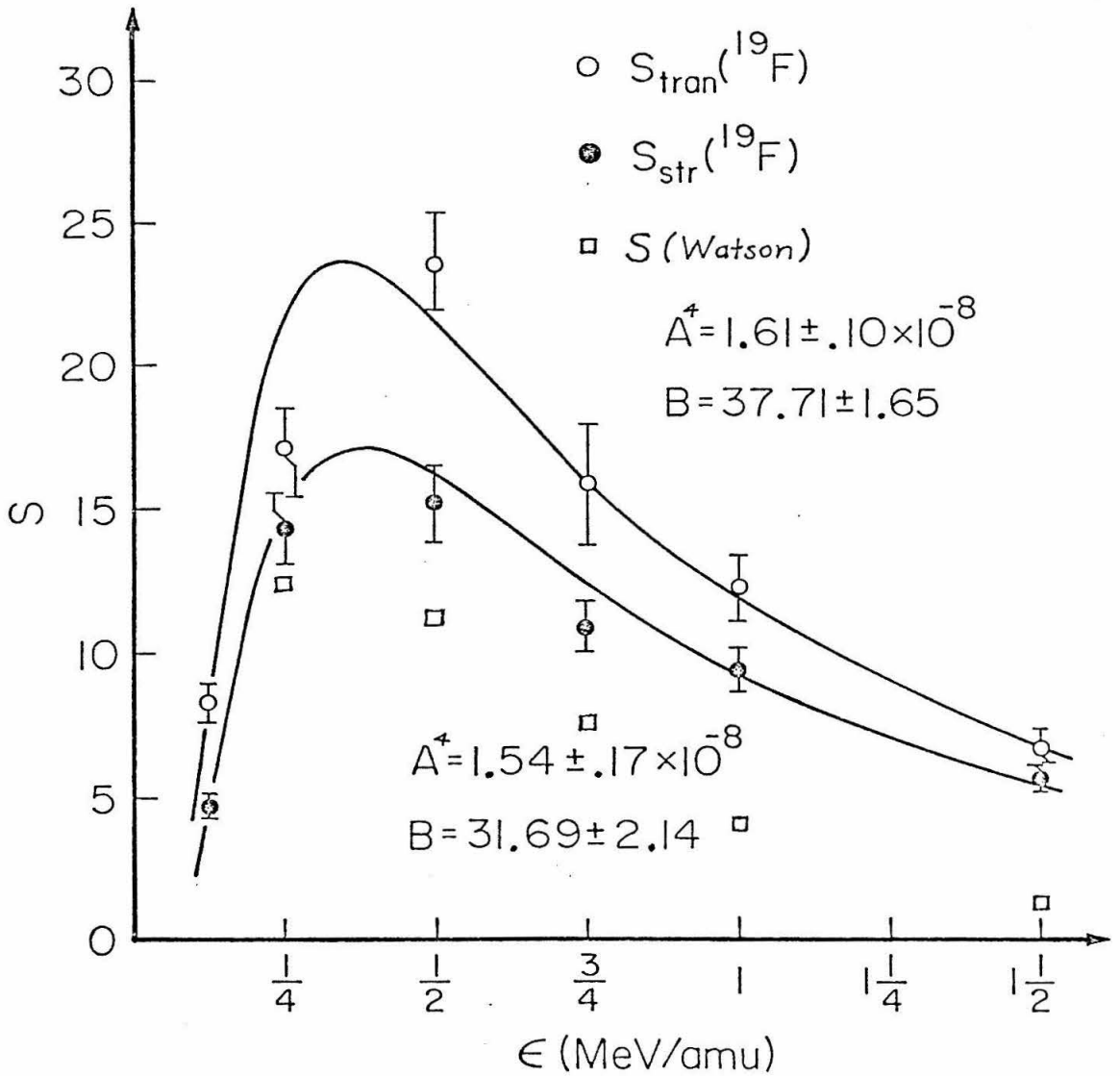
S
30
25
20
15
10
5
0
$S_{tran}(^{19}F)$
$S_{str}(^{19}F)$
S (Watson)
$A^4 = 1.61 \pm .10 \times 10^{-8}$
B = 37.71 ± 1.65
$A^4 = 1.54 \pm .17 \times 10^{-8}$
B = 31.69 ± 2.14
1/4
1/2
3/4
1
1 1/4
1 1/2
∈ (MeV/amu)

Figure 11

Yield of ^{235}U sputtered from UF_4 by ^{16}Cl in the stripped beam and transmission arrangements. The solid curves are fits to $\left[\frac{dJ}{dx}\right]^4$ with the values of A^4 and B shown. Also shown are the yields calculated by Watson(81).

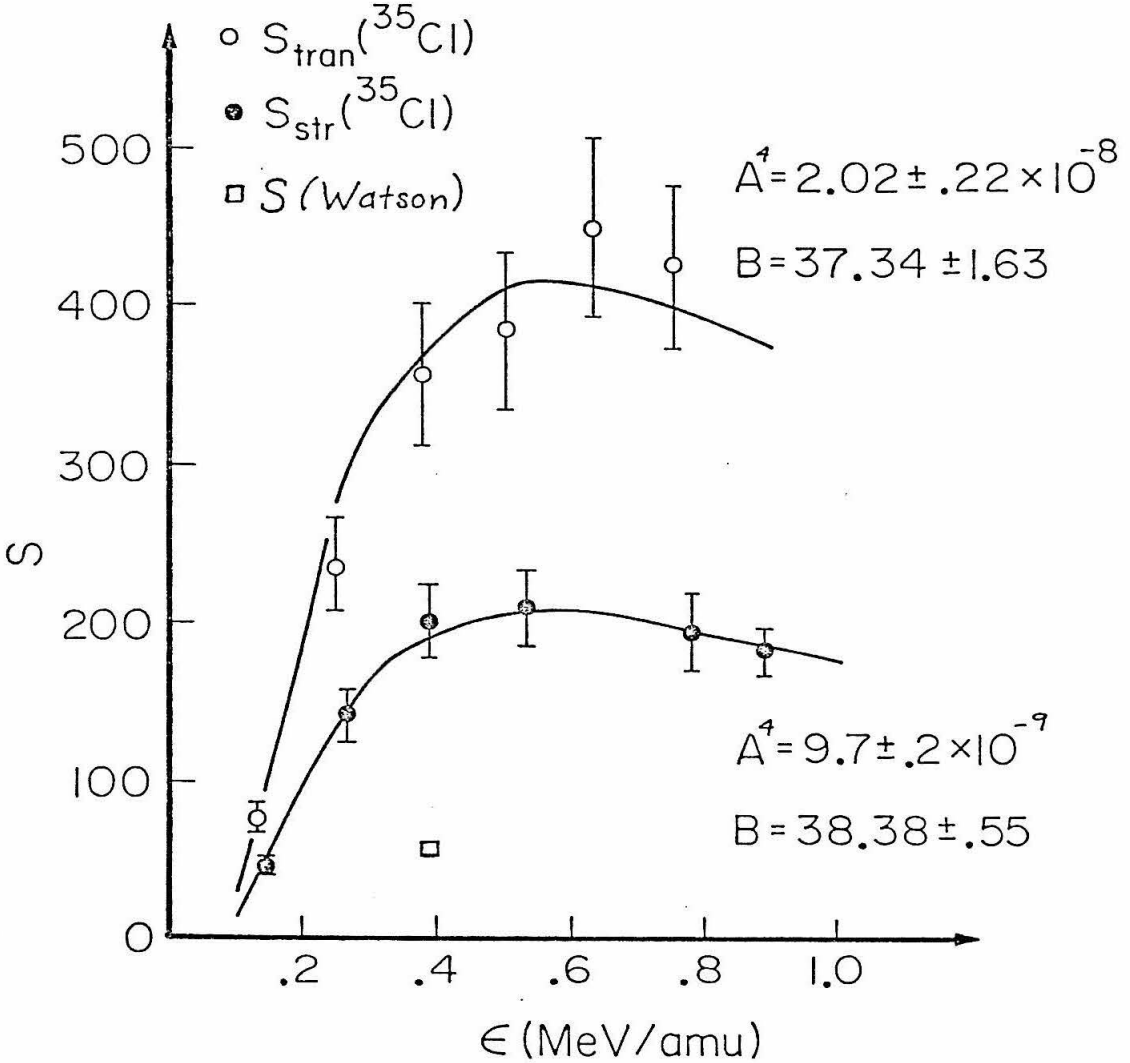
$S_{tran}(^{35}Cl)$
$S_{str}(^{35}Cl)$
S (Watson)
$A^4 = 2.02 \pm .22 \times 10^{-8}$
$B = 37.34 \pm 1.63$
$A^4 = 9.7 \pm .2 \times 10^{-9}$
$B = 38.38 \pm .55$
S
500
400
300
200
100
0
.2
.4
.6
.8
1.0
ϵ (MeV/amu)

Figure 12

Stripped beam yields for ^{19}F along with fits to $\left(\frac{dJ}{dx}\right)^2$, $\left(\frac{dJ}{dx}\right)^4$, $\left(\frac{dE}{dx}\right)^2$ and $\left(\frac{dE}{dx}\right)^4$ as determined by Rutherford scattering in section V.B.

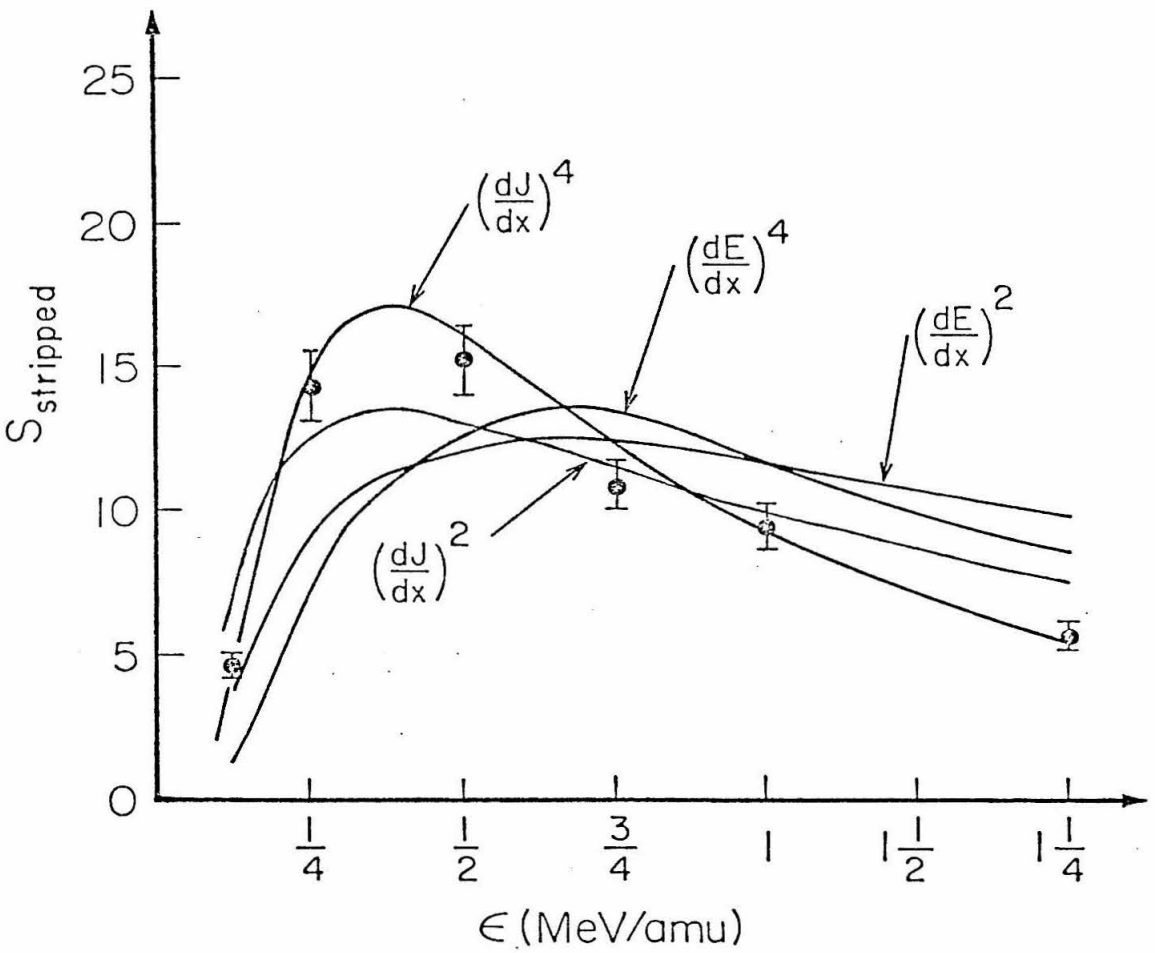
25
20
15
10
5
0
$S_{stripped}$
$\left(\frac{dJ}{dx}\right)^4$
$\left(\frac{dE}{dx}\right)^4$
$\left(\frac{dE}{dx}\right)^2$
$\left(\frac{dJ}{dx}\right)^2$
$\frac{1}{4}$
$\frac{1}{2}$
$\frac{3}{4}$
1
$1\frac{1}{2}$
$1\frac{1}{4}$
ϵ (MeV/amu)

Figure 13

Yields measured by Hakansson et al.(80) of Cs^+ sputtered from CsI by ^{16}O, ^{32}S, ^{63}Cu, and ^{127}I. The curves are fits to $\left(\frac{dJ}{dx}\right)^4$ with z_{eq} given by Heckman et al.(63). This form is

$$z_{eq} = z\left(1-e^{-4.87\,\varepsilon^{1/2}/z^{.55}}\right)$$

where z and ε are the nuclear charge and energy per mass of the ion in *MeV/* amu, respectively. This form differs from Zeigler(80) in that for heavier ions it gives a greater charge at low energies. The difference for an ion as light as ^{16}O is very slight while for ^{127}I the Heckman value is 54% greater than the Zeigler value at ε=.2*Mev/* amu.

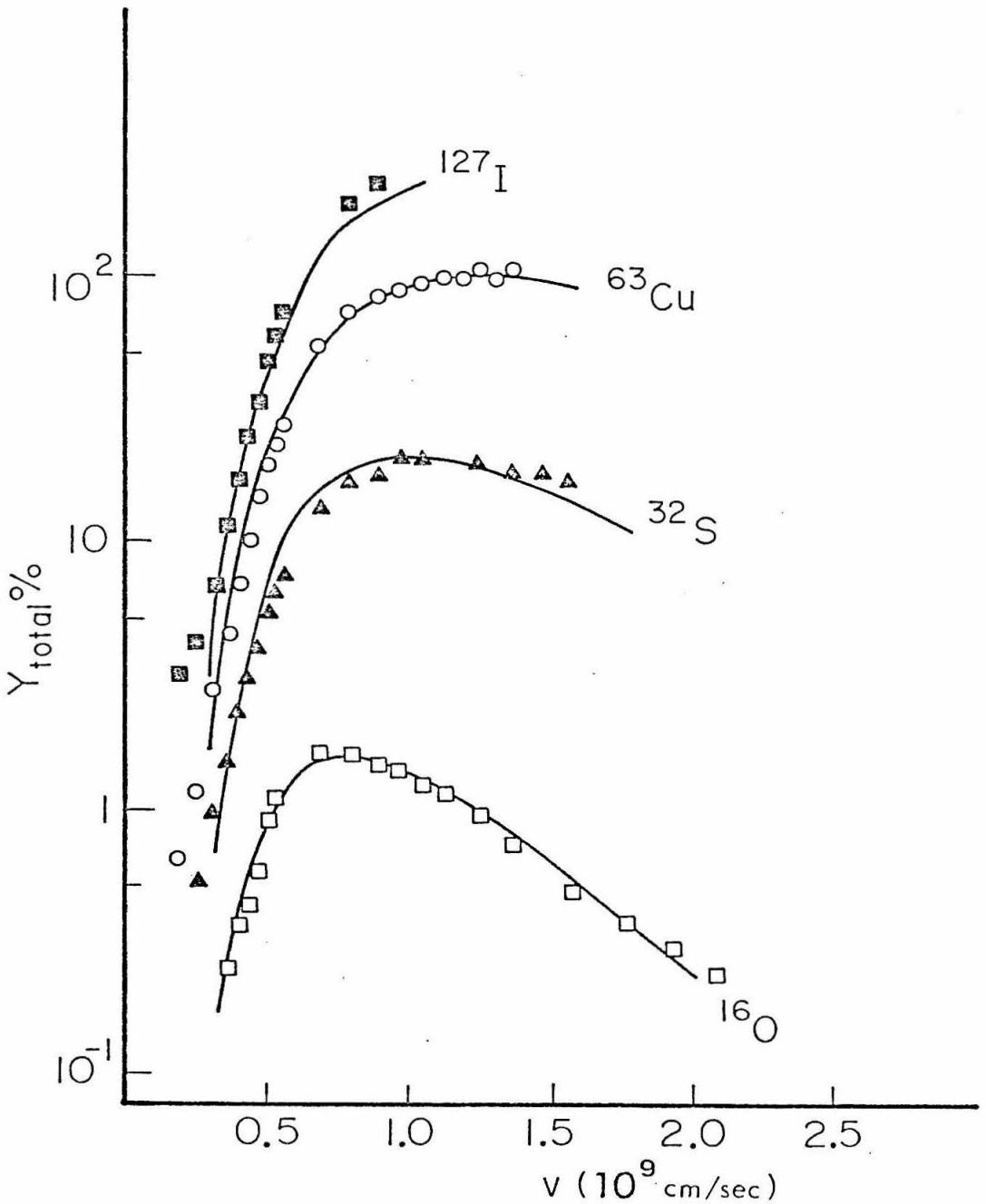
^{127}I
^{63}Cu
^{32}S
^{16}O
10^2
10
1
10^{-1}
Y_{total} %
0.5
1.0
1.5
2.0
2.5
V (10^9 cm/sec)

Figure 14

Sputtering yields of CsI, glycylglycine, and ergosterol by ^{63}Cu as measured by Hakansson(80). The observed sputter products were Cs^+ and $(M+H)^+$ where M was glycylglycine and ergosterol.

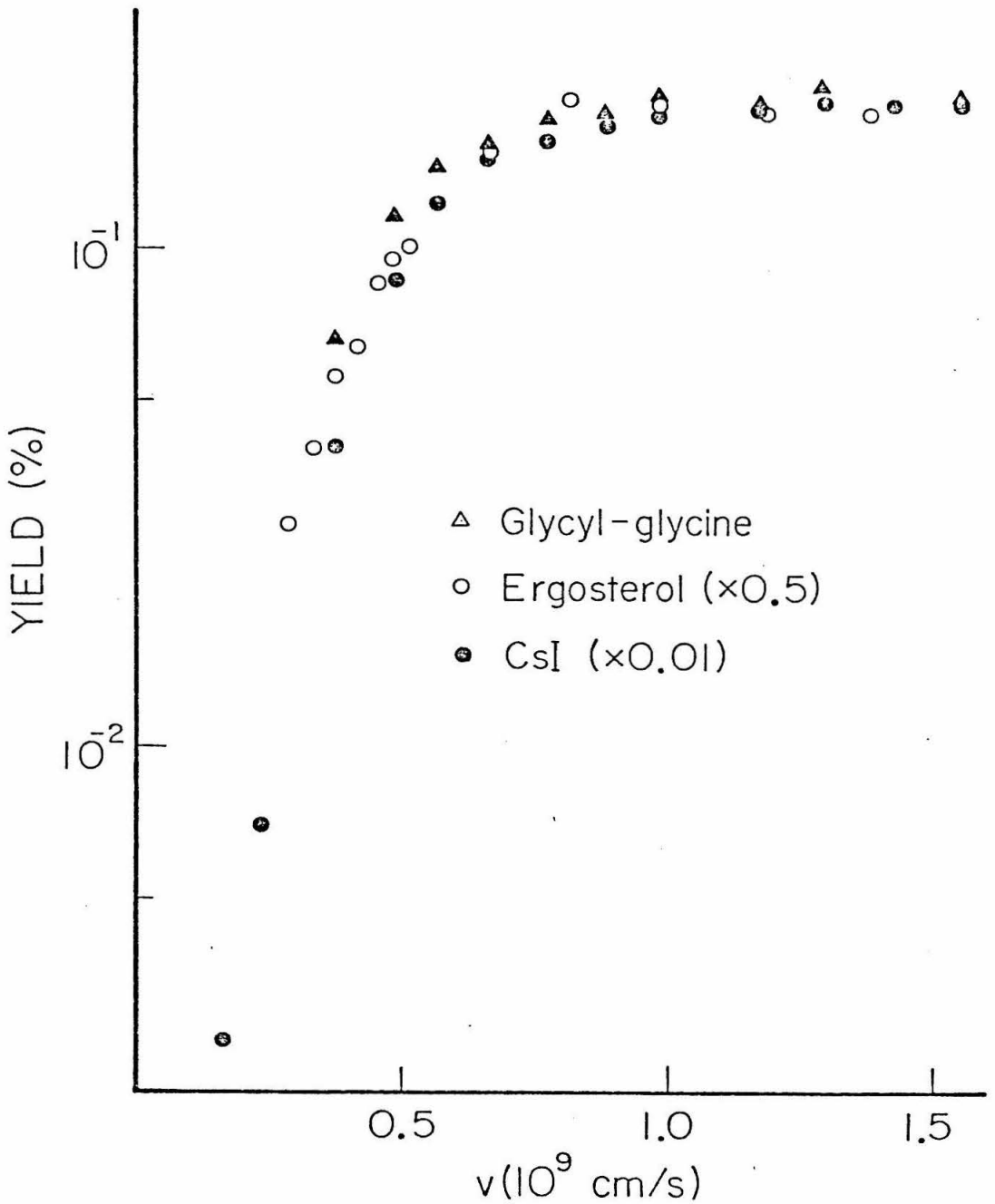
YIELD (%)
10^{-1}
10^{-2}
Glycyl-glycine
Ergosterol (×0.5)
CsI (×0.01)
0.5
1.0
1.5
v(10^9 cm/s)

Figure 15

Stripped beam and transmission yields of Cs^+ sputtered from CsI by 42.*MeV* ^{16}O (from Hakansson(81a)). The angle ϑ is the angle between the beam and the target normal.

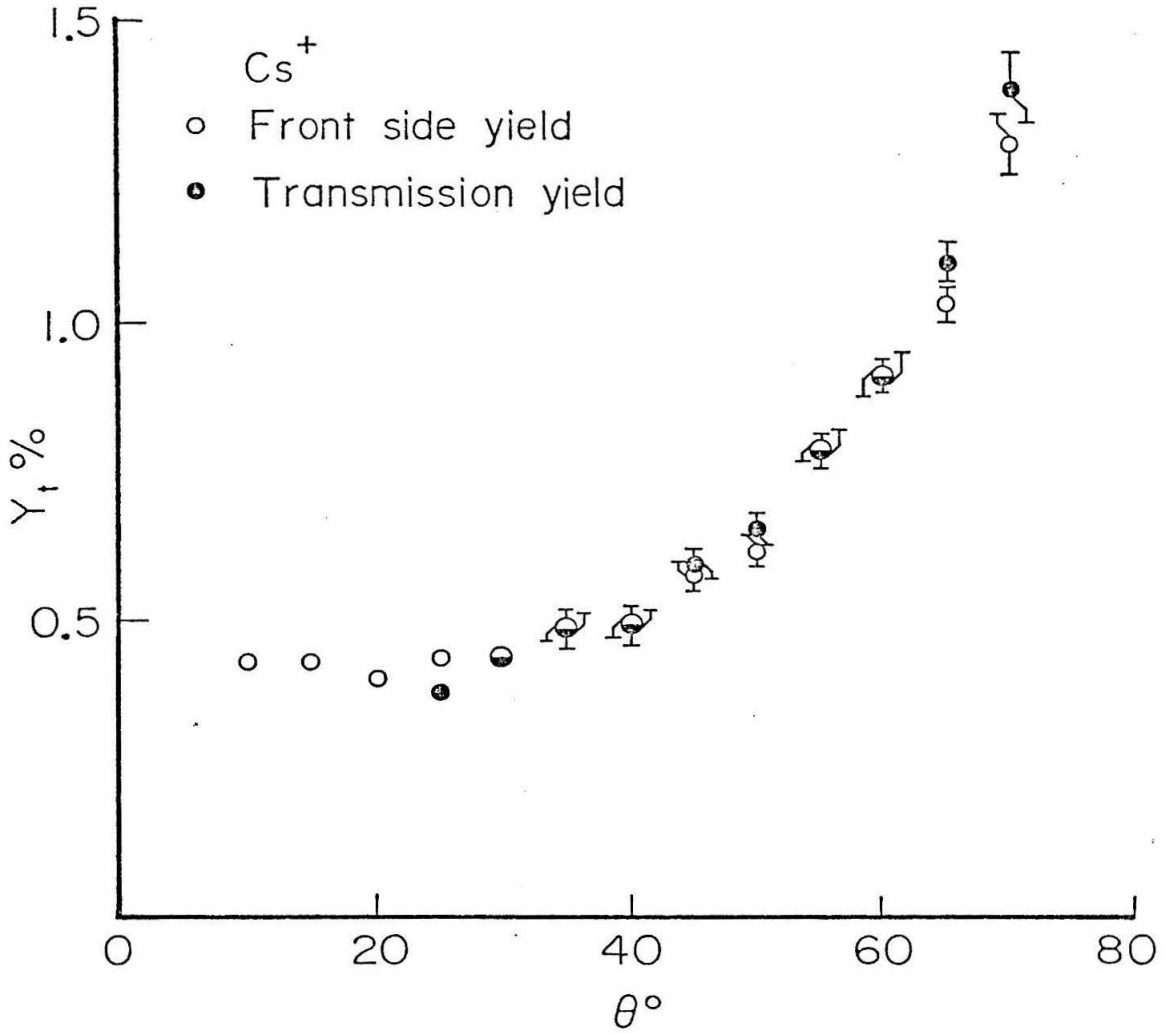
1.5
1.0
0.5
Y_t %
Cs^+
Front side yield
Transmission yield
0
20
40
60
80
θ°

Figure 16

The ratio of charge states $\frac{A(k)}{A(k+1)}$ versus charge number k for $28. MeV$ ^{19}F emerging from carbon. This ratio is related to the electron capture and loss cross sections, σ_c and σ_l, by

$$\frac{A(k)}{A(k+1)} = \frac{\sigma_c(k+1)}{\sigma_l(k)}$$

As the data show, it can be well fit by a simple exponential.

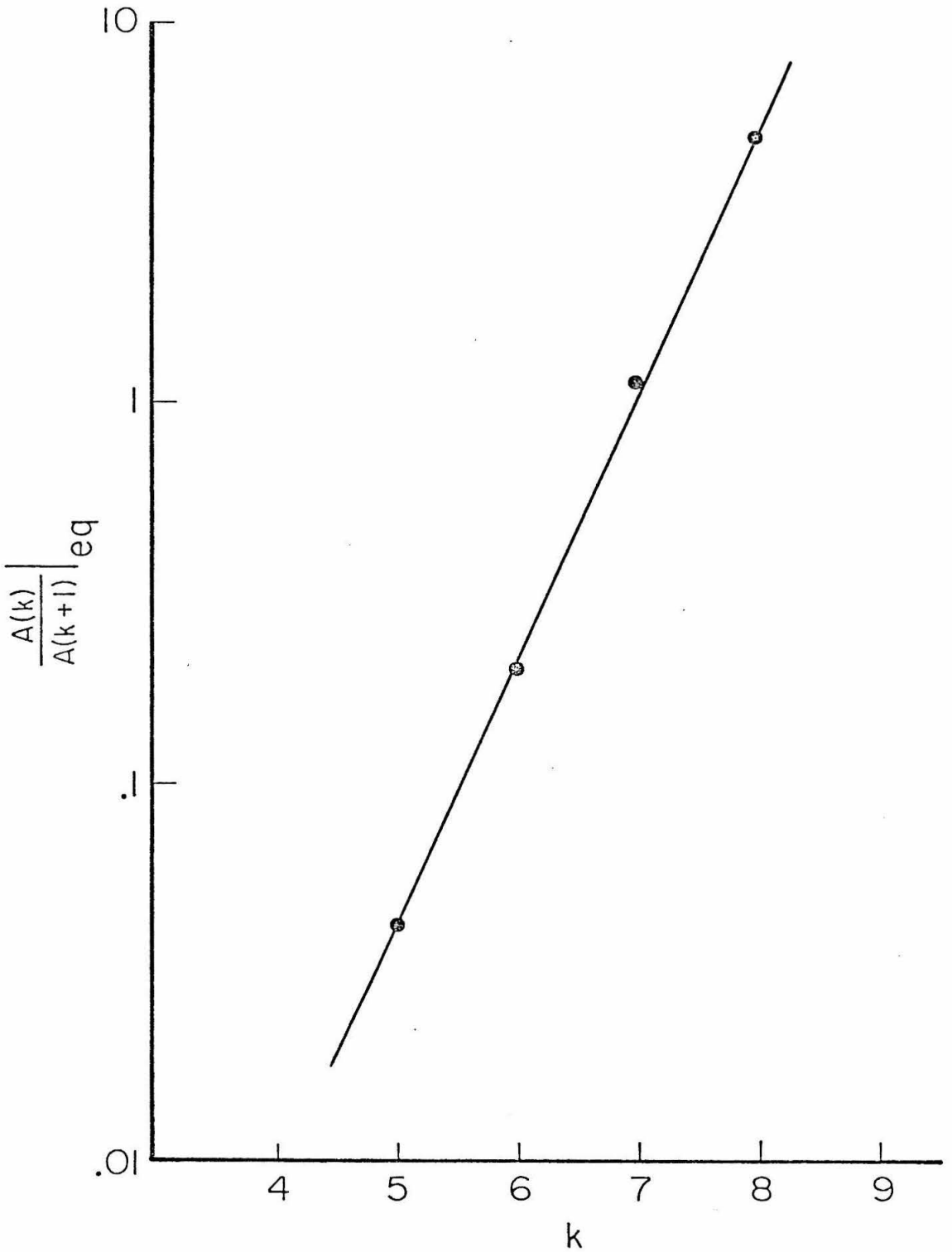
10
1
.1
.01
$\left.\frac{A(k)}{A(k+1)}\right|_{eq}$
4
5
6
7
8
9
k

Figure 17

Charge fractions in a 28.*MeV* ^{19}F beam versus depth into UF_4 for a beam initially in the +5 charge state.

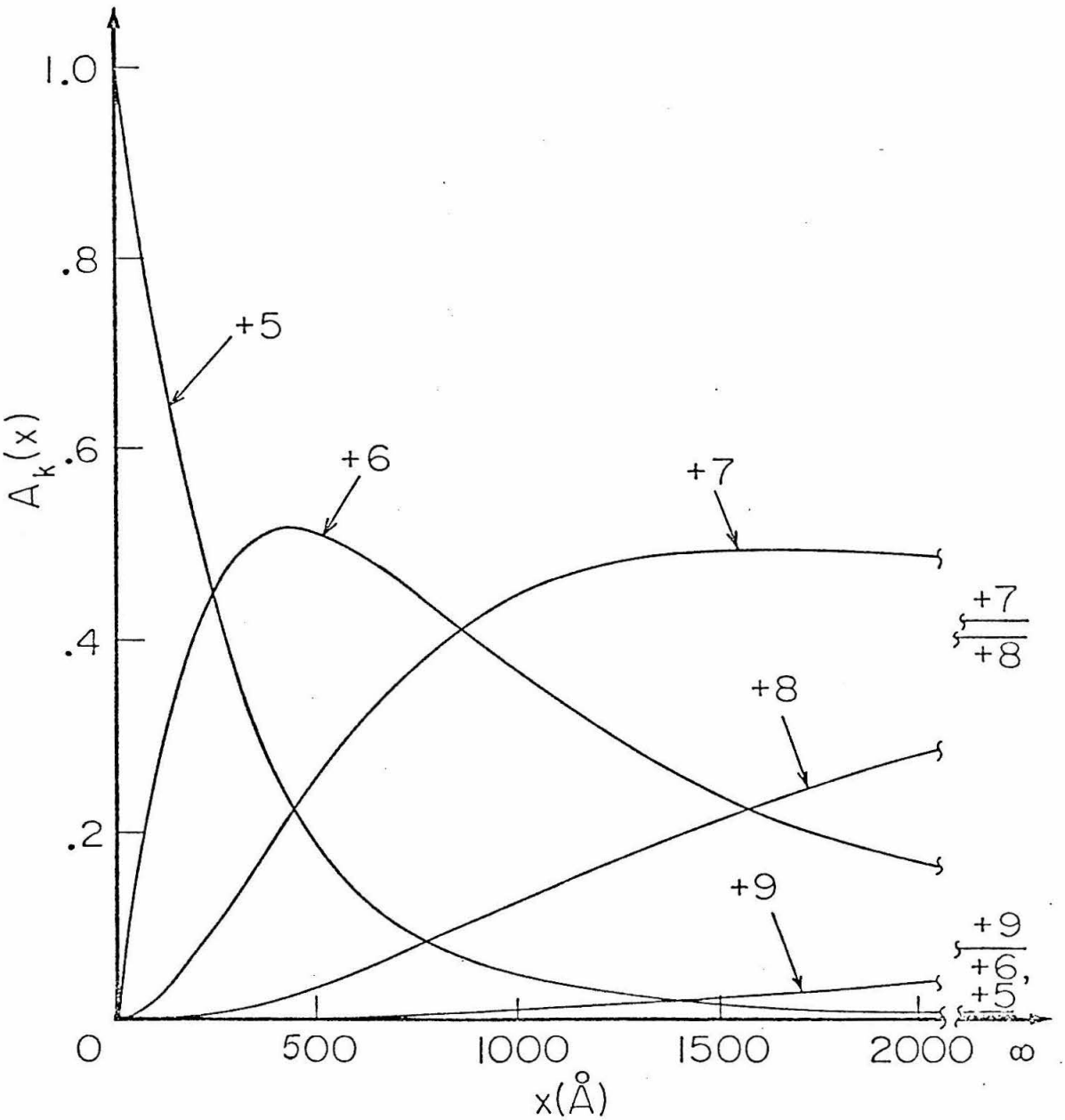
1.0
.8
.6
.4
.2
$A_k(x)$
+5
+6
+7
+8
+9
+7
+8
+9
+6,
+5
0
500
1000
1500
2000
∞
x(Å)

Figure 18

Incident charge data for 1½ *MeV*/amu ^{19}F with fits to the average charge and charge fraction forms.

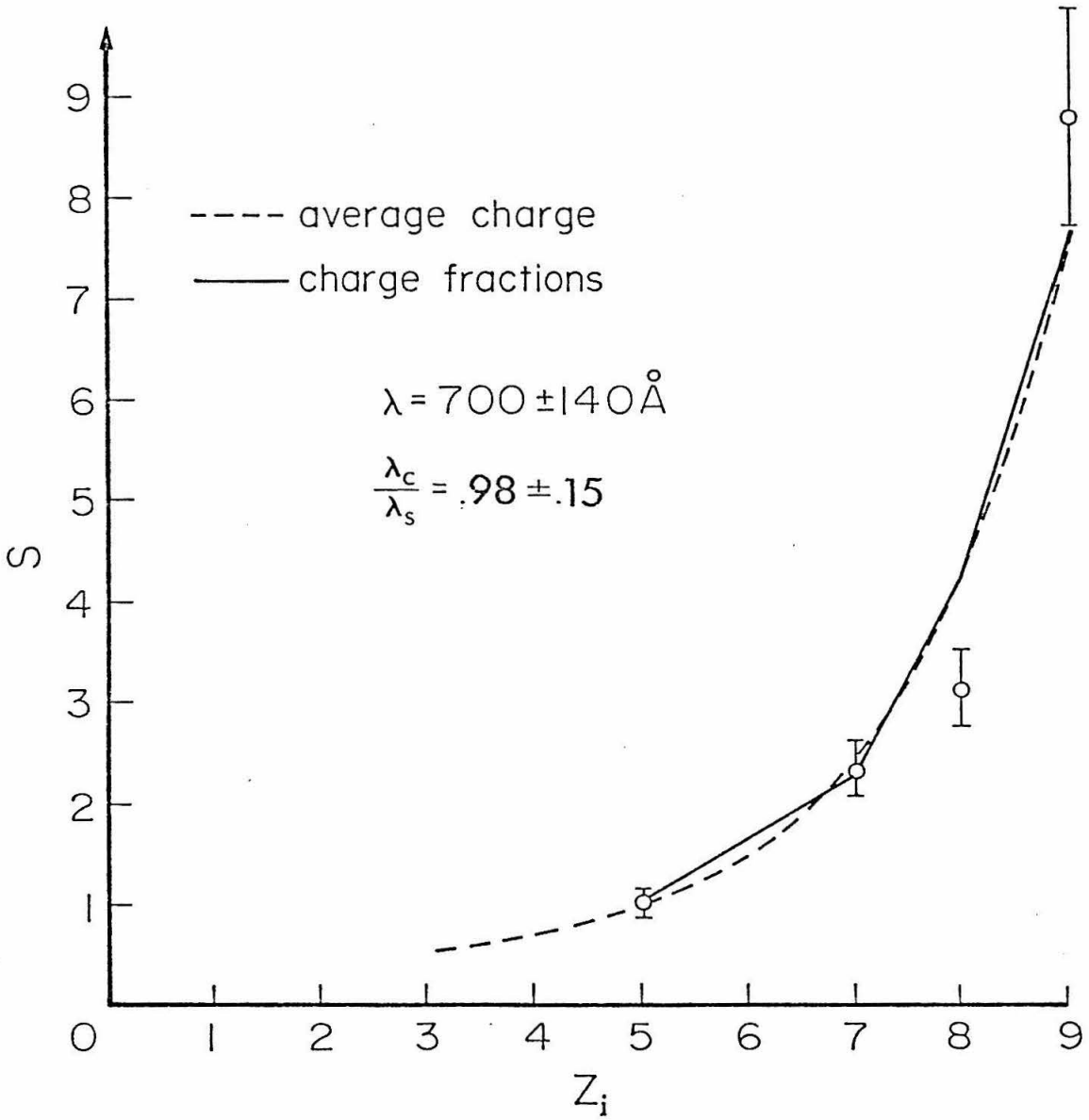
9
8
7
6
5
4
3
2
1
0
S
---- average charge
—— charge fractions
λ = 700 ±140Å
λc/λs = .98 ±.15
0 1 2 3 4 5 6 7 8 9
Zi

Figure 19

Incident charge data for ¼ *MeV*/amu ^{19}F with a fit to the average charge form.

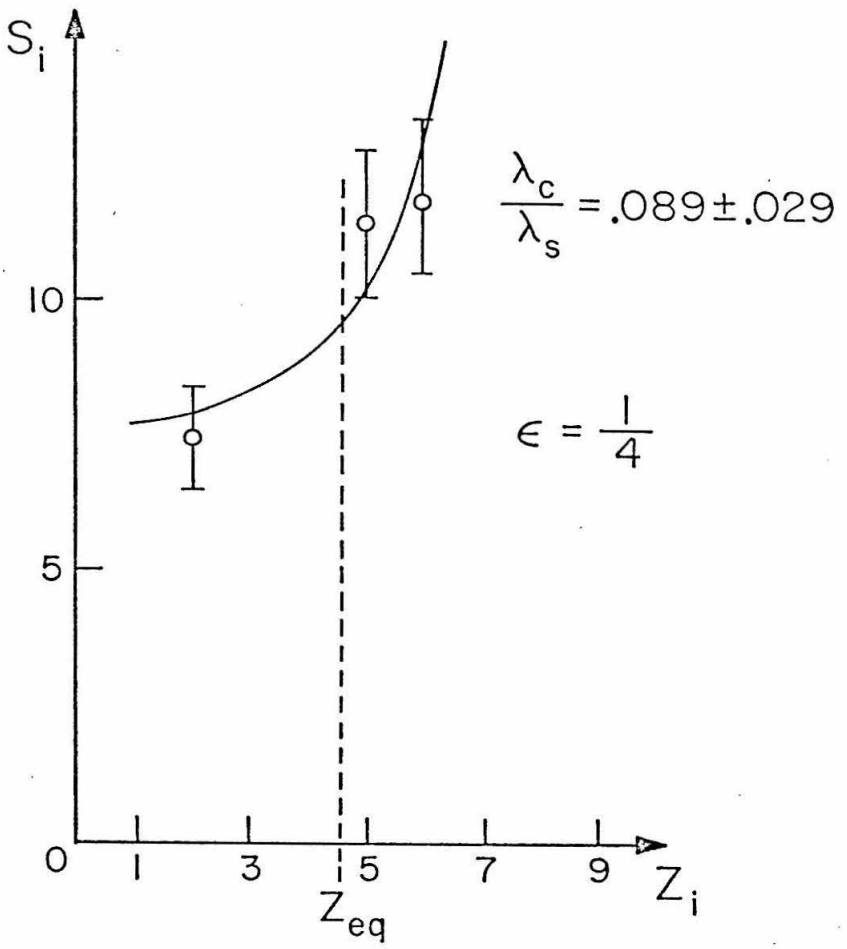
S_i
10
5
0
1
3
5
7
9
Z_i
Z_{eq}
$\frac{\lambda_c}{\lambda_s} = .089 \pm .029$
$\epsilon = \frac{1}{4}$

Figure 20

Incident charge data for ½ *MeV*/amu ^{19}F with a fit to the average charge form.

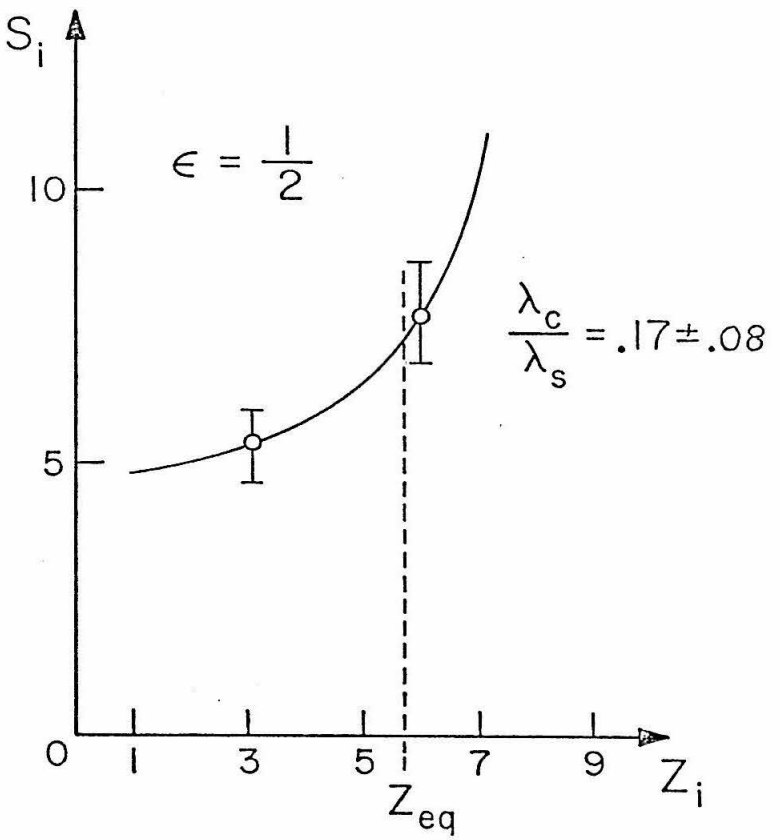
S_i
$\epsilon = \frac{1}{2}$
10
5
0
1
3
5
7
9
Z_i
Z_{eq}
$\frac{\lambda_c}{\lambda_s} = .17 \pm .08$

Figure 21

Incident charge data for 1 *MeV/* amu ^{19}F with a fit to the average charge form.

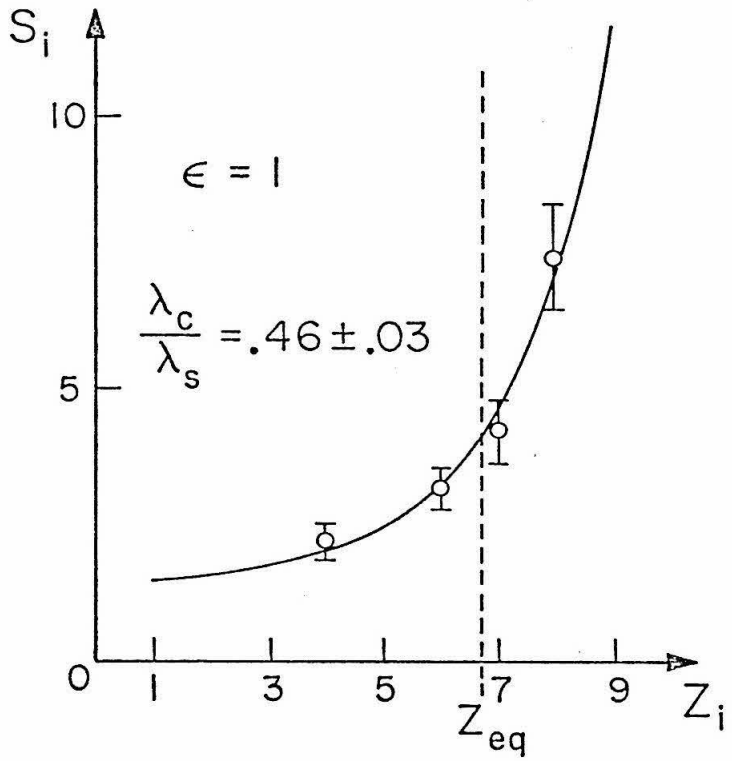
S_i
10
5
0
$\epsilon = 1$
$\frac{\lambda_c}{\lambda_s} = .46 \pm .03$
1
3
5
7
9
Z_i
Z_{eq}

Figure 22

Values of $\frac{\lambda_c}{\lambda_s}$ derived from fits to incident charge data versus energy. The solid curve is a power law fit to the data.

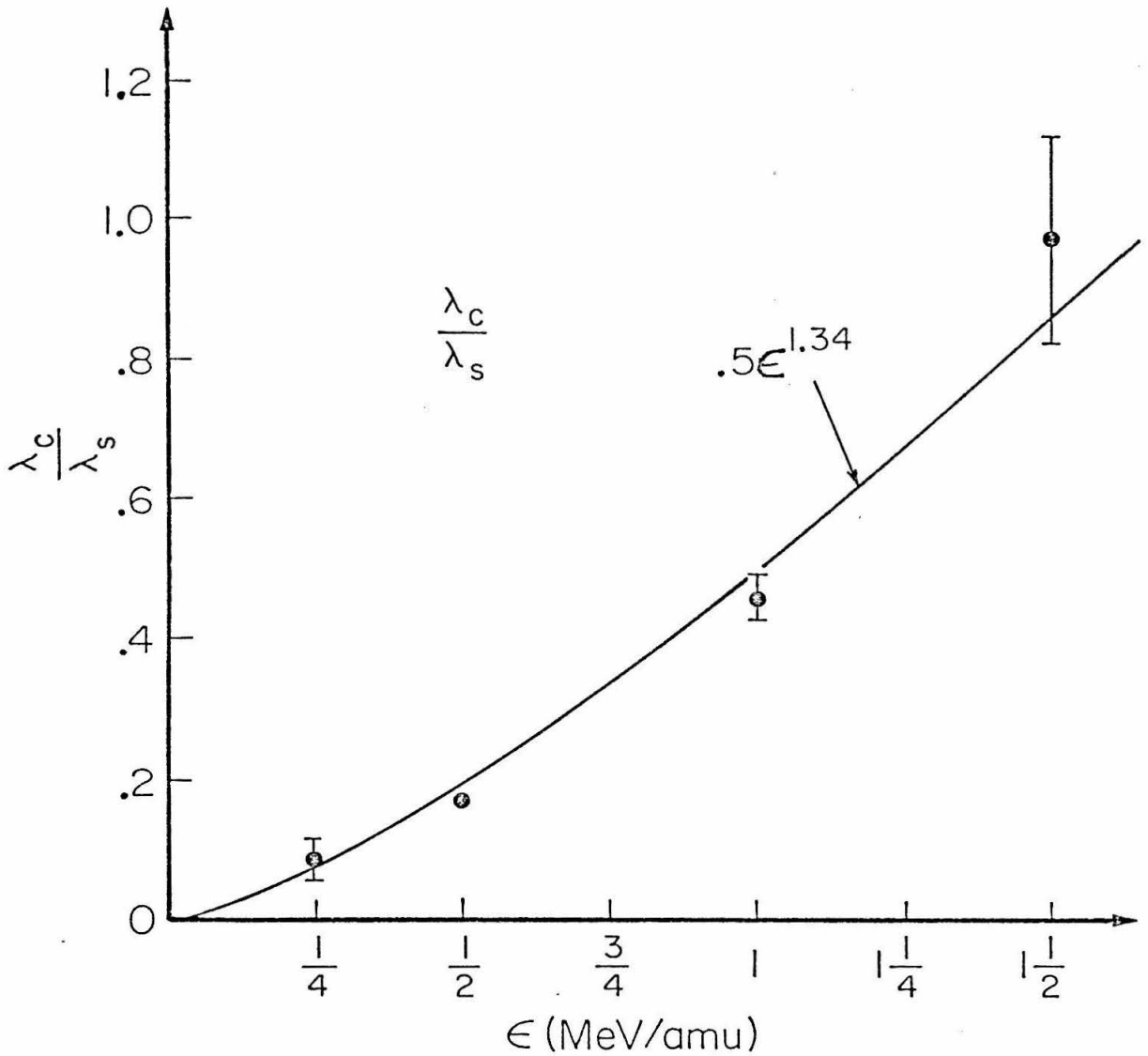
1.2
1.0
.8
.6
.4
.2
0
$\frac{\lambda_c}{\lambda_s}$
$\frac{\lambda_c}{\lambda_s}$
$.5\epsilon^{1.34}$
$\frac{1}{4}$
$\frac{1}{2}$
$\frac{3}{4}$
1
$1\frac{1}{4}$
$1\frac{1}{2}$
ϵ (MeV/amu)

Figure 23

S_{eq} derived from fits to incident charge data along with stripped beam and transmission yields for ^{19}F.

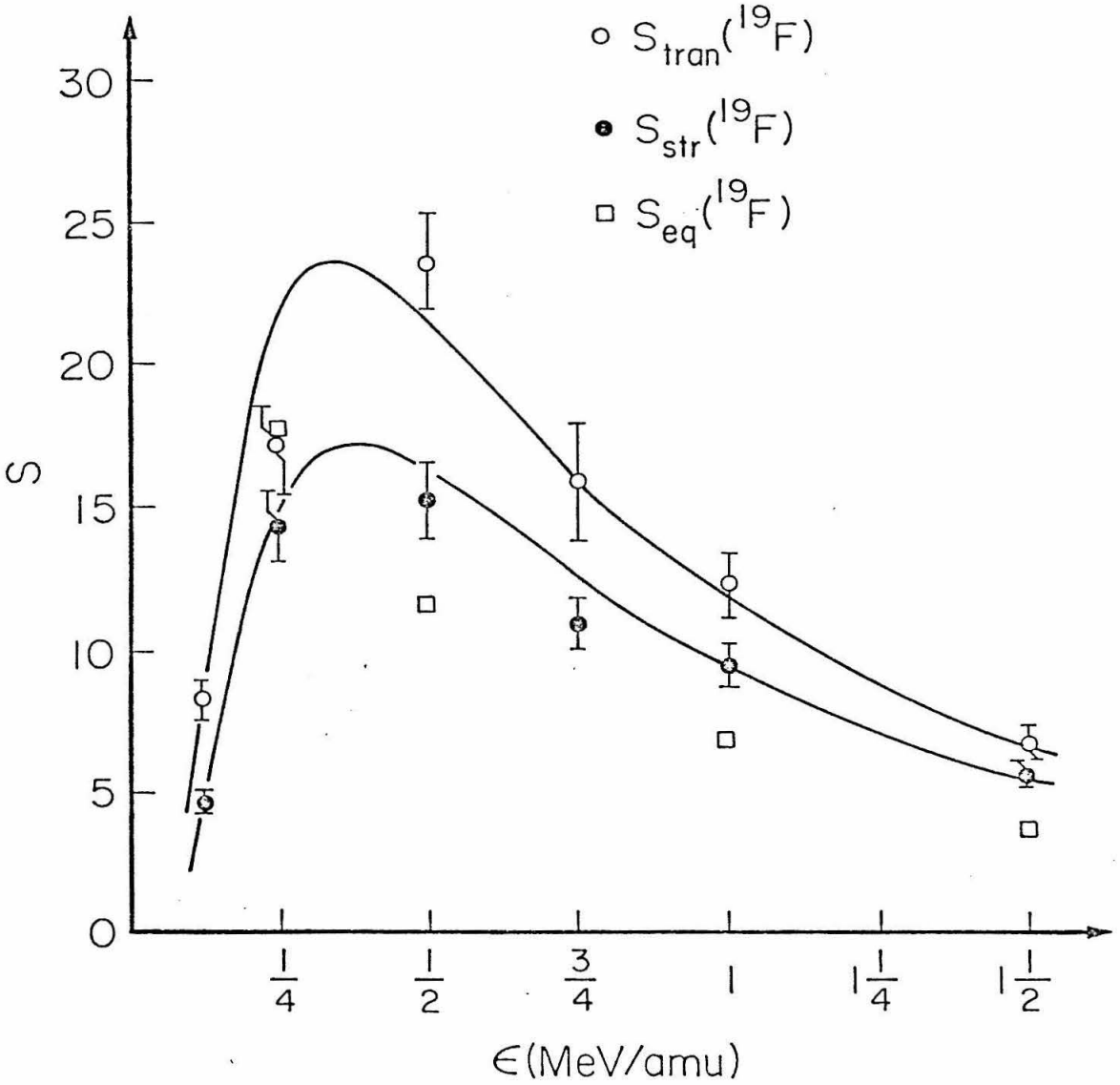
$S_{tran}(^{19}F)$
$S_{str}(^{19}F)$
$S_{eq}(^{19}F)$
S
30
25
20
15
10
5
0
1/4
1/2
3/4
1
1 1/4
1 1/2
∈(MeV/amu)

Figure 24

Incident charge data from Hakansson(81b) for 20.*MeV* ^{16}O on glycyl-glycine along with a fit to the average charge form.

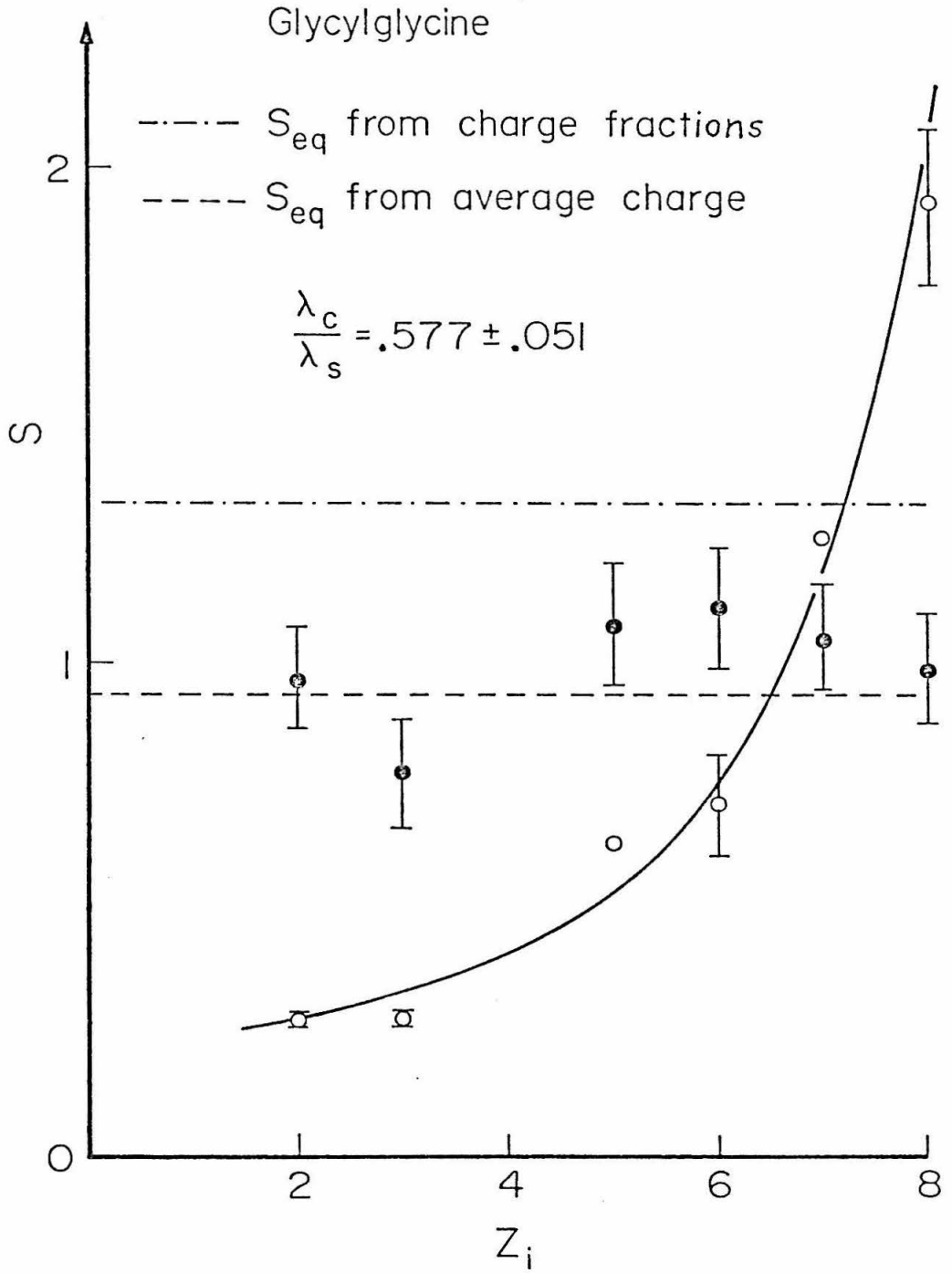
Glycylglycine
S_{eq} from charge fractions
S_{eq} from average charge
$\frac{\lambda_c}{\lambda_s} = .577 \pm .051$
S
2
1
0
2
4
6
8
Z_i

Figure 25

Incident charge data from Hakansson(81b) for 20.*MeV* ^{16}O on ergosterol along with a fit to the average charge form.

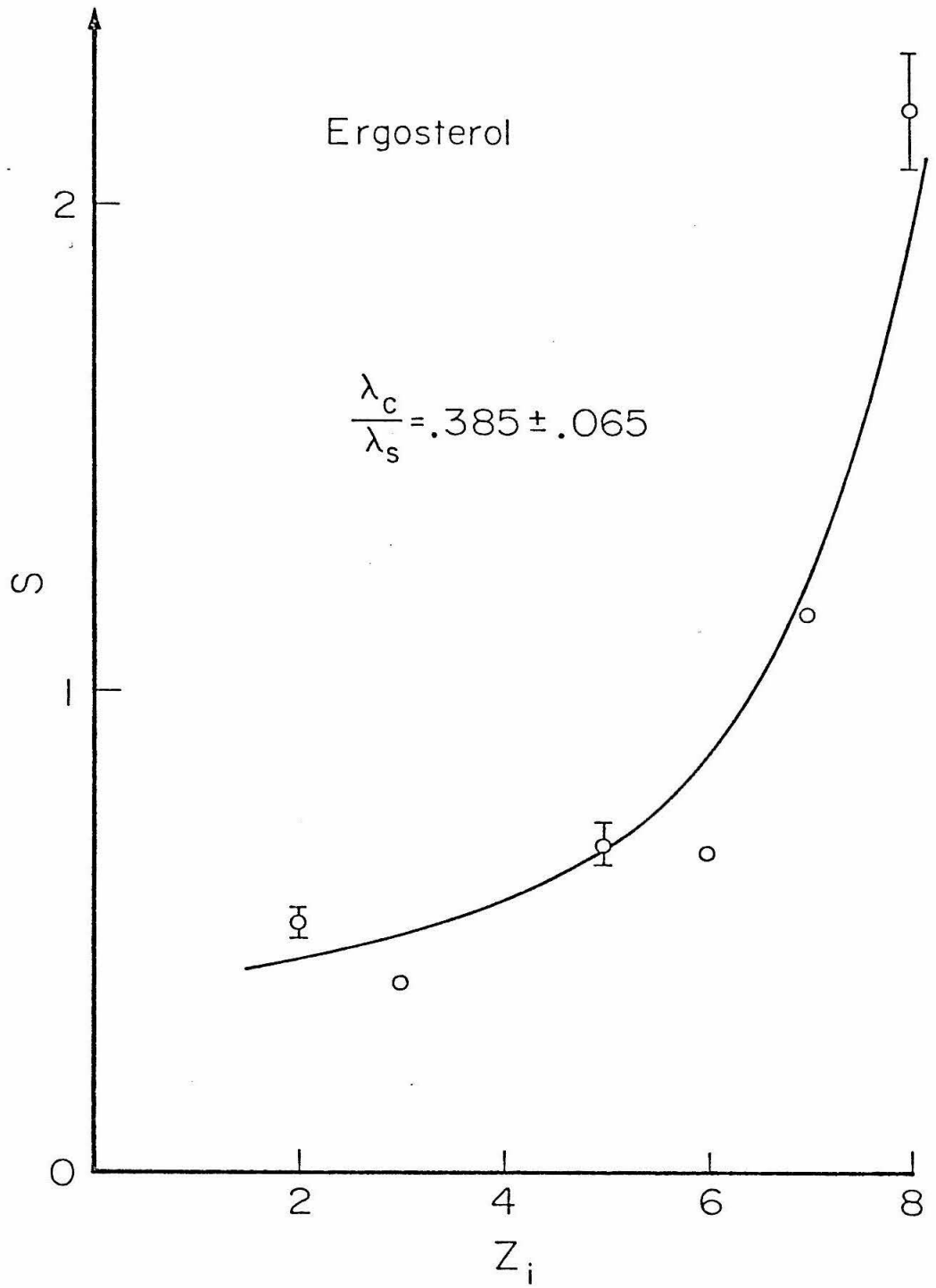
Ergosterol
$\frac{\lambda_c}{\lambda_s} = .385 \pm .065$
S
2
1
0
2
4
6
8
Z_i

Figure 26

Incident charge data from Hakansson(81b) for 20.*MeV* ^{16}O on CsI along with a fit to the average charge form.

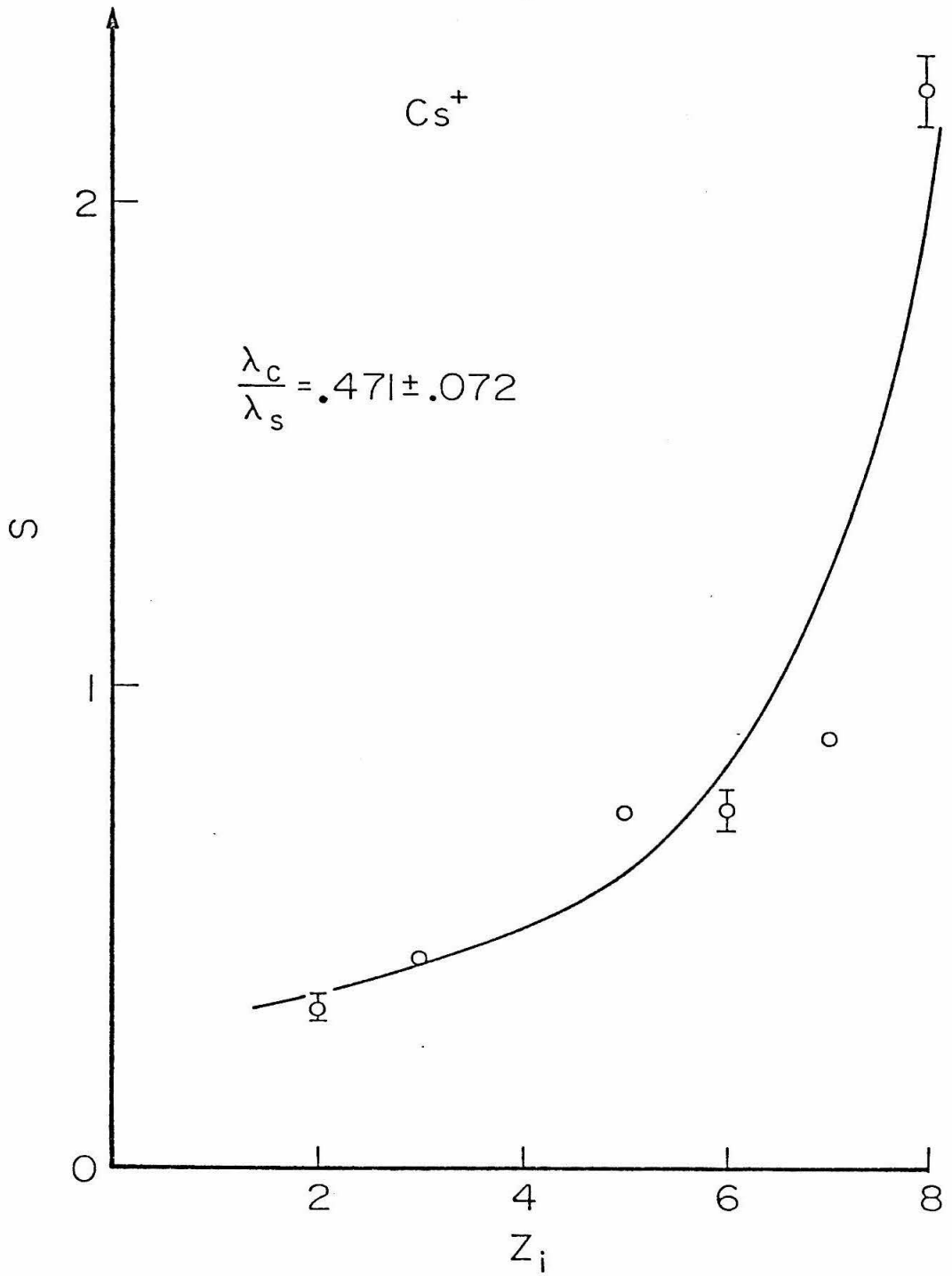
Cs^+
$\frac{\lambda_c}{\lambda_s} = .471 \pm .072$
S
2
1
0
2
4
6
8
Z_i

Figure 27

Equipment used for Rutherford scattering measurements. The targets were mounted on a vertical linear motion feedthru. A graphite beam dump was mounted behind the targets for use with foil targets. The surface barrier detector with its defining aperture was mounted on a rotatable arm centered on the target feedthru. The second arm was used to hold a carbon foil which could thus be moved in and out of the beam. For charge integration, the foil mount was insulated from the arm by a Lucite block and was attached to the targets by a copper wire. A cylinder made of copper mesh surrounded the target and foil holder and was biased to suppress secondary electron emission.

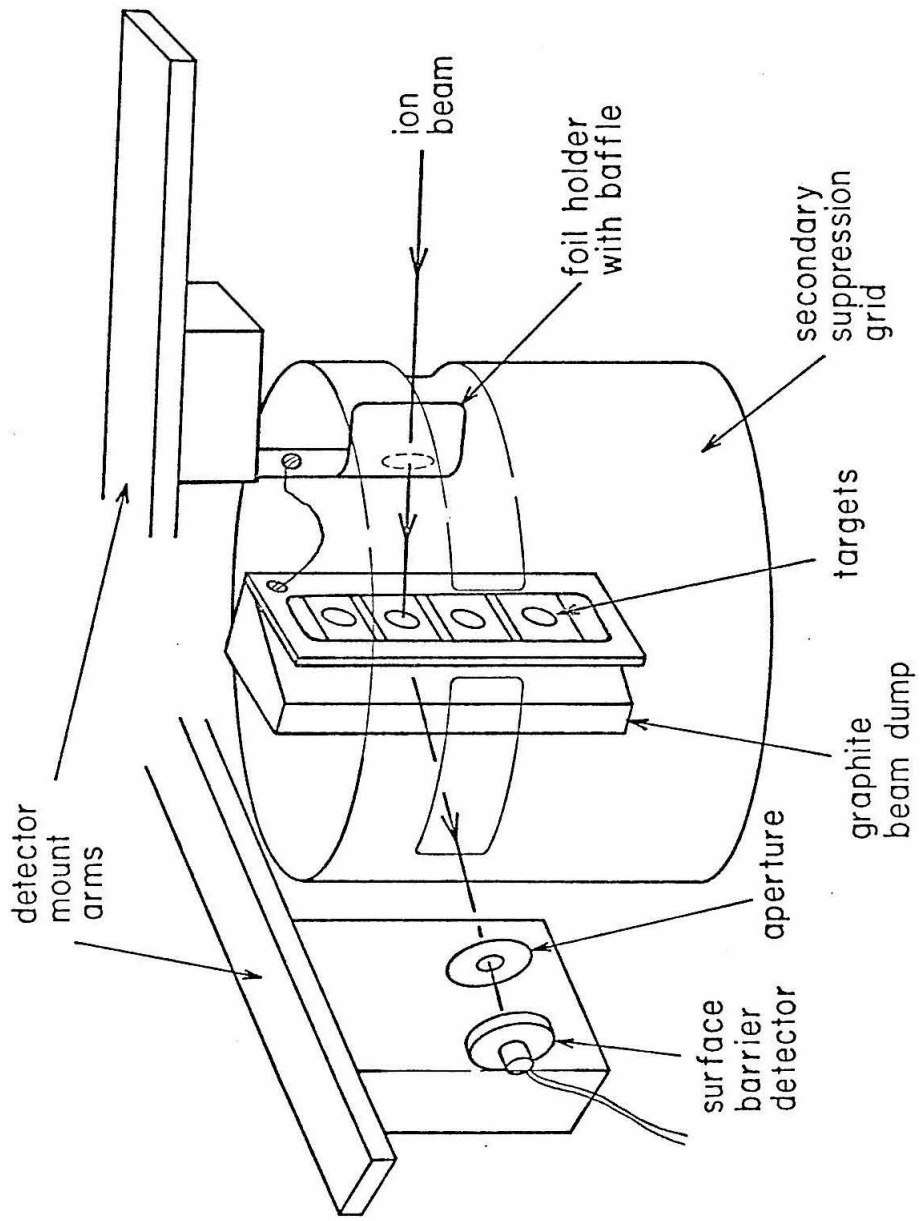
ion beam
foil holder with baffle
secondary suppression grid
targets
graphite beam dump
detector mount arms
aperture
surface barrier detector

Figure 28

Energy spectrum of 1.5 *MeV* alphas scattered at 55° from a carbon foil of nominal thickness 18.3 $\mu g / cm^2$. The foil had been used as a stripper foil for a stripped beam experiment and had thus been exposed to both the uranium and fluorine atoms sputtered from UF_4. The foil was analyzed in an attempt to measured the ratio of sputtered uranium and fluorine atoms. The points of the spectrum marked by the various nuclides were determined by assuming the two large peaks were due to ^{12}C and ^{235}U and that the energy was linear in the channel number.

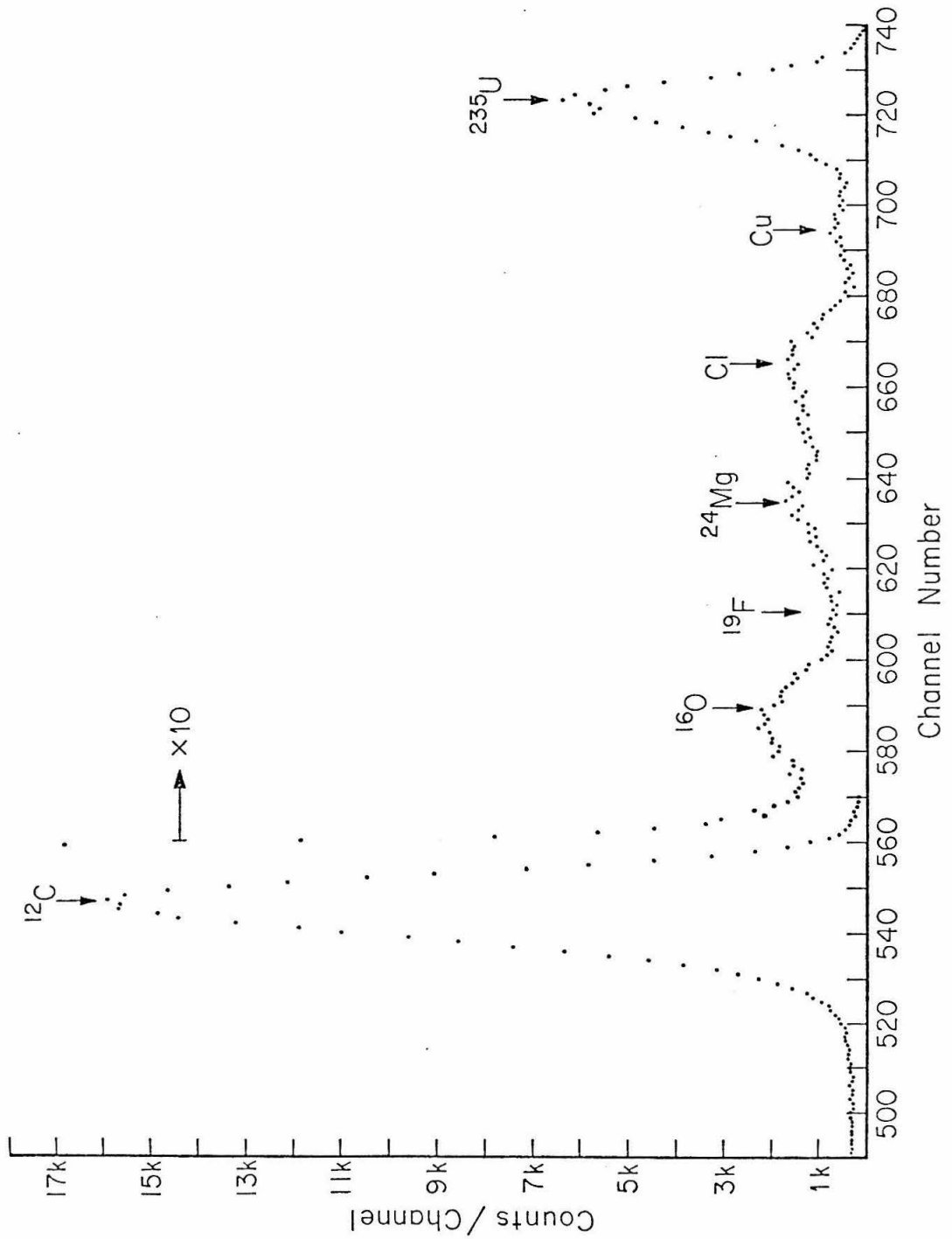
17k
15k
13k
11k
9k
7k
5k
3k
1k
Counts / Channel
500
520
540
560
580
600
620
640
660
680
700
720
740
Channel Number
^{12}C
×10
^{16}O
^{19}F
^{24}Mg
Cl
Cu
^{235}U

Figure 29

This figure shows the spectrum in fig.28 in the region where scatterings from ^{19}F would appear. The data in this region can be described by a flat background and the tails of the ^{16}O and ^{24}Mg peaks (the peaks were considered to have the same shape as the ^{12}C peak). From the standard deviation of the background, the ratio of fluorine to uranium atoms was

$$\frac{N(F)}{N(U)} \leq 4.$$

at the 3σ level.

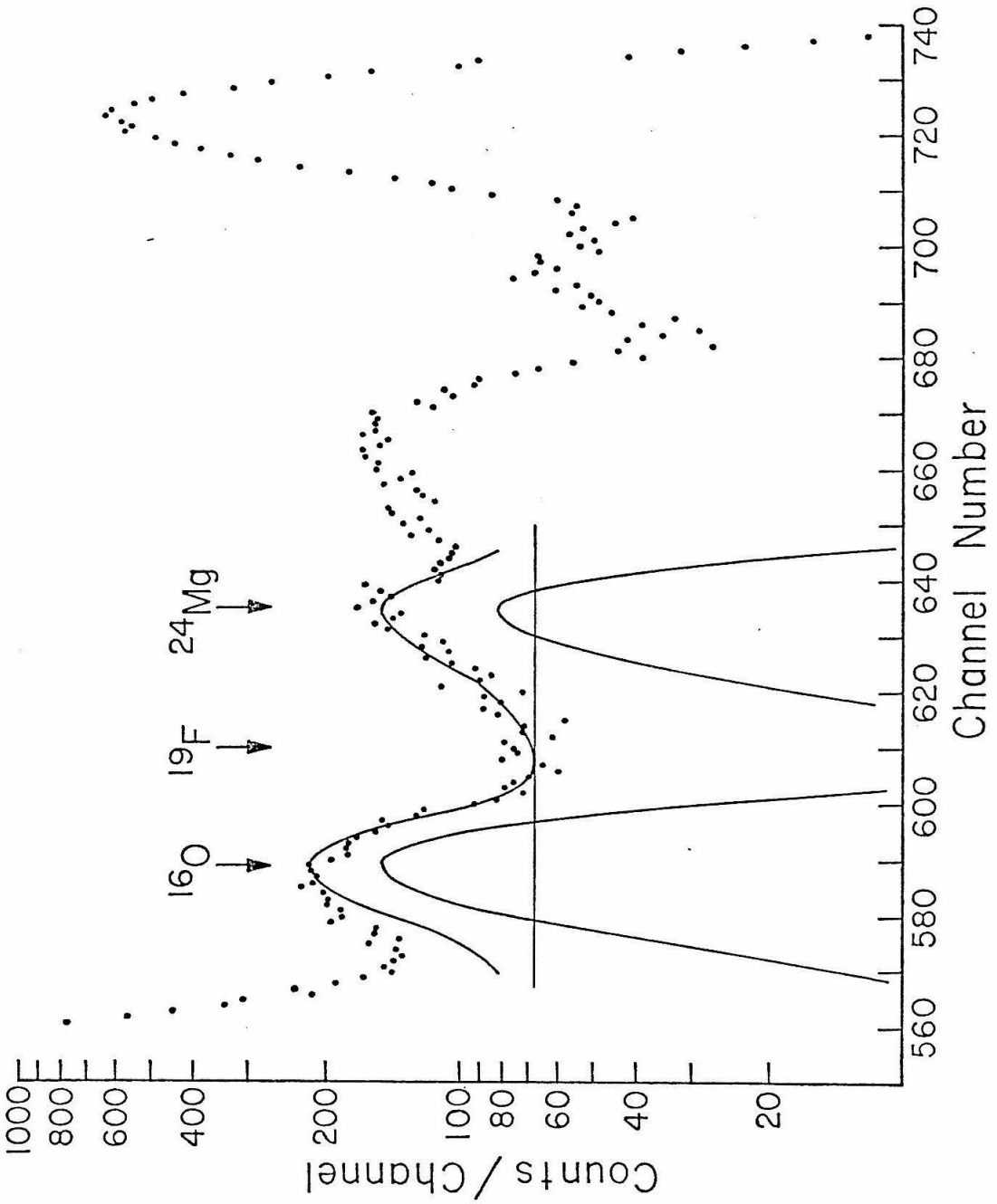
Counts / Channel
1000
800
600
400
200
100
80
60
40
20
560
580
600
620
640
660
680
700
720
740
Channel Number
^{16}O
^{19}F
^{24}Mg

Figure 30

Spectrum of 19.*MeV* ^{19}F scattered from UF_4 on copper at 160°.

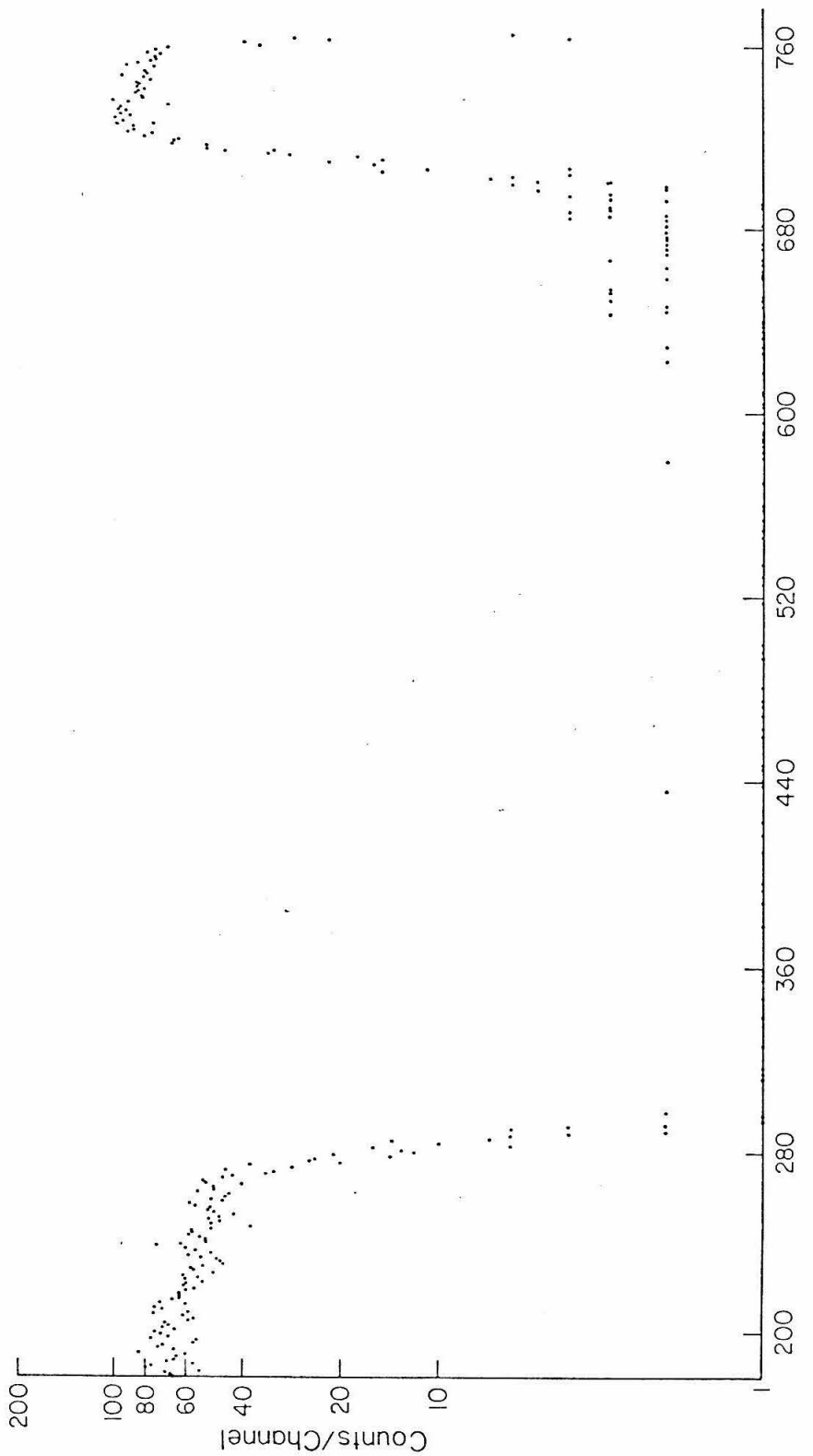
Counts/Channel
200
100
80
60
40
20
10
1
200
280
360
440
520
600
680
760
Channel Number

Figure 31

Comparison of $D_{\parallel}$ measured by Rutherford scattering and predicted by the $\frac{dE}{dx}$ tables of Northcliffe and Schilling(70) and Zeigler(80). The values of $D_{\parallel}$ predicted by $\frac{dE}{dx}$ have been reduced by the amounts shown to make them agree with the $\frac{1}{4}MeV/$ amu measurement.

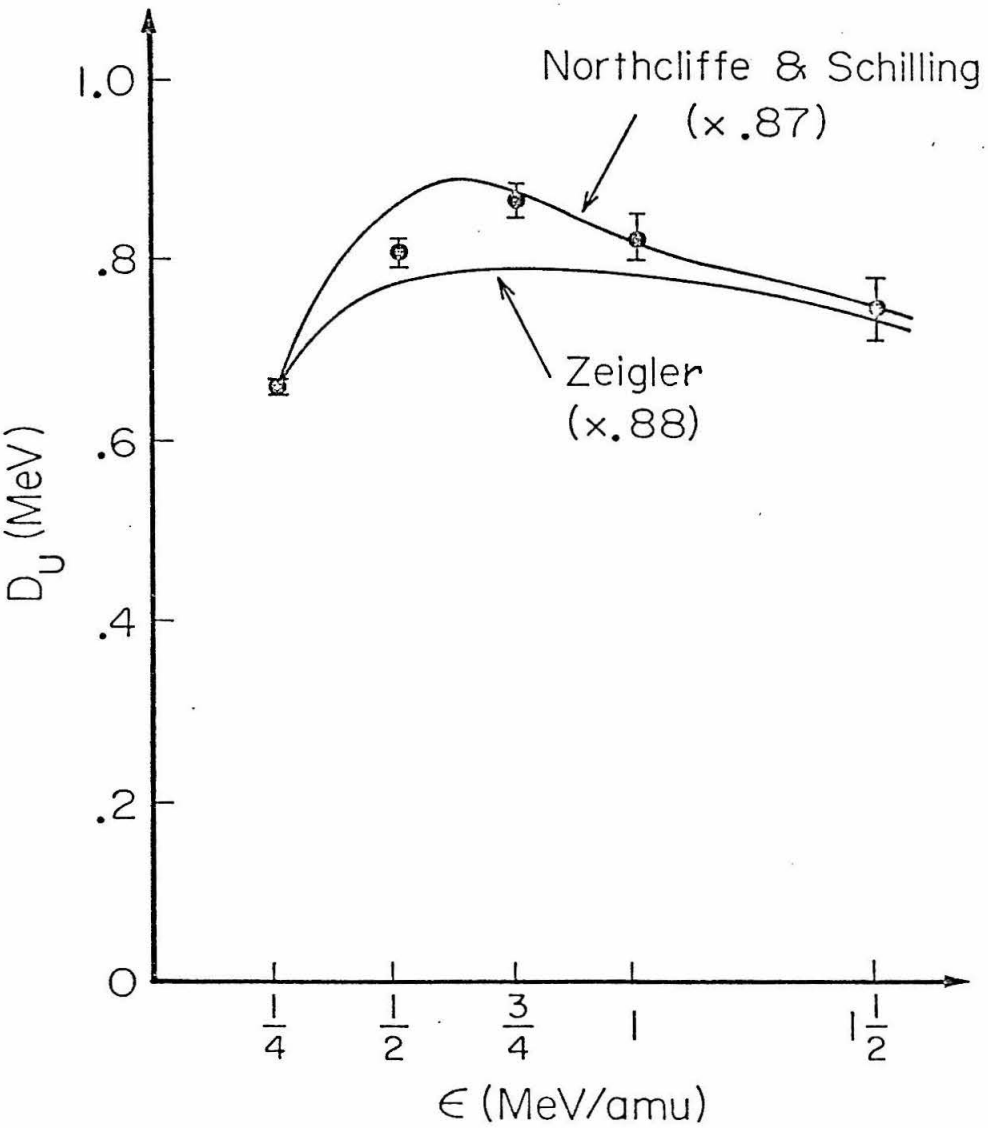
Northcliffe & Schilling
(×.87)
Zeigler
(×.88)
1.0
.8
.6
.4
.2
0
D_U (MeV)
$\frac{1}{4}$
$\frac{1}{2}$
$\frac{3}{4}$
1
$1\frac{1}{2}$
∈ (MeV/amu)

Figure 32

$\frac{dE}{dx}$ for ^{19}F in UF_4 as given by Northcliffe and Schilling(70) and Zeigler(80) and as implied by Rutherford scattering measurements. The implied $\frac{dE}{dx}$ curve is to be considered uncertain to ~1% at the low energy end progressing to ~5% at the high energy end.

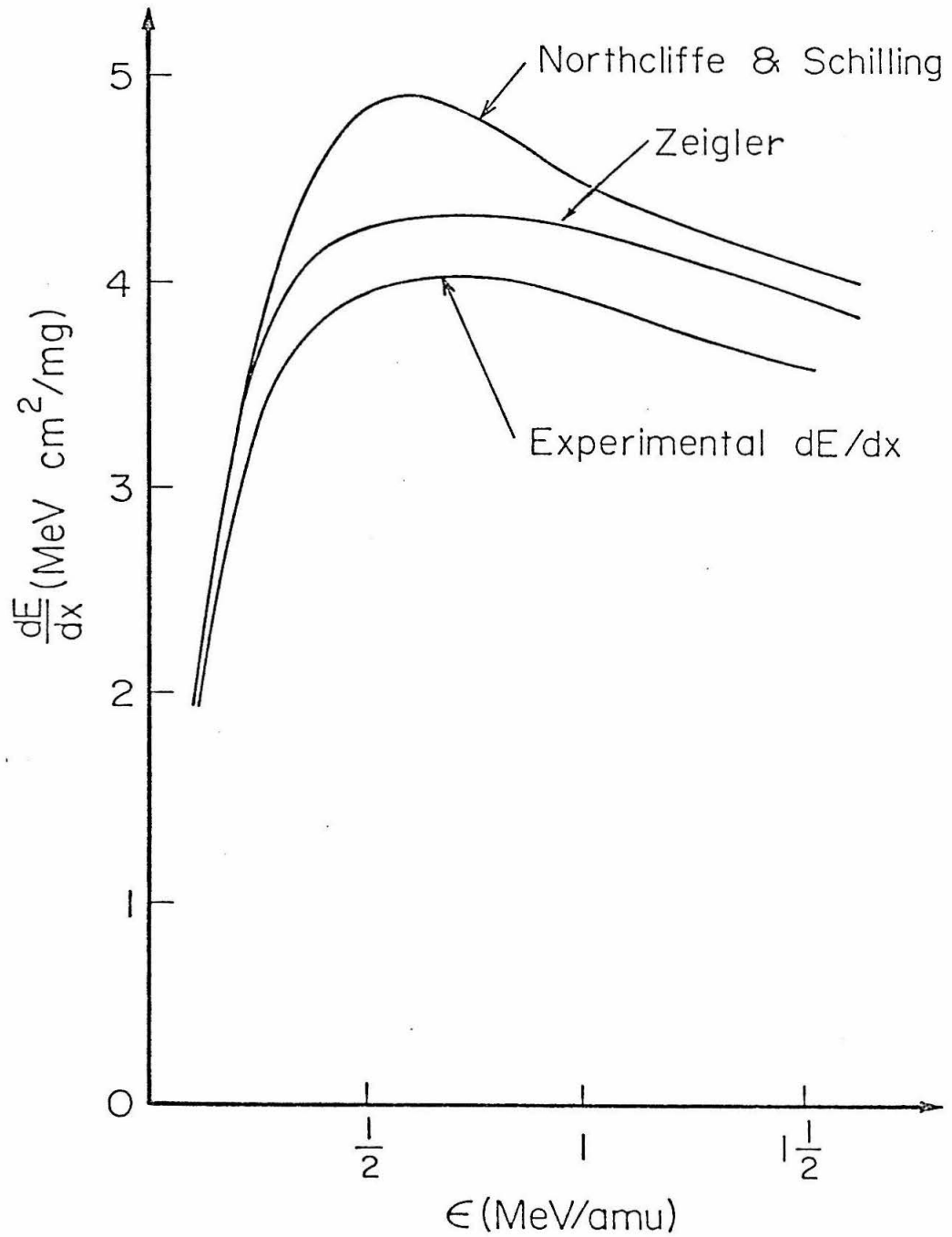
Northcliffe & Schilling
Zeigler
Experimental dE/dx
5
4
3
2
1
0
$\frac{dE}{dx}$ (MeV cm^2/mg)
$\frac{1}{2}$
1
$1\frac{1}{2}$
ϵ (MeV/amu)

Figure 33

Sputtering yield for 13.*MeV* ^{35}Cl on UO_2 (Seiberling et al.(81)). The magnitude and energy dependence are consistent with collision cascade sputtering.

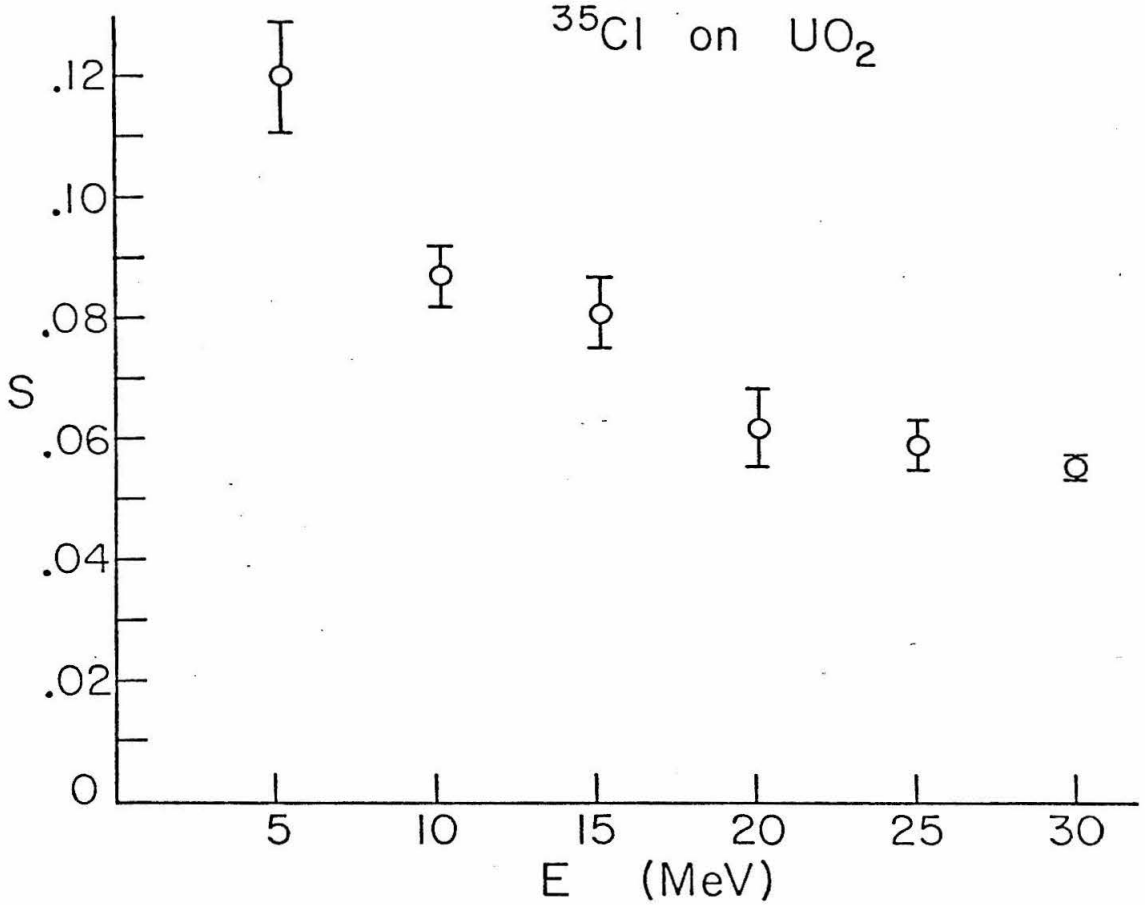
^{35}Cl on UO_2
.12
.10
.08
.06
.04
.02
0
S
5
10
15
20
25
30
E (MeV)